# Tracking changes in complex auditory scenes along the cortical pathway

Jennifer Lawlor

# THÈSE DE DOCTORAT

de l'Université de recherche Paris Sciences et Lettres
PSL Research University

**Préparée à École Normale Supérieure**

# Tracking changes in complex auditory scenes along the cortical pathway

**École doctorale n°158**

CERVEAU, COGNITION, COMPORTEMENT

**Spécialité** COGNITIVE NEUROSCIENCE

**COMPOSITION DU JURY :**

Dr. Stephen David
OHSU, Rapporteur, Président

Pr. Andrew King
Oxford University, Rapporteur

Dr. Kishore Kuchibhotla
Johns Hopkins University, Membre du jury

Dr. Srdjan Ostojic
Ecole Normale Supérieure, Membre du jury

Soutenue par **Jennifer LAWLOR**
le 26 October 2018

Dirigée par **Shihab Shamma**

ENS ÉCOLE NORMALE SUPÉRIEURE

PSL RESEARCH UNIVERSITY PARIS

My heartful thanks goes to Yves for being the most honest, thoughtful, cunning scientist. To Shihab for being supportive and always optimist. To Celian, for shared experimental frustration over extended period of time and chasing noise sources throughout the departement. To HiJee, the quiet force and sunday EEG experiments. To Sabrina, for chocolate and biased support. To Ljubisca, Jackson, Tarryn, Claudia, Bernhard, Andy... To Ben, the best lab/drone building partner. Pour Irma, Inf. A Vic. A Laurent pour une moitié de donughts au chocolat. A dodo pour son aide précieuse. A Sophie et sa soif de vivre. To Arthur for decent Sunday morning coffee. To David, à stoir, for coffee, twix and Yeats near the Arts building. To Pads, for pancakes at the metro and scones. To Pheobe, for being the smart one. To the calm litterary voice of Micheal. Pour Rémy, rends moi mes livres. To jess and Sam, respectively lovely and grumpy. To Antoine, Georges Sand sucks ! Pour Pam et son irrévérence. To Flo our, moral compass. To Agathe, for standing by for 25 years. Pour Arthur est son irrepressible ambition. Pour Pauline et son esprit logique. Pour Léo et le temps perdu. To Alyssa's ruthlessness. A Thibault, Pierre, Hugo, Max, Louis, Robin, Galahaad, Jason, Virgile, Uriel, Hoelle, Delorme, Marc, Léo, Brossart, Yanis, Antoine, Geoffroy, Eliott, Louis, Alex. To Dr. Buchin, wish the world would have been different. To Alejendro, modeling is too complex. To Manuel, no one ever thought "boite à sucres" was a good idea anyway. To Derek and cider near Malahide.

# Contents



[1] Boubenec et al. [2017]

# List of Figures

## Abstract

Complex, cluttered acoustic environments, such as a busy street, are characterised by their ever-changing dynamics. Despite their complexity, listeners can readily tease apart relevant changes from stochastic irrelevant variations in continuous acoustic streams. Such a capability requires continuously tracking the appropriate sensory evidence for detecting relevant changes in stimulus properties while discarding noisy acoustic variations due to stimulus inherent variability. Despite the apparent simplicity of this perceptual phenomenon, the neural basis of the extraction of relevant information in complex continuous streams for goal-directed behavior is currently not well understood. In particular there is no investigation about how this process is implemented throughout the auditory hierarchy during task performance. As a minimalistic model for change detection in complex auditory environments, we designed spectrotemporally broad-range tone clouds whose first-order statistics change at a random time. Subjects (humans or ferrets) were trained to detect these changes. Hence, they were faced with the dual-task of estimating the baseline statistics and detecting a potential change in those statistics at any moment, mimicking real-life challenges. To characterize the extraction and encoding of relevant sensory information along the cortical hierarchy, we first recorded the brain electrical activity of human subjects engaged in this change detection reaction-time task using electroencephalography. In a texture-based, change-detection paradigm, human performance and reaction times improved with longer pre-change exposure, consistent with improved estimation of baseline statistics. Change-locked and decision-related EEG responses were found in a centro-parietal scalp location, whose slope depended on change size, consistent with sensory evidence accumulation. The potential's amplitude scaled with the duration of pre-change exposure, suggesting a time-dependent decision threshold. Auditory cortex-related potentials showed no response to the change. A dual timescale, statistical estimation model accounted for subjects' performance. Furthermore, a decision-augmented auditory cortex model accounted for performance and reaction times, suggesting that the primary cortical representation requires little post-processing to enable change-detection in complex acoustic environments. To further this investigation, we performed a series of electrophysiological recordings in the primary auditory cortex (A1), secondary auditory cortex (PEG) and frontal cortex (FC) of the fully trained behaving ferret. A1 neurons exhibited strong onset responses and change-related discharges specific to neuronal tuning. PEG population showed reduced onset-related responses, but more categorical change-related modulations. Finally, a subset of FC neurons (dlPFC/premotor) presented a generalized response to all change-related events only during behavior. We show using a Generalized Linear Model (GLM) that the same subpopulation in FC encodes sensory and decision signals, suggesting that FC neurons could operate a conversion of sensory evidence to a perceptual

decision. In addition, PEG and FC population dynamics showed a time-dependent evolution within trials and before the change occurred, possibly reflecting an online estimation of the ongoing baseline statistics, a necessary process in this dual-estimation task. All together, these area-specific responses suggests a behavior-dependent mechanism of sensory extraction and generalization of task-relevant event.

## Résumé :

Les environnements acoustiques complexes et encombrés, comme par exemple une rue animée, sont caractérisés par leur variabilité. Les auditeurs peuvent pourtant facilement distinguer les changements pertinents des variations aléatoires du son dans ces scènes complexes continues. Cette capacité nécessite de suivre en permanence les aspects appropriés du stimulus tout en ignorant le bruit stochastique dans le stimulus dû à sa variabilité. En dépit de sa simplicité apparente, les processus cérébraux sous-tendant l'extraction d'informations pertinentes dans des flux continus restent actuellement peu explorés. Tout particulièrement, il n'y a pas de description de l'implémentation neurale des mécanismes sous-jacents à travers la hiérarchie auditive. Afin de décrire et caractériser ces processus, nous avons conçu des nuages de tons spectro-temporellement larges dont les statistiques de premier ordre changent à un moment aléatoire comme modèle pour la détection de changement dans les environnements acoustiques complexes. Les sujets ont pour consigne de détecter ces changements. Par conséquent, ils sont confrontés à une double tâche : ils doivent estimer les statistiques initiales du nuage de tons et détecter un changement potentiel de ces statistiques à chaque instant. Afin de caractériser l'extraction et l'encodage des informations sensorielles pertinentes par la hiérarchie corticale, nous enregistrons tout d'abord l'activité électrique du cerveau (EEG) de sujets humains détectant des changements dans les nuages de tons présentés. La performance et les temps de réaction sont respectivement plus haute et plus courts avec une exposition plus longue avant l'apparition d'un changement, ce qui correspond à une meilleure estimation des statistiques de base. Des réponses EEG centro-pariétales liées au changement et à la décision dépendent notamment de la taille du changement, un résultat en accord avec l'hypothèse d'une accumulation de l'information sensorielle au cours du temps. L'amplitude du potentiel est de plus corrélée avec la durée de l'exposition pré-changement, ce qui suggère un seuil de décision dépendant du temps. En outre, un modèle de cortex auditif auquel on ajoute un seuil de décision permet de reproduire la performance et les temps de réaction, suggérant que la représentation corticale primaire nécessite peu de post-traitement pour permettre la détection de changement dans des environnements acoustiques complexes. Pour préciser les mécanismes qui sous-tendent la détection du signal pertinent et amène au comportement adéquat, nous avons effectué une série d'enregistrements électrophysiologiques dans le cortex auditif primaire (A1), le cortex auditif secondaire (PEG) et le cortex frontal (FC) du furet entraîné à la détection de changements dans les mêmes stimuli. Les neurones A1 présentent des modulations fortes de leur taux de décharge spontané au début du son, ainsi que des modulations après le changement lorsque celui-ci correspond aux spécificités spectro-temporelles des cellules enregistrées. La population du PEG montre des réponses associées au début du son plus réduites,

mais des modulations liées au changement plus généralisées. Enfin, un sous-ensemble de neurones FC (dlPFC / prémoteur) présente une réponse généralisée à tous les événements liés aux changements pendant le comportement. Nous montrons en utilisant un Modèle Linéaire Généralisé (GLM) que la même sous-population dans le FC encode le signal sensoriel et de décision, suggérant que la conversion des évidences sensorielles en une décision pourrait se réaliser au niveau du FC. En outre, la dynamique des populations PEG et FC évolue avec le temps avant le changement, reflétant peut-être une estimation en ligne des statistiques du nuage de tons, un processus nécessaire dans cette tâche d'estimation double. Ces réponses spécifiques aux différentes zones corticales suggèrent un mécanisme d'extraction sensorielle et de généralisation dépendant du comportement.

# Chapter 1: Introduction

Simply observing an animal's behavior in its natural environment will lead to the conclusion that animals respond selectively to objects and events. Exposure to one type of relevant stimuli typically leads to one behavior, while another may elicit another response. The red color patch placed on the belly of a male stickleback elicits aggression in other males during breeding, but a model of a female with eggs elicits courtship (Tinbergen [1952], Shettleworth [2001]). Birds can be trained to peck at pictures of trees and refrain from pecking for other types of pictures (Herrnstein et al. [1976]). Both examples illustrate how common and widespread discriminative behavior are. Producing the adequate behavior in a timely fashion is crucial for an individual's survival. It relies on the correct classification and interpretation of external inputs. As a consequence, sensory systems have evolved to allow things in the world that have different significance to elicit different behaviors.

Unlike pure tones and wavelengths traditionally used in the laboratory, sensory inputs in natural environment are usually noisy and embedded in complex scenes. This means that in order to achieve a stable percept, the brain overcomes signal's variability and must select the relevant input. This task becomes more complex as context also changes with time. Robustness of speech recognition in noisy background exemplifies how a noisy signal unfolding over time leads to a reliable percept.

Understanding how relevant sensory information is processed by the brain to produce an adequate behavior is one of the major challenges in system neuroscience. Three main processing stages are thought to lead to a perceptual decision: sensory processing, decision formation, and motor execution (Sternberg [1969]). The present manuscript focuses on the first two stages. In the following chapter we will review underlying neural substrates and possible mechanisms leading to perceptual decisions within modality and introduce the paradigm developed throughout the thesis.

Three axes will explore how sensory flow is processed to lead to a decision. First, we will review evidence relating to emergence of abstract representations along the cortical hierarchy. We will then describe mechanisms underlying the conversion of sensory evidence into decisions. Finally, we will explore contextual effects that modulate both processes. Examples will be taken from different modalities, although an emphasis will be made on the auditory one when possible. Modality specificity will

not be discussed in the present manuscript.

## Bottom-up processing of sensory information

Within modalities, sensory information is thought to travel in a bottom-up fashion (Romo and de Lafuente [2013], van Vugt et al. [2018], Brincat et al. [2018], Atiani et al. [2014], Siegel et al. [2015]) from the periphery to higher associative cortical areas, where abstracted representations can be found (Roy et al. [2010], Swaminathan and Freedman [2012], Fritz et al. [2010]). The following section will focus on how sensory signals representation evolve from a feature-based representation to a categorical one.

**Feature-based representation in primary sensory cortices** Upon reaching primary sensory cortices, sensory information is already processed by the periphery and subcortical structures and nuclei (Kiang et al. [1965], Mountcastle [1957], BARLOW [1957]). Studies comparing stimulus-evoked activity in the primary auditory cortex (A1) of anesthetized animals have demonstrated that neurons are modulated by basic auditory features (Bizley et al. [2005]). A1 tonotopic organisation illustrates how cells in primary sensory regions respond in reliable fashion (Bizley et al. [2005]). Similarly orientation columns are found in the primary visual cortex (V1). Much is known about the anatomy and the functional mapping of the primary sensory areas (Bimbard et al. [2018], Bizley et al. [2005]), at least in some of the most commonly used species in neuroscience. Computational models have been used to reconstruct natural movies from the sluggish BOLD activity in visual cortex (Nishimoto et al. [2011]) or phonemes from extracellular electrophysiology recordings in auditory cortex (Mesgarani et al. [2009]) by taking into account functional response of cortical neurons such as spectral and temporal patterns.

**Features become more complex in secondary areas** Compared to primary responses in primary cortices, secondary cortices represent more complex features. For example responses in secondary auditory areas display longer latencies, less phase-locking, broader spectral bandwith, longer integration time-constant, and higher stimulus selectivity (Atiani et al. [2014], Bizley et al. [2005], Wang et al. [2005], Rauschecker et al. [1997]). Thus, even within auditory cortex functional responses suggest gradation of complexity.

**Abstract representation in the prefrontal cortex** Prefrontal cortex including the lateral prefrontal cortex receive afferents from higher-order auditory cortex (Romanski et al. [1999], Romanski and Goldman-Rakic [2002], Plakke and Romanski [2014]). Those areas have been involved in a number

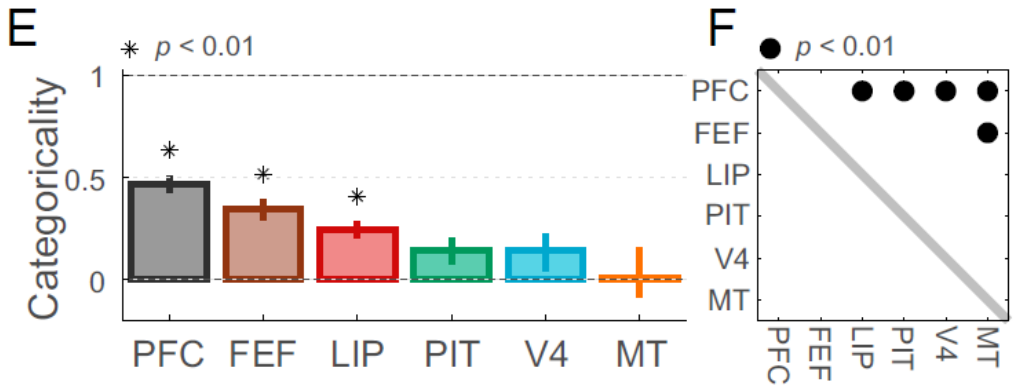


Figure 1: **Task-rule cue categoricality representation**
From Brincat et al. [2018] E) Task-rule categoricality index (±SEM) for each area, reflecting where its mean between-category rule-cue variance falls between its expected values for pure sensory (0) and categorical (1) representations. Only PFC, FEF, and LIP are significantly different from zero ($p < 0.01$). (F) Cross-area comparison matrix indicating which regions (rows) had significantly greater task-rule categoricality indices than others (columns) ($p < 0.01$). PFC was significantly greater than all others, except FEF.

of functions such as categorization (Roy et al. [2010], Cohen et al. [2006]) and decision-making (Romo and de Lafuente [2013], Romo et al. [2004], Rossi-Pool et al. [2016], Hanks et al. [2015]). In Fritz et al. [2010] a subset of neurons displayed higher responses to targets in the ferret cortical area equivalent of dlPFC (dorsal aspect of the Anterior Sigmoid Gyrus, ASG) regardless of the modality (visual and auditory).

**Encoding comparison along the sensory pathway suggest gradual increase in abstraction** In addition, studies specifically comparing how different part of the pathway encode stimulus- and task-related components (Rossi-Pool et al. [2016]) suggest a gradual progression towards abstraction. Brincat et al. [2018] compared neural representations in visual, temporal, parietal, and frontal cortices in monkeys engaged in a visual multiple-categorical task. Using electrophysiological recordings in the non-human primate and in six cortical areas along the visual pathway, they showed that categorization is gradual (see 1E & F).

**Population distributions of stimulus evoked response latency** If sensory information flow is hierarchical, then neurons response latency to a stimulus should increase along this hierarchy. Minimum response latency across areas of the visual pathways (Schmolesky et al. [1998] and 2(a)) showed that signal arrives first in V1, followed by V3, MT, MST and FEF and later V2 and V4, highlighting the separation between visual streams. In de Lafuente and Romo [2006] response latencies across

areas of the somatosensory system were measured as well as encoding of the animal's behavioral response. Both measure increase gradually and culminate with the prefrontal regions (Schmolesky et al. [1998] and 2(b)).

## Decision process stage

Forming a perceptual decision requires converting relevant sensory information into a decision that will lead to a discrete motor act. The field of perceptual decision-making has implicated sensori-motor areas, mostly parietal and dorsal prefrontal cortex, in this process in a number of species (humans: O'Connell et al. [2012], Twomey et al. [2015], non-human primates: Britten et al. [1996], Shadlen et al. [1996], Churchland et al. [2008], Drugowitsch et al. [2012], Romo et al. [2004], Huk [2005], Ratcliff and McKoon [2008], Kim and Shadlen [1999], rodents: Erlich et al. [2015], Hanks et al. [2015], Scott et al. [2017]) using a variety of visual (Britten et al. [1996], Churchland et al. [2008], Drugowitsch et al. [2012], Hanks et al. [2006, 2014], Huk [2005], Kim and Shadlen [1999], O'Connell et al. [2012]), vibrotactile (Romo et al. [2004], Rossi-Pool et al. [2016]) and auditory tasks (Brunton et al. [2013], Hanks et al. [2015]) requiring accumulation of information over time. Neural signals recorded in those areas have been shown to be scaled by the amount of sensory evidence on a given trial, even at the single neuron level, and predict the animal upcoming choice (Britten et al. [1996], Romo et al. [2004], Shadlen and Newsome [2001], Latimer et al. [2013], Kim and Shadlen [1999], Churchland et al. [2008]). The combination of responses are neither purely motor nor purely sensory and implicate those areas in the decision process.

**Neural correlates of a decision variable** To be considered as a decision variable a signal needs to be neither purely sensory, nor purely motor, and must instead integrate task-relevant sensory information over time (Shadlen and Kiani [2013], Kelly and O'Connell [2015], Hanks and Summerfield [2017]). Therefore this signal must vary with sensory inputs and should also show a clear relationship with the motor output, such as co-variation with reaction time. In the middle temporal area (MT) of monkeys performing a motion discrimination task, direction-tuned neurons' firing rates predict reliably the decisions in the absence of coherent motion ('choice probability') (Britten et al. [1996], Parker and Newsome [1998]). Neural activity identified as representing decision variables in other cortical areas all share two principal components: a build-up rate scaled by sensory evidence (see example in the lateral intraparietal cortex (LIP) 3c) and a threshold upon which an action is triggered (see example in LIP 3d). Decision variable signals have been observed in parietal and frontal areas (dlPFC, premotor) in a number of species and in a different modalities (Roitman and Shadlen [2002], Shadlen

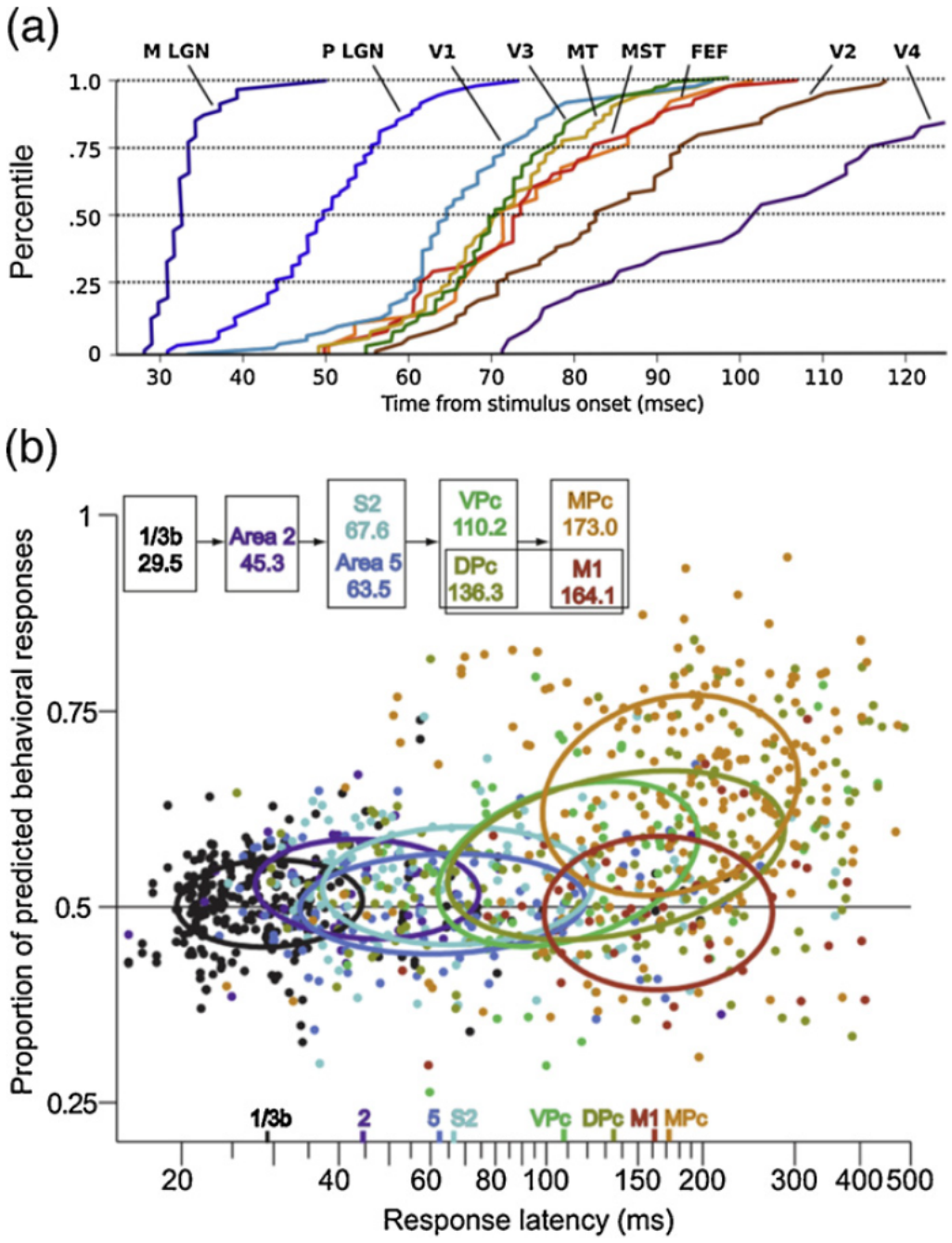


Figure 2: **Distribution of response latencies across cortical areas**
From Wohrer et al. [2013] (b) Latencies and choice probabilities in different areas involved in a tactile discrimination task. Latencies and choice probabilities increase along the putative processing pathway of information. Reproduced from de Lafuente and Romo (2006), Copyright (2006) National Academy of Sciences, U.S.A. V3,

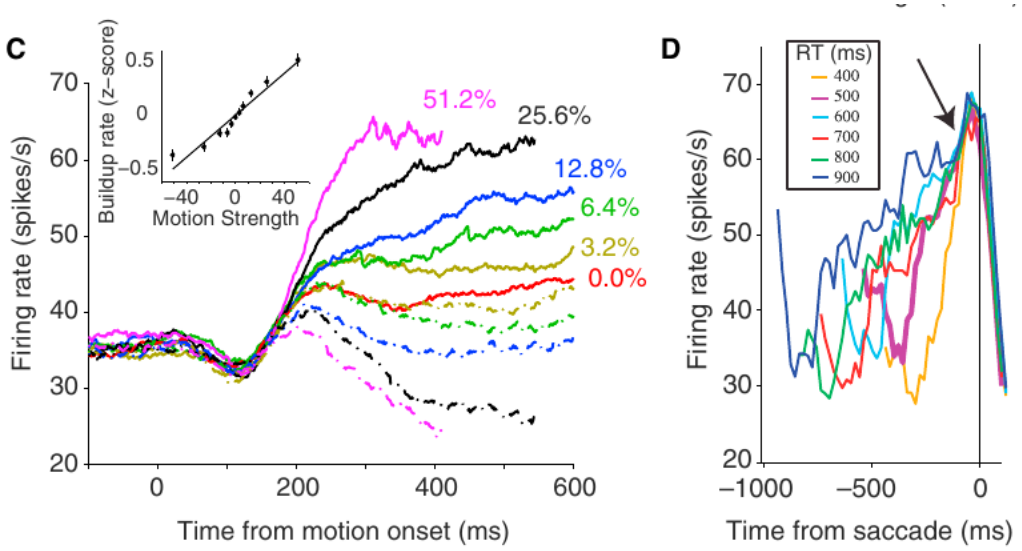


Figure 3: **LIP responses during decision formation**
From Shadlen and Kiani [2013](C) Response of LIP neurons during decision formation. Average firing rate from 54 LIP neurons is shown for six levels of difficulty. Responses are grouped by motion strength (color) and direction (solid/dashed toward/away from the receptive field (RF)); they include all trials, including errors. Firing rates are aligned to onset of random-dot motion and truncated at the median RT. Inset shows the rate of rise of neural responses as a function of motion strength. These buildup rates are calculated based on spiking activity of individual trials 200–400 ms after motion onset. Data points are the averaged normalized buildup rates across cells. Positive/ negative values indicate increasing/decreasing firing rate functions. (D) Responses grouped by reaction time and aligned to eye movement. Only saccades to the cells' RF are shown. Arrow shows the stereotyped firing rate ~70 ms before saccade initiation. Adapted from Roitman and Shadlen (2002)

and Newsome [2001], Brunton et al. [2013], Erlich et al. [2015], O'Connell et al. [2012], Hanks et al. [2015], Erlich et al. [2011]), suggesting invariance of the decison process.

**Causality** The above-mentioned signals were obtained by recordings neural activity (neurons or EEG) during behavior. If the presence of the decision-related activity is ascertained, its exact role in the decision process is not. Causation can only be established by disrupting the system and quantifying how behavior is impacted. Katz et al. [2016] pharmacologically inactivated (muscimol, a GABA receptor agonist) MT and LIP in the monkey performing a motion-discrimination task. If MT inactivation impacted behavior significantly (see Fig. 4c), inactivation of LIP did not (see Fig. 4d). LIP decision-related activity is therefore not necessary to perceptual decision formation in this particular task. Furthermore, Erlich et al. [2015] inactivated the posterior parietal cortex (PPC) and the frontal orienting field (FOF) in the rat performing on a click train accumulation task (Brunton et al. [2013]). Only inactivation of FOF impacted behavior significantly. The same group have recently used a combination of pharmacological inactivation and optogenetic and proved that anterior dorsal striatum (ADS)

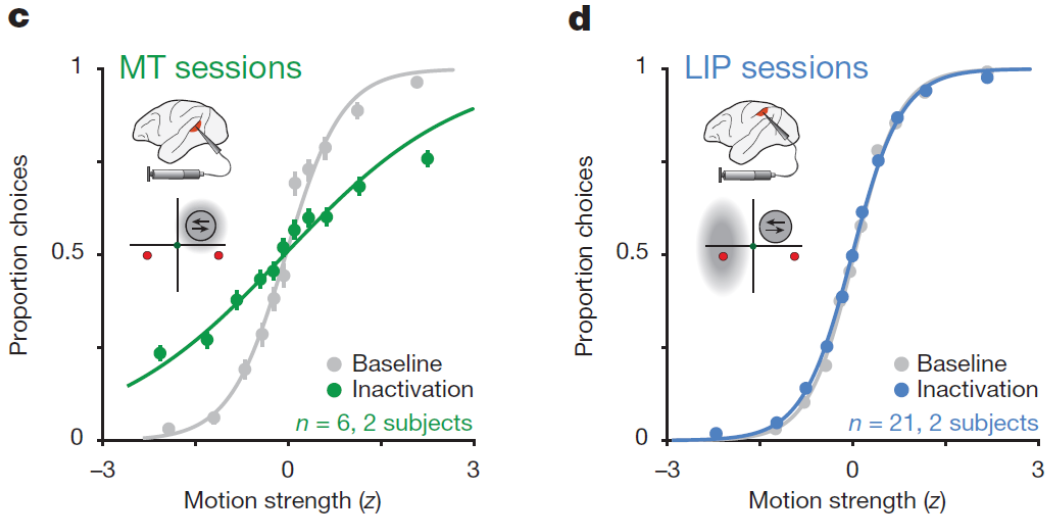


Figure 4: **MT and LIP inactivation**
From Katz et al. [2016]**c, d,** Psychophysical data for averaged pairs of baseline and muscimol treatment sessions in MT (c), and LIP (d). Insets illustrate the brain region inactivated (top) and the corresponding experimental geometry (bottom), along with the estimated inactivated field (grey cloud). Error bars on points show ± 1 s.e.m. over all trials.

is responsible for evidence accumulation (Yartsev et al. [2018]).

**Models** Accumulation of evidence from noisy observations over time improves estimates. It requires keeping an estimation in memory and updating it when new evidence is presented until a threshold is reached. This principle underlies a popular model in the decision-making field. The "drift diffusion model" provides quantitative explanation for behavior in perceptual tasks (Gold and Shadlen [2007], Ratcliff and McKoon [2008], Ossmy et al. [2013], Brunton et al. [2013]). A decision variable (see Fig. 5, decision variable a), varies with sensory evidence over time until a threshold is reached ("decision bound"). It has been suggested however, that integration-to-bound signals may only be created by averaging neuronal responses (Park et al. [2014]) and may not capture the heterogeneity of the encoding (Rigotti et al. [2013]). Heterogeneous encoding could allow information to be maintained on multiple timescales.

## Overcoming signals' variability

Sensory inputs in natural environment are usually noisy and embedded in complex scenes. Even within a category object properties vary greatly. For instance phonetic distance between identical phonemes said by different speakers can be larger than distance between different phoneme said by the same speaker (Peterson and Barney [1952]). In other words, the environment is highly variable

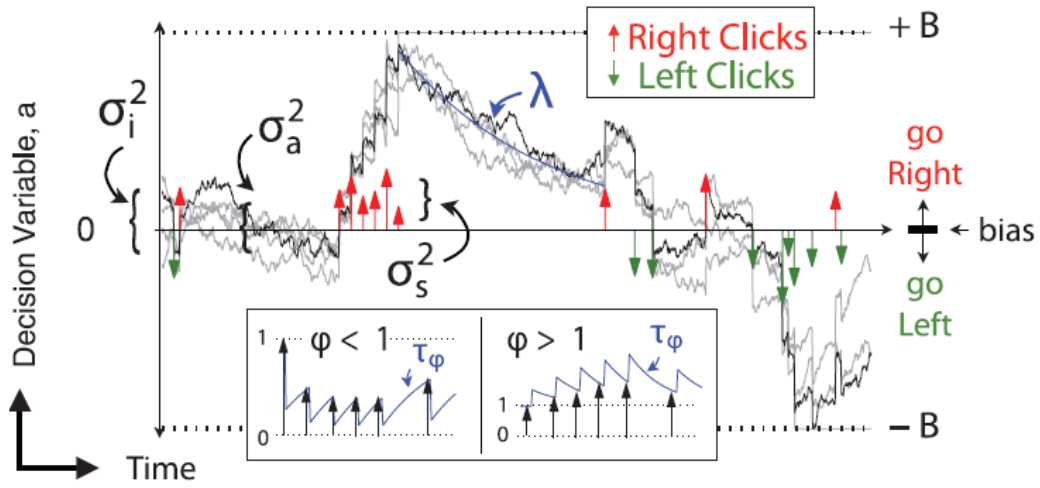


Figure 5: **Drift Diffusion Model illustration**
From Brunton et al. [2013]
At each time point, the accumulator memory a (black trace) represents an estimate of the right versus left evidence accrued so far. At stimulus end, the model decides right if a > bias and left otherwise, where bias is a free parameter. The light gray traces indicate alternate runs with different instantiations of model noise. Right ↑ (left ↓) pulses change the value of a by positive (negative) impulses of magnitude C.
$\sigma_i^2$ parameterizes noise in the the initial value of a.
$\sigma_a^2$ is a diffusion constant, parameterizing noise in a.
$\sigma_s^2$ parameterizes noise when adding the evidence from a right or left pulse: For each click, variance s2 s is scaled by the amplitude of C and then added to the evidence contributed by the click.
$\lambda$ parameterizes consistent drift in the memory a. In the "leaky" or forgetful case ($\lambda$ <0, illustrated), drift is toward a = 0, and later pulses affect the decision more than earlier pulses. In the "unstable" or impulsive case (l >0), drift is away from a = 0, and earlier pulses affect the decision more than later pulses. The memory's time constant $\tau = 1/\lambda$.
B is the height of the sticky decision bounds and parameterizes the amount of evidence necessary to commit to a decision.
$\varphi$ and $\tau\varphi$ parameterize sensory adaptation by defining the dynamics of C. Immediately after a click, the magnitude C is multiplied by $\varphi$. C then recovers toward an unadapted value of 1 with time constant $\tau\varphi$. Facilitation is thus represented by $\varphi$ > 1, whereas depression is represented by $\varphi$ < 1 (inset).

and still individuals must extract abstract categories from it. Therefore, there is a discrepancy between the environment's variability and the stability of a percept. In order to overcome that variability the system must build noise-invariant representation of inputs. In this section we will review the different level of neural mechanisms associated with constructing of a noise-invariant representation of the sensory input.

**Mechanisms of neural adaptation** Individual neuron firing rate is modulated by sensory context (Rabinowitz et al. [2011], Wark et al. [2007], Benucci et al. [2013], Watkins and Barbour [2008], Bar-Yosef et al. [2002]). Benucci et al. [2013] manipulated this context by changing the orientation distribution of grating stimuli from uniform to biased. By shifting the underlying statistics of the ensemble while recording a large population of cells in V1 of the anesthetized cat, they observed that neurons adapted their responsiveness and selectivity so that population response stays the same. This adaptation mechanism "counteracted" the sensory bias. One of their interpretation is that adaptation's role is to match the statistics of the environment by subtracting responses to the bias sensory component. Adaptation to the presented statistics provides a possible mechanism to construct noise-invariant representations. The underlying neural computation termed 'divisive normalization' consists in dividing neurons' responses by a common factor, such as the summed activity of a pool of neurons (Carandini and Heeger [2012], Schwartz and Simoncelli [2001])

**Time integration** In some cases the signal is inherently variable either because it unfolds over time or because it is embedded in noise. Achieving a good estimation of such signals requires integration over time. McWalter and McDermott [2018] use specific stimuli that are thought to be represented by their statistics to probe the the time integration process. Auditory textures are variable on a short time scale but can be represented on a longer time scale by their statistics (McWalter and Dau [2017], McWalter and McDermott [2018], Mcdermott et al. [2013], McDermott et al. [2011]). They introduced subtle shifts in stimulus statistics that biased the texture judgment seconds later, indicating of a multi-second averaging window. In addition, this window may adapt to the ongoing stimulus statistics.

## Context dependence

We have described so far mechanisms thought to underly the processing of sensory inputs along the cortical hierarchy and the conversion to a decision. Cortical activity also reflects task-relevant parameters (Brincat et al. [2018], Fritz et al. [2010], Atiani et al. [2014]) in a gradual manner.

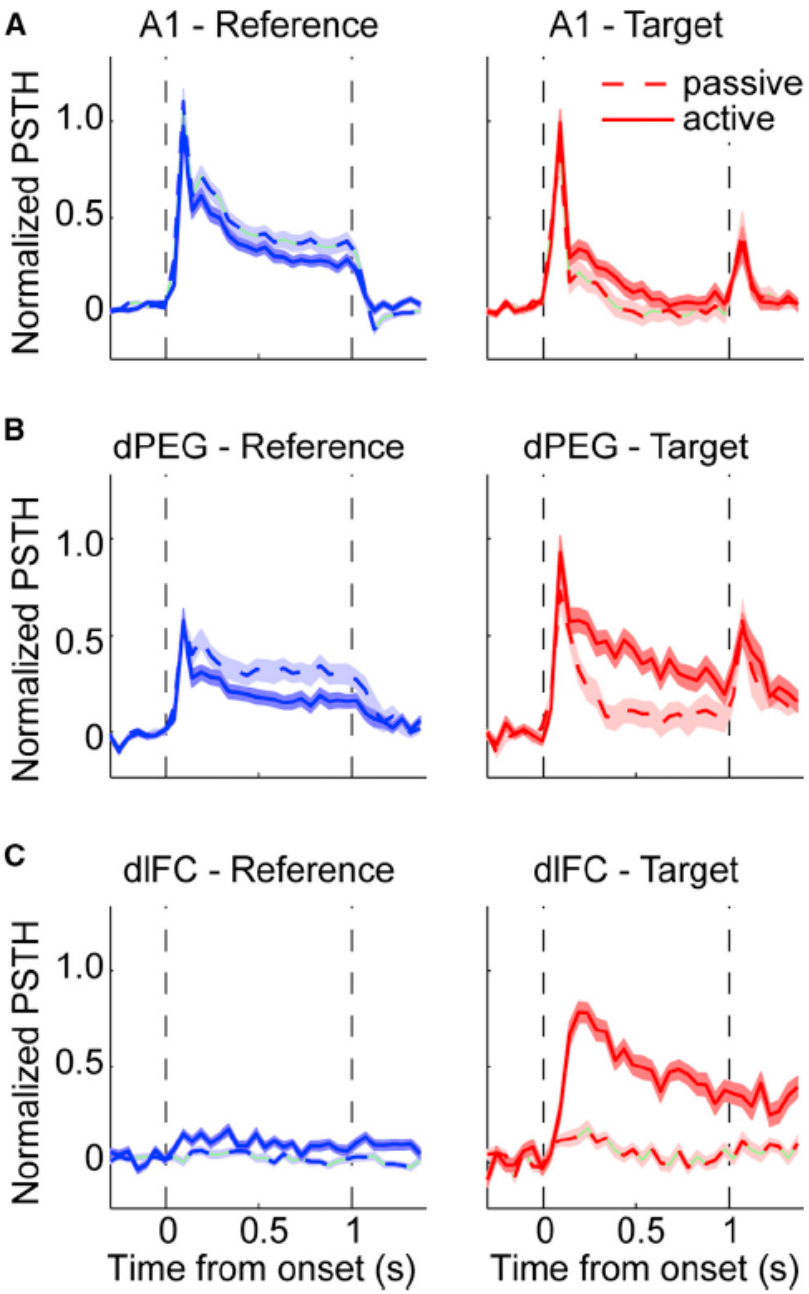


Figure 6: **Target enhancement and behavioral gating along the cortical pathway**
From Atiani et al. [2014] (a) Average behavior-dependent change in reference and target responses in A1. Left panel plots pre-passive (dashed) versus active (solid) normalized PSTH response to reference noise across all neurons that underwent a significant change in evoked response during behavior (n=155 neurons significantly modulated during behavior). The average reference response decreases slightly in these neurons. Right panel compares the average PSTH response to target tones for the same set of A1 neurons. The average target response does not change significantly during behavior. (b) Target and reference PSTH comparison for dPEG, plotted as in a (n=110). In addition to a slightly larger decrease in reference response during behavior in dPEG (right panel) than observed in A1, the average target response also increases in dPEG. (c) Target and reference PSTH comparison for dlFC (n=266). Here both the sign and magnitude of responses has been normalized so that suppression of activity by target or reference, which occurs in about 40% of cells, is plotted as a positive modulation. In dlFC, neurons show consistently very little response during passive listening and respond only to the target during behavior.

**Concept of relevance** Decisions are usually not based on one stream of data. The brain must somehow process the relevant one and filter out others. In animal studies the relevance of a stimulus is dependent on the reinforcement context. Fritz et al. [2010] and later Atiani et al. [2014] have compared the neural activity in multiple cortical areas in a Go/NoGo task in the ferret between 'Reference' (safe sound) and 'Target' (sound paired with a mild electric shock) stimuli. Averaged activity of recorded populations across areas (see Fig. 6, left against right panels) shows a enhancement in target representation compared to reference. Thus illustrating that representation of similar sound class is dependent on the behavioral contingencies.

**Task-engagement** Relevance may also depend on the state of the animal, engaged or not. To come back to the male stickleback example (Tinbergen [1952]), the behavior elicited is dependent on the breeding season. The same stimulus can produce different outcomes. In the Fritz et al. [2010] and follow-up studies, task-engagement effect on stimulus class representation is assessed by recording the same population during passive presentation of the stimulus (before and after behavior). Task-engagement modulates averaged population responses for the target condition in a gradual fashion (for PEG and drastically for FC, see Fig. 6). Together those results indicate behaviorally-gated enhancement of relevant sensory information.

**Gating mechanisms** Neural activity is driven by external output but is also internally regulated (Luczak et al. [2013], Stringer et al. [2018], Marguet and Harris [2011], Harris and Thiele [2011], McGinley et al. [2015b]). Cortical spontaneous activity of the auditory cortex and its synchronization (Luczak et al. [2013]) has been implicated in the shaping of sound-evoked responses. It is currently unclear what that activity represents and its effect on sensory processing, for some it is mere noise, for other it correlates with states and behavior. In Stringer et al. [2018] ~10000 neurons were simultaneously recorded and the analysis suggested that arousal (running speed and pupil area) explained most of the variance in the high-dimensional activity.

**Top-down control** So far we presented a simplistic view of a sensory signal gradually shaped along the cortical hierarchy. It is known that higher order regions such as the PFC project back to sensory areas (Bimbard et al. [2018]) and shape the activity. For example, top-down inputs may be responsible for change in A1 receptive fields (Fritz et al. [2010], Winkowski et al. [2013]).

## Project summary

In the present manuscript, we investigated how the brain tracks complex, ever-changing acoustic scenes to detect embedded target events using a combination of psychophysics, EEG, computational modeling, electrophysiology and pupillometry. For that purpose, we developed a novel paradigm that requires a dual-estimation strategy. Subjects have to estimate baseline of stimulus' statistics while monitoring possible deviation from those statistics. Similarly to Thura and Cisek [2014], the stimulus was continuous and probabilistic. In addition, a reaction time design allowed use to obtain a more precise estimation of the decision process. The multiplicity of techniques allowed us to describe different aspects of noisy, dynamic perceptual decision. Our project is presented in four parts.

**Chapter 2** First we investigated how human listeners detected changes in spectrotemporally broad acoustic textures, as a model for change detection in complex auditory environments. Listeners were presented with a continuous sound, whose statistics change at a random time. We used a combination of psychophysics, EEG and computational modeling to describe underlying neural processes.

**Chapter 3** The second part of the project focused on how subtle but relevant auditory events are selected, extracted and enhanced along the auditory pathway. For that purpose we used extracellular electrophysiology to record the activity of three different cortical areas in the behaving ferret. Similarly to Atiani et al. [2014] and Brincat et al. [2018] we compared the hierarchical representation of sensory inputs and the effect of task-engagement.

**Chapter 4** Once the relevant information is extracted and present in higher cortical region it still needs to be converted into a decision process. In the present chapter we try and ascertain the relationship between FC activity and the behavior. Computational analysis of recordings in FC of the ferret performing the dynamic change detection task allowed us to examine how sensory evidence leads to decision formation.

**Chapter 5** Finally, using the same paradigm we investigated how pupil diameter was influenced by subjects' expectation and subsequent shift in strategy.

# Chapter 2: Detecting changes in dynamic and complex acoustic environments[2]


## Abstract

Natural sounds such as wind or rain, are characterized by the statistical occurrence of their constituents. Despite their complexity, listeners readily detect changes in these contexts. We here address the neural basis of statistical decision-making using a combination of psychophysics, EEG and modeling. In a texture-based, change detection paradigm, human performance and reaction times improved with longer pre-change exposure, consistent with more accurate estimation of the baseline statistics. EEG responses from auditory cortex did not show a response related specifically to the change. Instead, change-locked and decision related responses were found in parietal cortex, scaling with duration of pre-change exposure and consistent with sensory evidence accumulation. A dual time-scale, statistical estimation model successfully accounted for subjects' performance. Furthermore, an auditory cortical model with a decision stage also accounted accurately for performance and reaction times, suggesting that the primary cortical representation requires little post-processing to enable change-detection in complex acoustic environments.


## Introduction

Many natural and environmental sounds are composed of shorter, elementary events, whose occurrence can be described on a statistical level (Lederman [1979], McDermott and Simoncelli [2011], Thoret et al. [2014], Turner and Sahani [2007]). For example, individual drops of water can add together to sound like rain or like a dripping faucet, depending on their number, rate, and relative timing

[2] Boubenec et al. [2017]

(Mcdermott et al. [2013]). However, in real-life, listeners face a dynamic acoustic environment, where statistics do not remain constant for very long. Changes in the statistics of the sound of rustling leaves amidst the sounds of an ongoing storm, or changes in the acoustic composition of a busy cityscape, provide relevant information of putative threats. We investigate here determinants of human performance and their neural representation in these contexts, exploring the hypothesis that the behavior and neural representation are consistent with statistical estimation.

Changes in sound statistics can only be detected if the statistical properties before the change have been estimated sufficiently well (Kaya and Elhilali [2014], Mcdermott et al. [2013]). Without this estimate, the listener cannot distinguish between 'what to ignore' given the current statistics and 'what to recognize' as a change. Moreover, the quality of this estimate can influence the speed and certainty of detection, which are essential in real-life contexts. The present study thus investigates the factors influencing detection of deviations in sound statistics, and where it may be represented in the human brain. For this purpose, listeners are presented with a continuous sound, whose statistics change at a random time. Hence, they are faced with the dual-task of estimating the baseline statistics and detecting a potential change in those statistics at any moment, which mimics real-life challenges.

The estimation of sound statistics depends on many factors, but most importantly on the complexity of a stimulus in relation to the time available to sample it (Kaya and Elhilali [2014]). A simple stimulus, governed by only few parameters, can be reliably estimated more quickly than a complex stimulus. We introduce a statistically controlled stimulus that combines simplicity with broad spectral distribution. In contrast to previous studies with narrow-band complex stimuli (Andreou et al. [2015], Cervantes Constantino et al. [2012], Overath et al. [2010], Teki et al. [2013]), the sounds here form a minimalistic, but well-controlled model for natural, acoustic textures that are only defined by first order statistics. The task for the subjects was to listen to the texture of the stimulus (for a variable pre-change duration), and then to signal the detection of a change in the texture as soon as possible.

We found that detection performance improves with the time available to sample the baseline statistics before the change. As expected, detection performance also depended on the saliency of the change. EEG recordings from the auditory cortex responded strongly to the onset of the sound, but did not exhibit any further responses specifically related to the subsequent change in stimulus statistics. By contrast, EEG responses from the parietal cortex appeared after the time of change, and displayed a build-up rate that depended on the pre-change interval, or the time available to the subjects to sample the stimulus baseline statistics. Performance and reaction times were well predicted by a minimal model of statistical estimation with two time-scales. In addition, a model of auditory cortical processing (Chi et al. [2005], Overath et al. [2008]) augmented with a basic decision stage, could

also account for the EEG responses and subjects' behaviors, thus suggesting that decision-making in such statistically complex acoustic environments may only require minor post-processing (channel-selection and averaging) beyond the primary auditory cortex.

## Materials and Methods

### Participants

In the main psychophysical study, 15 normal hearing subjects (mean age: 24.8y, 6 females) participated, 10 of which could be included for final analysis (see below for criteria). A different set of 8 subjects participated in the combined psychophysics and EEG experiment (mean age: 22y, 4 females), 6 of which could be included for final analysis (see below for criteria). All experiments were performed in accordance with the guidelines of the Helsinki Declaration. The Ethics Committees for Health Sciences at Université Paris Descartes approved the experimental procedures.

### Experimental Setup

**Acoustic Stimulation** Subjects were seated in front of a screen with access to a response box in an acoustically-sealed booth (Industrial Acoustics Company GmbH). Acoustic stimulus presentation and behavioral control were performed using custom written software package in MATLAB (BAPHY, from the Neural Systems Laboratory, University of Maryland, College Park; available upon request). The acoustic stimulus was sampled at 100 kHz, and converted to an analog signal using an IO board (National Instruments, PCIe-6353) before being sent to diotic presentation using high-fidelity headphones (Sennheiser i380, calibrated flat, i.e. ±5 dB, within 100-20000 Hz). Reaction times were measured via a custom-built response box and collected by the same IO card at 1 ms resolution.

**Electroencephalogram (EEG) acquisition** EEG recordings were collected in 6 subjects while listening and subsequently responding to the texture change stimuli. Continuous EEG data were recorded using a 64-channel system (Active Two, Biosemi, Amsterdam) at a sampling rate of 1024 Hz with 2 additional reference electrodes on the mastoids recorded in parallel. In order to standardize electrode placement on the skull, we used default fabric head-caps that hold the electrodes (Electro-Cap International Inc., Eaton). The analysis of EEG responses was carried out offline (see section Data Analysis).

## Stimulus Design & Trial Procedure

We investigated the conditions under which listeners could detect a change in the statistics of complex acoustic stimuli. More specifically, we wondered how subjects capture the percept of a spectrotemporally complex stimulus, and then use it as a background to detect changes relative to it. Concretely, in an experimental trial, we presented a sound texture, allowed the subjects a randomly varying period of time to form a percept of the stimulus (i.e. "estimate the baseline statistics"), and then a change in the frequency distribution of the tones was introduced (while maintaining the overall sound level). After the change, subjects had up to 2 s to indicate that they detected it. The timbre of the stimulus resembled that of a broadband acoustic flicker (see below, Fig.7 and stimulus examples in Supplementary files 2-5), which captures the central textural properties of statistical predictability and complex spectrotemporal structure. Both the stimulus design and the procedure are described in detail below.

### Stimulus Design

In brief, the stimulus was a 'cloud' of tones, i.e. a train of short pure tones chords (30 ms) drawn from a range of 2.2 octaves (400 to 1840 Hz), where the occurrence probability of each tone was governed by a marginal distribution (see below, Fig. 7). The frequency resolution of the tone distribution was 12 semitones per octave, i.e. 26 logarithmically spaces pure tones covered the used frequency range. To limit the number of experimental conditions, these were grouped into 8 spectral bins, each comprising 3-4 of the pure tone frequencies (see Fig. 7 for illustration). The marginal distribution was chosen to ensure that the actual rate of tones per bin was controlled, independent of the number of pure tone frequencies constituting the bin. The entire stimulus can be described by a spectrogram denoted by S(t,f) as a function of time and frequency.

The minimal temporal unit of the stimulus was a 30 ms chord, i.e. a synchronous presentation of multiple pure tones. The number of tones for each chord was drawn from a Poisson distribution with a fixed mean of 2 tones per octave. The mean number of tones per chord was kept fixed as a function of time to avoid changes in level (see below). The frequency of each tone in a chord was chosen in two successive steps: First, one of the 8 spectral bins was selected according to a marginal probability distribution (see below). Second, within this bin, one of the pure tone frequencies constituting the bin was randomly selected. Chords at different times were drawn independently from each other.

The baseline marginal probability distribution was composed of 8 frequency bins with discrete probability values (Fig. 7A, left). These values were chosen pseudo-randomly for each trial, forcing subjects to always reestimate the stimulus statistics. The probability in each bin could take one of 3 values: 0.083, 0.125, 0.188. To avoid differences in spectral density, the number of bins with each probabil-

ities was fixed to 3 bins with P=0.083, 2 bins with P=0.125 and 3 bins with P=0.188. The marginal distribution is thus normalized, i.e. the sum across bins equals 1. Since multiple pure tone frequencies constituted each of the 8 bins, the probability per pure tone frequency bin was correspondingly lower: based on this marginal distribution and the number of tones per chord, the effective probability of a tone falling in a pure tone frequency bin thus ranges between 0.021-0.063 per chord duration, corresponding to an average rate of ~147 tones / s.

The change in statistics consisted in a change in the baseline marginal distribution. Two out of the 8 spectral bins were increased in probability at a random point in time (referred to as change time, more details below) during stimulus presentation, i.e. the stimulus continued uninterrupted. The increment size will be referred to as change size and was drawn from a set of discrete values: 30, 50, 80, 110, 140 % (inset in Fig. 8A), relative to the single bin probability in a uniform distribution (for 8 bins this is 0.125, i.e. a 50 % change size would be an increment of 0.0625). In order to exclude cues from global level changes, the marginal distribution was simultaneously renormalized, thus keeping the global level constant within a trial (i.e. as mentioned above the rate of tones per chord was kept constant at all times). Since the 30 % condition was only collected for 3 subjects, it is omitted from most plots, although results were generally consistent with the other conditions.

The relative spectral locations of the 2 changed bins were separated into two conditions:

(1) Localized: the frequency bins containing the change were adjacent. To limit the number of conditions, only 4 pairs of bins, {1,2}, {3,4}, {5,6}, {7,8} were tested at all increment levels.

(2) Non-localized: the frequency bins containing the change were separated in frequency. To limit the number of conditions, we chose a subset of distances (D=[2, 3, 5, 7] bins, i.e. [6.6, 9.9, 16.5, 23.1] semitones (st)) and only used the change size 110 % (determined as intermediate difficulty from pilot studies). Since certain inter-bin distances are more frequent (i.e. 6 for D=2, 5 for D=3, 3 for D=5, 1 for D=7), the number of trials going into each distance differs, which scales the error bars accordingly (see Fig. 10B).

The time at which the change occurred (change time) was drawn randomly from an exponential distribution (mean: 3.2 s) limited to the interval of [0,8] s (Fig. 7B). This choice of distribution prevents subjects from developing a timing strategy, by keeping the probability of a change constant over time. The associated flat hazard rate minimizes participants' ability to anticipate the end of the trial (Janssen and Shadlen [2005], Kiani et al. [2008]). The change time is an important parameter with respect to the estimation of the first marginal distribution, with the hypothesis that greater change times improve detection of changes.

Given the slow range of rates (see above), individual tones remained distinguishable. Hence, the

density was low enough to avoid fusion into a single stream per channel, although the present study still has some parallels with previous paradigms, e.g. spectral shape analysis (Green et al. [1992], Green [1988], Green and Berg [1991]) (see Discussion).

**Procedure**

The experiment proceeded in three phases: instruction, training, and main experiment. After reading the instructions, subjects went through 10 minutes (60 trials) of training, where they were required to obtain at least a detection performance of 40 %. The training comprised only stimuli of the two largest change sizes (110 %, 140 %). Three subjects did not attain the criterion level of performance and were not tested further.

The main experiment was composed of two sessions of about 70 min each, comprising a total of 930 trials. The two sessions were never more than two days apart. Each session contained three blocks of about 20 min, for a total of 465 trials per session, corresponding to 30 repetitions of each condition (for the 3 subjects in which the 30 % condition was tested the total trial number increased to 1050). In between blocks subjects could take a short break.

The instructions specified that subjects would be compensated according to their performance, although an easily attainable threshold of proficiency would give them the maximal compensation. Upon reaching this threshold, all subjects were compensated equally according to the length of the experiment (10euros/hour).

After reading the instructions, subjects were aware that the change could arise at any moment on each trial and that their task was to detect it within a 2 s window. Following the change, the second stimulus continued for a maximum of 2 s. When subjects heard a change, they pressed a response button. This terminated the trial and the sound. Hence, the subject had up to 2 s after the change to detect the change in stimulus statistics.

Visual feedback was always displayed on a screen in front of them after the trial. A red square was displayed, if the button was pressed before the change (false alarm), or if the button was not pressed within the 2 s time window after the change (miss). A green square was displayed, if the button was pressed after the change, but within the 2 s window (hit).

In addition, stimulus level was roved from trial to trial, chosen randomly between 60 and 80 dB SPL. This procedure is classically applied to prevent subjects from adopting an absolute level strategy (Green and Berg [1991]). Overall level was not found to significantly influence performance ($p=0.89$, ANOVA). The inter-trial interval was ~1 s with a small, random jitter (<0.1 s) depending on computer load.

### Psychophysics procedure during EEG recordings

During the EEG recordings, stimuli and experimental procedures identical to those of the psychophysics experiments were used. In addition, subjects were required to continuously fixate a white cross on the screen. They were asked not to blink and to keep fixation especially during the sound presentation. After the end of the trial (i.e. either the end of the sound or their response), they received a visual text feedback after 0.5 s. After the feedback disappeared, eye blinks were allowed during the intertrial interval indicated by on-screen text underneath the fixation cross. At 1 s before the next stimulus, the text disappeared, indicating that blinking should be prevented subsequently.

## Data Analysis

The ability of the subjects to detect the change in stimulus statistics was quantified using two measures, performance and d-prime, denoted d'. These analyses were performed on the data obtained during the psychophysics experiments, and restrained to the trials embedding localized changes unless stated in the text. In addition, reaction times dependences over stimulus parameters were analyzed.

### Performance

We computed a subject's performance as the fraction between successful detection (hits) out of the total trials for which the change occurred before the response (hits + misses). False alarms were excluded from the performance computation, since the responses occurred before the change arose (see d' for an inclusion of false alarms).

### d' Analysis

We developed a time-dependent d' measure, in which longer trials serve as catch trials before the change occurs (Green and Swets [1966]). We computed d' values to assess the ability to detect changes (Egan et al. [1961]), while taking their false alarm rate into account, as classically analyzed using signal detection theory. Due to the present task structure, d' could be computed as a continuous function of time from stimulus onset. We used the usual approximation $d'(t) = Z(HR(t)) - Z(FAR(t))$, where Z(p) is the inverse of the Gaussian cumulative distribution function (CDF). HR(t) is the hit rate as a function of time since stimulus onset. HR was computed as the fraction of correct change detections, in relation to the number of trials with changes occurring at t (Macmillan and Creelman [2005]). As detailed above, a correct detection had to occur within 2 s of the change time (Fig. 7D). Similarly,

the false alarm rate FAR(t) was computed as the number of false alarms that occurred over all 2 s windows (starting at t), in which no change in statistics occurred. This brought an artificial reaction time for each false alarm, that we used for comparing the distributions of the actual reaction times resulting from the Hits (Yin et al. [2010]). d' was computed for different times and change sizes, yielding only a limited number of trials per condition. To avoid degenerate cases (i.e. d' would be infinite for perfect scores), the analysis was not performed separately by subject, but over the pooled data. Confidence bounds (95 %) were then estimated by bootstrapping within the dataset. The analysis was verified on surrogate data from a random responder (binomial with p=0.01 per time bin at 40Hz sampling rate), providing d' close to 0 as expected.

**Reaction Times**

We obtained reaction times by subtracting the change time from the response time in each hit trial. For each condition, the distribution of reaction times was assembled and the median reaction time computed. Note that very early and late reaction times will in some cases not correspond to actual reaction to the change in statistics, but are coincidental, which can, however, not be distinguished on a trial-by-trial level. The results presented for the effect of change size on performance and reaction time were computed using only the data with change in contiguous bins (localized change). Results for the trials with non-localized bins (at 110 % change size) were qualitatively the same, however, they were excluded from this analysis to keep the number of trials per condition equal.
These measures were computed as a function of change size and change time. While change times were drawn without binning from an exponential distribution for the experiment, they were binned for analysis using bins of exponentially increasing width (in order to achieve comparable numbers of trials in each bin).

**Performance Dynamics**

In order to compare the performance dynamics for different change sizes, we fitted an adapted version of the Erlang CDF to the data according to:

$$P(\Delta_c, t_c) = P_0(\Delta_c) + P_{max}(\Delta_c) * \gamma(k, tc/\tau(\Delta c))/(k-1)!$$

where $t_c$ is change time,$\Delta_c$ change size, $\gamma$ the incomplete gamma function, $\tau$ the function rate, and $k$ controls the function shape. $k$ was kept constant across subjects and change sizes, assuming the shape of the performance curves is invariant. Optimizations were performed using nonlinear least-squares minimization on the residuals of the fit (via "lsqnonlin" in Matlab).

To control for inattentive subjects, we set a 30 % threshold for the total false alarm rate. Two subjects were discarded according to this criterion leaving a total of 10 subjects for the data analysis, with false alarm rates below 25 %.

**Analysis of EEG Recordings**

We analyzed two signals based on the EEG: the classical auditory event-related potential (ERP), and the centro-parietal positive potential (CPP). First, slow trends were removed from all electrodes using a low-dimensional polynomial fit ("nt_detrend", from the NoiseTools Matlab toolbox by de Cheveigné and Parra [2014]). All trials with at least one scalp channel exceeding 500 μV at any time after referencing were discarded. Two of the subjects had a high rate of blinks and eye movements and had to be excluded, leaving 6 subjects for final analysis.

Classical auditory ERPs were estimated as the average of a set of medial electrodes (C1, Cz, C2, FC1, FCz, FC2; Nie et al., 2014). All electrodes were referenced to the average mastoid potential. EEG data were segmented into epochs locked on stimulus onset or change time. The epochs were then baseline-corrected relative to the 150 ms interval prior to their starting point.

The CPP signal was based on a set of parieto-occipital electrodes (POz,Oz,Pz, similar to Twomey et al., 2015). Electrodes were low-pass filtered below 30 Hz with a 45th order Chebyshev filter using the "filtfilt" function in MATLAB to avoid phase distortion. In addition, all electrodes were referenced to the common average of all electrodes and then normalized by the standard deviation over time and electrodes of interest. Trials were then extracted in the period encompassing 0.5 s before and 3 s after the sound presentation and time-shifted to their corresponding change times. Individual trials were baseline corrected using a time window of 400 ms before the change. Topographic distributions of the EEG signal were plotted with EEGLAB ("topoplot" function) (Delorme and Makeig [2004]).

Post-change buildup rates of CPP activity were compared across conditions with an analysis of covariance (ANCOVA) where time was the continuous variable, change time and trial type the categorical independent variables (in total 6 categories with 3 sound durations [2.75, 3.6, 5 s] and 2 types of trials, catch and signal). As the activity from these electrodes reached a plateau for the condition with change times of 3 s, only the first second after the change was considered for the 2 conditions where the trial lasted 5 s. The full post-change period (0-2 s) was taken into account for the other experimental conditions.

The neural generators of both onset and change activity were estimated using dipole source localization. Preceding the source analysis, data was filtered 0.3 - 30 Hz, downsampled to 128 Hz and artifact rejected based on the threshold level (+/-100 μV), abnormal trends (max slope of 150 μV) in EEGLAB

(Delorme et al. [2011]). Next, eye movements and abnormal activity were identified using a blind source separation algorithm (ICA). In order to localize equivalent independent components (ICs) we used the DIPFIT2 plugin (Oostenveld et al. [2011]) based on a Montreal Neurological Institute (MNI) template head model. The localization of the neural generators was performed separately for the onset- ([0,400] ms) and change-locked ([0,2000] ms after the change) activity. In both cases, ICs whose residual variance (RV) of dipole location was greater than 15% were rejected (Hammon et al. [2008]). Due to the binaural auditory stimulation, we additionally checked for symmetrical components. In order to group functionally similar ICs, k-means clustering was performed based on auditory ERPs, scalp maps and dipole locations. The initial number of clusters (k) to be searched was 15, but further inspection indicated 6 clusters for onset and 5 for change condition, while the threshold level for outliers was always 2.5. Finally, Talairach coordinates of independent components and their centroids were computed (Lancaster et al. [2000]). Some of the estimated dipoles were located around midline, an effect that was already observed previously for auditory stimulation (e.g. Wisniewski et al. [2014]). We therefore report only dorso-lateral and anterior-posterior coordinates.

### Dual Timescale Model

We assume that subjects continuously estimate a wide range of statistical properties of the acoustic environment, and are able to detect unexpected deviations in these properties for the purpose of detecting changes in the ongoing sound. Among these properties are the probabilities of having a tone in the different frequency channels. Since these are the only determining properties in our stimulus design, we developed a phenomenological model, which estimates and detects changes in the marginal tone probabilities across multiple frequency channels (see next section for a more biologically motivated model based on a cortical filter-bank).

The model consists of change-detector modules, which operate independently on a limited spectral range and whose output is combined to enable change-detection on a full spectrum. For simplicity, the spectral division of the modules was matched to the presently relevant division of the psychophysical stimulus $S(t, f)$ (see above), i.e. we here consider 4 modules, one for each pair of frequency bins, whose marginal probability could change. Since the modules operate independently, frequency separation is not relevant in the present model (but see below in the cortical model). For the present model, these frequency bins are referred to as $S_i(t)$ (with i[1,4]), which contain a random set of tones, adhering to the same marginal probabilities as the psychophysical stimulus.

For each frequency bin $S_i(t)$, a pair of dynamical processes $P_{slow}(t), P_{fast}(t)_i$, acts as a change detector. $P_{slow}$ estimates the long-term probability of the presence of a tone at a given time in $S_i(t)$,

and $P_{slow,i}$ estimates the more recent probability of the presence of a tone in $S_i(t)$. The dynamics of the processes are given by:

$$\frac{dP_{fast,i}(t)}{dt} = -\frac{P_{fast,i} - S_i(t)}{\tau_f}$$
$$\frac{dP_{slow,i}(t)}{dt} = -\frac{P_{slow,i} - S_i(t)}{\tau_s}$$

where $\tau_s > \tau_f$, which separates the speed of the processes. Normally, $P_{fast,i}$ and $P_{slow,i}$ are going to have similar values, since $P_{fast,i}$ is simply tracking faster than $P_{slow,i}$. However, if a change in the probability of occurrence occurs in the stimulus, the difference between the two processes will grow, since $P_{fast,i}$ will react faster to this change. A change in the environmental statistics is hence detected, if $|P_{fast,i} - P_{slow,i}| > T$, where T is a threshold and a free variable of the model. Identical models exist for different frequency channels $S_i(t)$. If T is exceeded in a particular $S_i(t)$, this is considered as a detected change in the environment at the corresponding time $T_i$. Hence, only the first detected change in any $S_i$ is recorded as the response. The time of actual response is then given by $T = T_i + T_m$ , where $T_m$ is a constant time equals to 250 ms to account for the non-integration related process, such as stimulus representation and motor execution, up to the button press (akin to the non-decision time, by Ratcliff and McKoon [2008]). The model is termed a dual time-scale model.

If we use the model as described so far, it would - correctly - detect a change in statistics at the onset of the stimulus (transition from silence to stimulus). In the present task design, the subjects were instructed to ignore the change associated with the start of the stimulus, but only detect the change in statistics within the stimulus. As laid out in the introduction, two estimations needed to be performed simultaneously: (1) estimate the probability from stimulus onset, (2) compare this estimate to the changed probability in the latter part of the stimulus (which occurs at an unknown time). To account for this initial period of estimation, we change the dynamics of $P_{slow}$ (the slower tracking process) as a function of stimulus time. Intuitively this means that $P_{slow}$ and $P_{fast}$ initially operate on the same time scales, and thus Θ is never exceeded. The modified equations therefore become

$$\frac{dP_{fast,i}(t)}{dt} = -\frac{P_{fast,i} - S_i(t)}{\tau_f}$$
$$\frac{dP_{slow,i}(t)}{dt} = -\frac{P_{slow,i} - S_i(t)}{\theta(t)}$$
$$\theta(t) = -(\tau_s - \tau_f)e^{-t/\tau_a}$$

The speed at which the tracking dynamics diverge is regulated by $\tau_a$. Overall, the model has 4 free parameters (T, $\tau_f$, $\tau_s$, $\tau_a$), which were matched to account for the experimentally collected data. The phenomenological model accounted for the dependence of performance on change time. Simulations were run at a sampling rate of 100 Hz. Fitting was performed by exhaustive search in the parameter space to avoid local minima and biasing by initial values.

The model structure is inspired by earlier accounts for decision-making in random-dot motion stimuli, i.e. so-called drift-diffusion models (Bogacz et al. [2006], Britten et al. [1996]), which have also recently been used to account for acoustic click-rate comparison tasks (Brunton et al. [2013]). In contrast to these models, the dynamical process $P_{slow}$ in our case becomes an estimate of the medium-term occurrence probability, and $P_{fast}$ an estimate of the recent occurrence probability, and a decision is made across the set of estimators (similar to Churchland et al. [2008]) Note, that the processes can transiently exceed 1, however, on average the right hand side of the dynamical equations is zero, when the dynamical process equals the probability that Si is drawn from.

## Auditory Multiresolution Cortical Model

The cortical model is an approximation to the analysis performed up to primary auditory cortex, which has been used successfully in a range of different auditory projects. A full description of the model can be found in Chi et al. [2005], Yang et al. [1992], but an outline of its basic principles is provided below.

### Computational structure of the cortical model

The cortical model processes the audio signal via two stages, inspired by the auditory pathway up to the midbrain and by the primary auditory cortex. The first stage transforms the sound into an auditory spectrogram, and the second performs a spectrotemporal analysis on this spectrogram.

The processing of the acoustic signal in the cochlea is modelled as a bank of 128 constant-Q, asymmetric bandpass filters, equally spaced on the logarithmic frequency scale spanning 5.3 octaves. The cochlear output is then transduced into inner hair cell potentials via a high-pass and low-pass operation. The resulting auditory nerve signals undergo further spectral sharpening via a lateral inhibitory network. Finally, a midbrain model resulting in additional loss in phase locking is performed using short term integration with time constant of 4 ms, resulting in a time-frequency representation (the auditory spectrogram $z(t, f)$) (top panel in Fig. 14A). The central stage further analyzes the spectrotemporal content of the auditory spectrogram using a bank of modulation selective filters centered at each frequency along the tonotopic axis, mimicking neurophysiological receptive fields. This step

corresponds to a 2D affine wavelet transform, with a spectrotemporal mother wavelet, defined as a Gabor-shape in frequency and exponential in time. Each filter h is tuned (Q=1) to a specific rate (ω in Hz) of temporal modulations and a specific scale of spectral modulations (Ω in cycles/octave), and a bidirectional orientation (+ for upward and - for downward). The response of each cortical filter in the model is given by

$$r\pm(t, f; \omega, \Omega; \Theta, \Phi) = z(t, f) *_{t,f} h\pm(t, f; \omega, \Omega; \Theta, \Phi)$$

where $*_{t,f}$ denotes convolution in time and frequency and $\Theta$ and $\Phi$ are the characteristic phases of the cortical filter, which determine the degree of asymmetry in the time and frequency axes respectively (middle panel in Fig. 14A). Because changes were isotropic within the sound spectrum, we averaged the upward and downward components of the scale modulation filter. To simplify the analysis, we limited our computations to the real cortical outputs across frequency (i.e. responses corresponding to zero-phase filters). The resulting modulation response is denoted R(t;ω,Ω) (bottom panel in Fig. 14A). Simulations were run at a sampling rate of 100 Hz.

**Decision process based on the cortical model output**

On a single trial basis, the stochastic nature of the stimulus was reflected in the noisy outputs of the cortical model. To facilitate change detection on single trials, we post-filtered the modulation response R(t;ω,Ω) using the average response to a change in statistics. Concretely, the shape of the trial-averaged response in R(t;ω,Ω) was convolved with single trials, to improve detection of change. Due to the different modulation rates, the length of the average response shape varied by modulation rate ω as 1/(2ω) ms. An unique combination of rate ω and scale Ω was used across all trials to characterize the modulation response. Next, we implemented a decision criterion on top of the filtered R(t;ω,Ω). Due to the comparative nature of the present paradigm and because the onset peak was not driven by any task-relevant feature of the sound, a time-dependent decision boundary was better suited to match the experimentally observed reaction times in both models. This was inspired by previous studies that described either time-varying collapsing boundaries (Ditterich [2006]) or linearly increasing emergency-related gain (Cisek et al. [2009], Drugowitsch et al. [2012]). We designed the time-dependent threshold as follows:

$$T(t) = be^{-t/\lambda} + a$$

where a and b scales the amplitude of the threshold and λ sets its time-dependence. The first peak exceeding the time-dependent threshold was labelled as the decision timing.

In total, the decision stage is controlled by five parameters: the time-varying threshold (λ, a, b), the scale Ω, and the rate ω, while other parameters of the cortical model were kept fixed. The threshold parameters tune the balance between conservative and liberal decisions. To take into account this aspect we fitted both performance and false alarm rate across all subjects for all change sizes and change times. Motor-related delay was accounted for by a 250 ms offset added to the estimated reaction times, as was done for the phenomenological model.

### Statistical Analysis

If not specified otherwise, nonparametric tests were used. When data were normally distributed (for performance), we checked that statistical conclusions were the same. One-way analysis of variance was computed with the Kruskal-Wallis' test; two-way using Friedman's test. Error bars are ±2 SEM (standard error of the mean), unless specified otherwise. Significance of EEG signals over multiple time-steps was assessed using the FDR algorithm by Benjamini and Hochberg [1995], which includes appropriate corrections for multiple comparison testing. Post-hoc pairwise multiple comparisons between buildup rates were assessed using Bonferroni correction. All statistical analysis was performed using Matlab (The Mathworks, Natick).

## Results

We investigated the neural mechanisms of detecting changes in the statistics of auditory stimuli, on the basis of human behavioral performance, neural response and their underlying mechanisms. In a set of psychoacoustic experiments, listeners were presented with complex acoustic stimuli, whose statistics could change at a random time. Several parameters of the change were varied in order to estimate their influence on the change's saliency. In a subset of listeners EEG responses were collected to localize the first stage in the brain where the neural response reflects the change in statistics. We propose a simple model to account for the listener's behavior, which is based on the estimation of stimulus statistics on two time-scales. Finally, we suggest a neural implementation of this principle based on a model of auditory cortical processing.

### Detection of changes in statistics is consistent with estimation of marginal distribution

The ability to detect a change in stimulus statistics improved in trials that provided more time before the change ("change time" in Fig. 7A) for subjects to listen to the baseline statistics of the texture. Performance also increased monotonically to different asymptotic levels for the four tested change

sizes (50, 80, 110, 140 %, Fig. 8A). Asymptotic performance depended on change size, with bigger changes in marginal probability leading to greater asymptotic performance especially between levels, from 50 % to 95 % (Fig. 8A, $p_{size} < 10^{-5}$, Friedman; $p_{time} < 10^{-5}$, Friedman). Change size also influenced the shape of dependence on change time, such that greater change sizes led to improved performance at shorter change times than for smaller change sizes (Fig. 8A). This translates to a combined steepening and leftward shift of the performance curves with change size. The significance of this effect was assessed by fitting the performance curves for individual subjects with a parametric function of sigmoidal shape (an Erlang CDF, see Methods) in order to extract the change size-dependent time constant (Fig. 8B). The characteristic time constant $\tau$ decreased significantly as a function of change size (8B; $p < 10^{-6}$, Kruskal-Wallis).

Alternatively, the observed performance could be explained by a timing strategy or a pattern recognition strategy. Both of these explanations can be rejected based on the data and the paradigm: if subjects had used a timing strategy, their instantaneous false alarm rate (as a function of change time) should never reach a constant value, which is not observed (Fig. 8D). Instead, the false alarm rate exhibits an initial linear increase, followed by a constant false alarm rate per unit time (embodied in the behavior of the models; see Fig. 13E/14F). Furthermore, the initial rising portion of the false alarm rate is a consequence of the dual estimation task design. The uniform regime of false alarm rate is consistent with the use of an exponential distribution of change times, which keeps the change occurrence probability constant per unit of time (see Fig. 7B and Methods).

Some subjects could have attempted to use a pattern recognition strategy, i.e. effectively ignoring the statistics of the first stimulus. However, based on the stimulus design, a pattern recognition strategy would have failed, since the first stimulus was drawn randomly for each trial, and the second statistic was a stochastic modification of the first. Furthermore, detection performance would not have depended on change time. Therefore, altogether, these results are inconsistent with both a pattern recognition or a timing strategy.

Using the time-dependent false-alarm rate, the sensitivity of the subjects to detect a change can be analyzed with a time-dependent d' (see Fig. 7D and Methods for details of computing this d'). This analysis exhibited similar monotonically increasing shapes as a function of both change time and size (Fig. 8C). Further, probability in a frequency bin was positively correlated with change detection (Fig. 15), consistent with the idea that a high rates of samples provided a better estimate of the probability value in a frequency bin. We can rule out that only large probability bins were attended to, since the performance for equal size chances in large probability bins is dominated by the change in other, lower probability bins (Fig. 16). Finally, larger stimulus duration in the current trial predicted a reduced

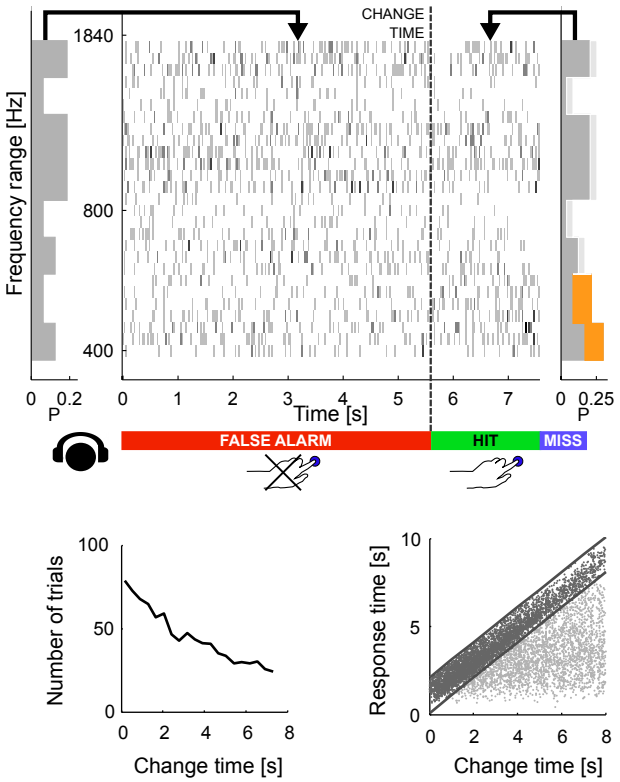


Figure 7: **Dynamical change-detection paradigm with auditory textures.**
(A) Subjects listened to an acoustic textural stimulus, whose predictability was governed by its marginal frequency distribution (grey curve, left panel). Tones in individual frequency bins were drawn independently consistent with the marginal (middle panel). Listeners were instructed to report changes by a button press. The frequency marginal was modified (indicated in orange in the right panel distribution) after a randomly chosen point in time ('change time'). The probabilities in two adjacent or non-adjacent frequency bins were increased together, and the distribution over the bins renormalized to maintain average global level. (B) The distribution of change times was chosen from an exponential distribution. This ensured that the probability of a change in the next time-bin remained constant (shown here is the empirical distribution). (C) Response times occurred before (false alarms) and after the change time (hits). Subjects usually responded only after an initial listening duration, allowing them to acquire the sound statistics.

performance in the following trial (Fig. 17), suggesting that the converged estimate in the previous trial could 'contaminate' the estimation process in the subsequent trial. This is another indication that subjects were not using a pattern recognition strategy, since such a strategy completely ignores the statistics presented in the previous trial.

In summary, those findings indicate that change detection (i) improves with time allowed to sample the stimulus, (ii) improves with the size of the change and (iii) saturates with longer observation intervals. These properties are consistent with statistical decision-making, where a decision can only be made if the observed change in a stimulus property is substantial compared to the current uncertainty about the same property. Subjects using statistical decision making can (i) reduce their uncertainty by collecting more stimulus information over time, (ii) use larger differences in the stimulus property to overcome the uncertainty more rapidly, and (iii) will not be able to improve their performance once the estimation of the stimulus statistics has saturated.

### Reaction times are consistent with statistical estimation

The dependence of performance on change time suggests a dynamical mechanism performing an on-going estimation of the initial statistics. To gain insights into these dynamics, we examined the dependence of reaction times on the parameters of the change, especially its size, which intuitively correlates inversely with task difficulty according to Piéron's law (Pins and Bonnet [1996]) and time of occurrence (or "change time").

Reaction time distributions changed both in duration and shape as a function of change size (Fig. 9A). Median reaction time decreased with larger change sizes ($p< 10^{-3}$; Kruskal-Wallis, Fig. 9B), in accordance with the increase in performance with larger change sizes. Receiver operating curve (ROC)-based analysis indicated that the distributions of reaction times were different across change sizes and chance level (Fig. 18; $p< 10^{-7}$; Friedman). More specifically we found a significant difference between the most difficult condition and chance level ($p< 10^{-5}$; Kruskal-Wallis), confirming that subjects were performing the task at all change sizes. This suggests that the time necessary to detect the deviation between the pre- and post-change stimulus statistics was reduced for larger change sizes.

For shorter change times, reaction time distribution changed in a qualitatively similar manner than what was observed for smaller change sizes, although the effect was less pronounced (Fig. 9C). Median reaction times decreased with change times, mirroring dependence of performance on change times ($p< 10^{-5}$; Kruskal-Wallis, Fig. 9D). This dependence can already be seen in the raw data (Fig.

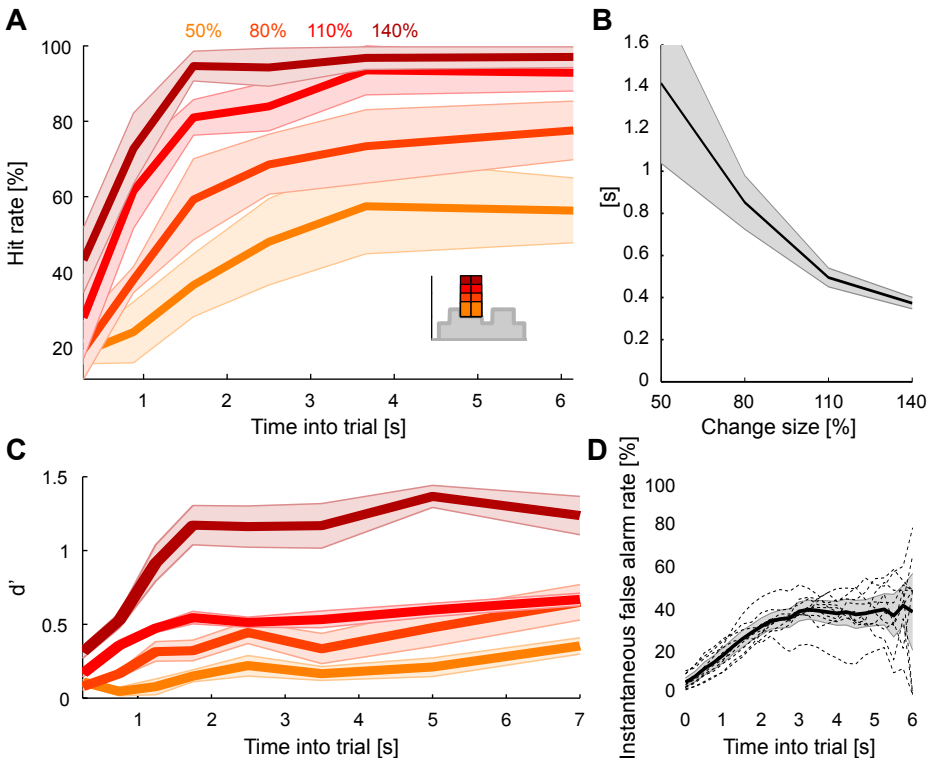


Figure 8: **Detecting a change in statistics improves with size and time of change.**
(A) Performance of change detection depended significantly on change time (abscissa) and change size (shades of orange indicate the step size as percent of the original bin probability, see inset). Only changes in contiguous bins were used presently, to maintain identical trial numbers across difficulties. (B) The dynamics of the performance curve varied with change size, indicated by the speed parameter t of an Erlang CDF fitted to the data (see Materials and methods). (C) Dynamical d' confirms the dependence of performance on change time and change size. The dependence on change time suggests an improved detection relying on a converged estimate of the baseline statistics, whereas the dependence on change size indicates a higher level of certainty can be attained more rapidly if the amount of evidence is larger. (D) Instantaneous false alarm rate is uniform across time, after an initial hesitation to respond in the first 2 s. The initial hesitation is likely due to the task-design, requiring an initial estimation of the sound statistics.

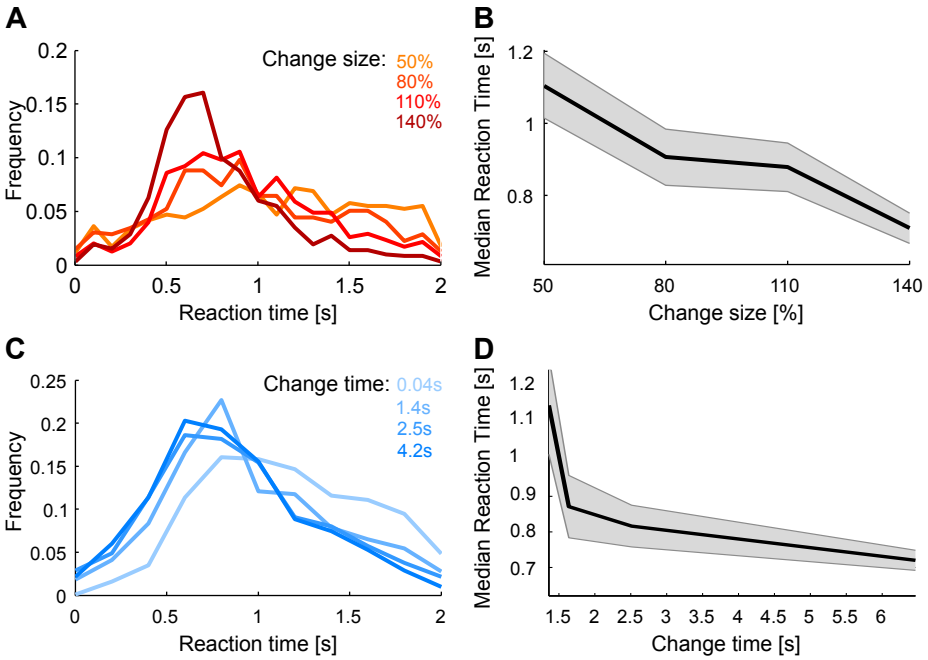


Figure 9: **Reaction times also reflect estimation of pre- and post-change stimulus properties** (A) Reaction time distribution sharpens with change size. (B) Median response time significantly reduces by 20% ($p < 10^{-4}$ , Kruskal- Wallis) with larger change size (different colors indicate different change sizes). These effects indicate a faster, temporally more constrained decision, which could indicate more rapid evidence accumulation for larger changes. (C) Reaction time distribution sharpens with change time and D) median reaction time reduces rapidly with change time by 25% ($p < 10^{-5}$ , Kruskal-Wallis). Both effects indicate a higher degree of certainty in decision making, which could indicate a more converged estimation of the pre-change statistics.

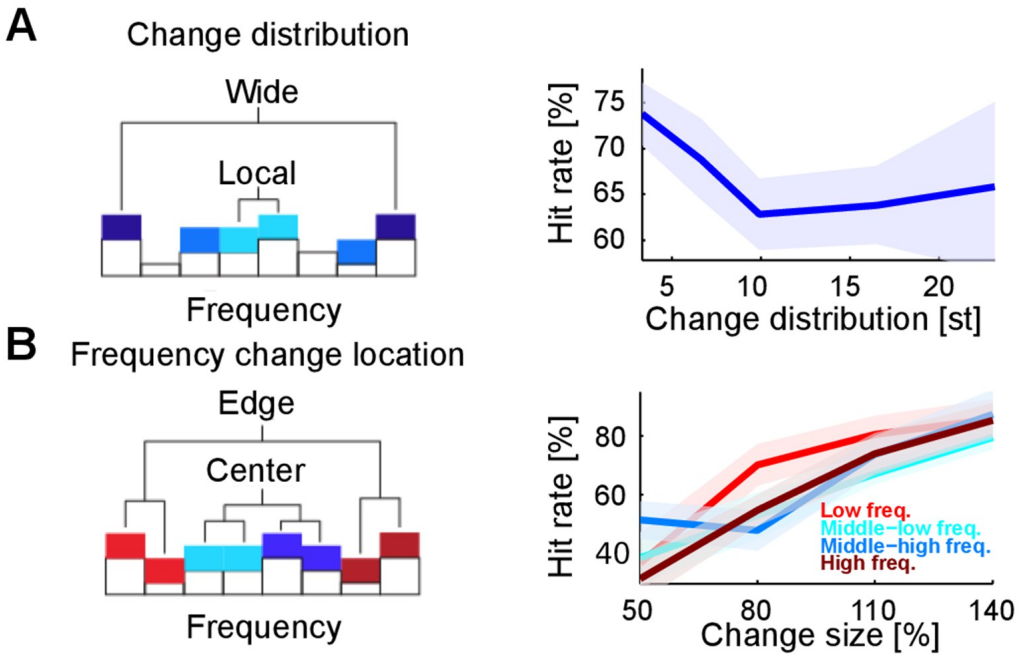


Figure 10: **Detectability of changes depends on spectral properties of the change.**
(A) Spectral distance between the changed bin centers ('change distribution', measured in semitones, st) significantly reduces performance (p=0.01, Kruskal-Wallis test). Spectral distance ranged from neighboring (three st) bin centers to locations at the edges of the tested range (23 st). (B) Absolute spectral position of the changed bins does not influence performance (p=0.85, Kruskal-Wallis). Absolute spectral position was not significantly correlated with the detectability.

7C), where hit trials (black) for longer change times exhibited shorter reaction times. Again the timing of the first correct responses decreased correspondingly with longer change time, suggesting more accurate estimation of the initial statistics.

## Dependence on spectral location of acoustic change

Changes in stimulus statistics are effectively a redistribution of the stimulus energy in the spectral (frequency) domain. Therefore, we hypothesized that a detection process acting in a spectrally localized manner should perform better when the total energy of the change is concentrated in a restricted frequency region. Indeed, we found that performance decreased for non-localized changes when compared with localized ones (Fig. 10A). This effect was significant only when distances below and above 8 semitones were grouped (Fig. 10A; $p < 5.10^{-3}$). Finally, we found that performance did not vary as a function of relative position along the frequency axis (p=0.28; Fig. 10B), contrary to the predictions of a recent study (Catz and Noreña [2013]) showing that cortical representation at the extreme edges of the stimulus spectrum could be enhanced for sharp contrast, resulting in lower change detection thresholds.

## EEG responses correlate with accumulation of sensory evidence

We collected neural responses using electroencephalography (EEG) in human subjects performing the above psychoacoustic task to study the relationship between behavioral performance and neural responses, and to narrow down the scalp regions whose neural response reflects the change in sta- tistics. The analysis was focused on a subset of the recording electrodes, namely an auditory (central location, El.1; corresponding to the center in Nie et al. [2014]) and a centro-parietal (14,27,28; corresponding to Twomey et al. [2015]) set. Depicted potentials show averages across each set of elec- trodes. Subjects exhibited similar performance and reaction time dependencies on change time as in the psychophysical experiments (Figure 19). Change times were binned into four bins based on their distribution and Hit rate to equalize trials per bin.

At stimulus onset, the average auditory potential exhibited a classical, large and rapid event- related potential (ERP) (Figure 11A,C, composed of N1 and P2), followed by a negative sustainedpotential (indicated as NS in the figure) previously described for prolonged stimulus duration (Hari et al. [1980], Lammertmann and Lütkenhöner [2001], Lütkenhöner et al. [2011]). However, there was no system- atic evidence for a response to the change in statistics (Figure 11B1, EEG of Hit trials aligned to change times). EEG aligned to subjects' response time also did not show a signifi- cant response (Figure 11B2, EEG of Hit trials aligned to button-press, different colors indicate differ- ent change sizes, averaged over all change times, see below for differences in change time). This suggests that the detection of the change in statistics was not accompanied by an overall response in the auditory cortex comparable to other stimulus changes such as stimulus onset or offset (compare also to the model responses in Figure 14B, see also **Discussion**). While this does not preclude the informa- tion about the change to be available in early auditory cortex, there is no specific, overall reaction to the change, compared to the continuous representation of the stimulus. The centro-parietal elec- trodes exhibited a centro-parietal positivity (CPP) reported previously (O'Connell et al. [2012], Kelly and O'Connell [2013], Twomey et al. [2015]) in a similar location (see Figure 11F for its topography at response time). In contrast to the central electrodes, the CPP did not display any clear response to sound onset (Figure 11D) but exhibited a long-lasting response fol- lowing change events (Fig- ure 11E1). This increase in the EEG signal was building-up and preceded subjects' responses across change sizes (Figure 11E2), outlasting the timing of the button press. The difference between change sizes was colocalized with the CPP (Figure 11F, inset), indicating that the difference in amplitude is not due to a global shift in potential). In previous studies, the CPP potential was clearly linked to evidence integration in decision making tasks, e.g. in simple visual and audi- tory detection tasks (O'Connell et al. [2012]) and a complex visual discrimination task (Kelly and O'Connell [2013]). We

therefore hypothesized the CPP to also be indicative of evidence integration in complex auditory detection tasks. In order to assess this, we examined how the CPP potential depended on the amount of evidence, and whether it exhibited accumulation-to-threshold dynamics. Both the slope (Figure 11G) and the height (Figure 11K) of the response-aligned CPP potential depended on the stimulus parameters. The slope increased significantly with change size (Figure 11H, $p<0.001$, 2-way ANOVA across change size and change time), but was not significantly dependent on change time (Figure 11I, $p=0.074$, same ANOVA). The effect of change size on slope is consistent with a representation of task-related evidence in the CPP signal, as reported previously in other change detection tasks (O'Connell et al. [2012]). The height of the potential also increased significantly with change size (Figure 11L, $p<0.001$, 2- way ANOVA across change size and change time), and decreased significantly as a function of time (Figure 5M, $p<0.001$, same ANOVA). Such a change size dependence has been reported before (see Figure 2 in O'Connell et al. [2012]), and at first appears inconsistent with a fixed threshold. However, since the execution of the button press requires some time, the application of the threshold has to precede the button press by some delay. The observed difference in heights could thus reflect a continued accumulation of evidence at different slopes, during the time interval between decision commitment and response completion, until the execution of the decision is communicated to the CPP source. Consistent with this interpretation, CPP height did not exhibit a dependence on change size, if measured in a window of 200–100 ms preceding the response time ($p=0.16$, same ANOVA, close to the crossing in Figure 11E2). In addition, we verified that the CPP height did not depend on the reaction time (Figure 6), as expected from an evidence accumulator signal (Kelly and O'Connell [2013]). The height decrease as a function of change time is indicative of a reduction in threshold as a function of time (Figure 11M). However, we did not observe an increase in FA rate later in the trial (Figure 8D), suggesting no increase in unfounded decisions. Although the time-dependence of CPP height could result in a decrease of CPP height for late versus early reaction times, we did not find any significant decrease in CPP height for late reaction times, which may be due to a rather small effect-size (Figure 12B). Finally, CPP responses aligned to false alarms exhibited similar slope and amplitude as the lower signal conditions (50%, 80%), however, were overall significantly lower than the overall signal conditions ($p<0.001$, 1-way ANOVA, across change size). Neither slope nor height displayed a depen- dence as a function of time into the trial (Figure 11J/N, $p=0.76$, $p=0.43$, respectively, 1-way ANOVA, across different time-into-trial bins). Together these results suggest that the decision threshold on the CPP is close to the lowest change size / false alarm height. Neither of these results depended on the detrending method, as verified by the alternative use of a classical high-pass filter (see Materials and methods and Figure 20). In summary, we found

central and centro-parietal electrodes to respond in a diametrically opposed manner to stimulus onset and (detection of) change in statistics. The CPP potential remained practically silent to stimulus onset, but reflected properties of the stimulus/task when aligned to button press. These results reinforce the notion that the CPP potential reflects sensory evidence accumulation and exhibits accumulation-to-threshold dynamics, with the possibility of continued integration until actual response execution. As a function of change time, only the CPP potential's height reduced, suggesting a time-dependent threshold.

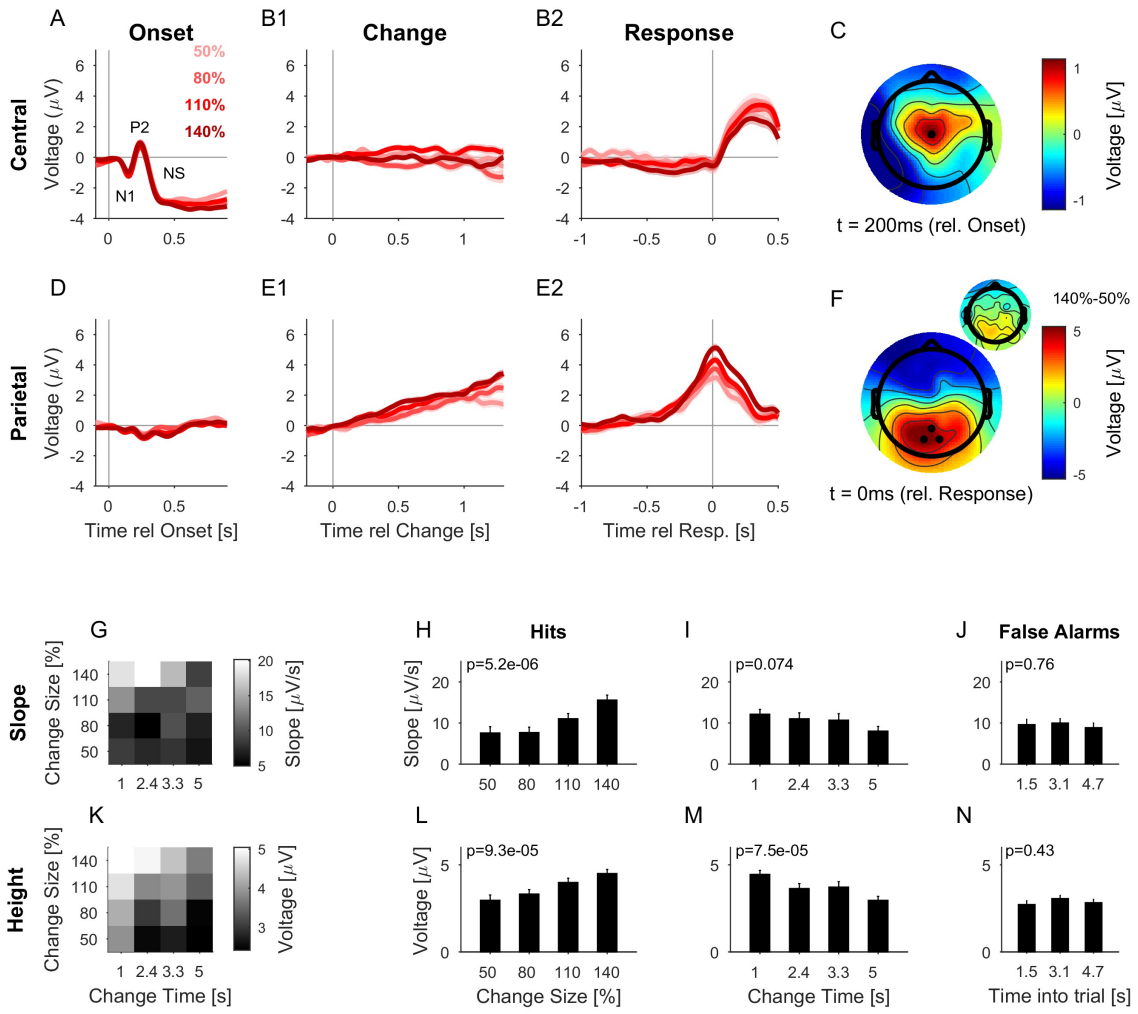


Figure 11: **The CPP potential shows a dependence on both time and size of change, while the central potential remains unaffected**
(A) After stimulus onset, the central potential (Ch. 1, black dot in C) shows a classical N1-P2 progression, followed by a sustained negative potential (labelled NS here). Different shades of red indicate different change sizes. Curves are average over all change times, to avoid crowding the plots. Note that the lowpass filtering at 20 Hz (common for all potentials) reduces the N1/P2 amplitudes below their typical size. (B1) Locked to the time of change, the central potential shows a slow negative trend, which, however, does not depend systematically on change size. (B2) Preceding the response, the central electrodes show no significant change in potential, which only starts to deviate from 0 after the button press. (C) At 200 ms after stimulus onset, the topography of the potential indicates a typical auditory onset response for bilateral stimulation, i.e. centered on Cz (El.1 in the equidistant layout, black dot). (D) The potential above the central parietal cortex (average over Ch. 14,27,28 in the equidistant cap, black dots in F) shows no substantial change at stimulus onset. (legend continued on next page)

(E1) Aligned to the time of change, the CPP electrodes show a progressive increase in potential, with some staggering according to change size. In comparison to the response-locked potentials, the present potential is wider and smaller since it is composed of responses at different times. (E2) In contrast to the central electrodes, the CPP electrodes show a clear increase before the response, peaking at or slightly after the response time. (F) The topography locked to the response is found to be centered over the parietal cortex, tending towards the occipital cortex (black dots mark Ch. 14,27,28). The inset shows the difference between the 140% and 50% condition, indicating that the difference in potential is also localized consistently with the average topography. Note, that there was no display change in the entire tone presentation, and a 0.5 s gap after the response, before the screen changed, hence, visual responses can be excluded. (G) CPP slope of the potential leading up to the response in relation to the different change time and size conditions was measured in a window of 300–50 ms before the response. (H) CPP slope depended significantly on change size (2-way ANOVA with change time and change size as factors, $p<0.001$ for the change time as a factor). (I) CPP slope did not depend significantly on change time (ANOVA as above, $p=0.07$). (J) CPP slope for false alarms showed no significant dependence on the time into the trial ($p=0.76$, 1-way ANOVA). (K) Peak height of the CPP was measured in a symmetric window of 80 ms around the response time. (L) Peak height of the CPP showed a significant increase with change size (2-way ANOVA with change time and size as factors, $p<0.001$ for change size). (M) Peak height depended significantly on change time, decreasing with longer change times (ANOVA as above, $p<0.001$ for change time). (N) Peak heights for false alarms showed no dependence on time into the trial ($p=0.43$, 1-way ANOVA) but were significantly smaller than the hit trials ($p< 10^{-9}$, 1-way ANOVA). Error bars indicate single SEMs for all plots.

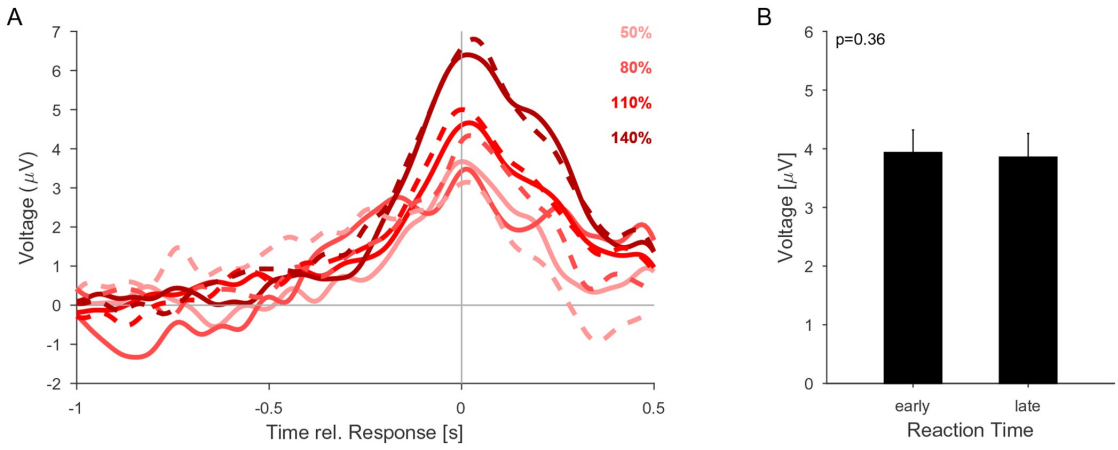


Figure 12: **The CPP potential shows no dependence on whether responses occur early or late after the change**
(A) CPP potentials aligned to response as in Figure 11E2 (for second change-time bin, i.e. around 2.4 s). The solid lines are the early responses (up to median reaction time) and the dashed lines are the late responses (median reaction time to end of response-window). (B) Across all conditions the reaction time did not significantly influence the height of the CPP potential (p=0.36 for reaction time, 3-way ANOVA over reaction time, change size and change time).

## Dual timescale statistical estimation model matches human response behavior

The psychoacoustic results demonstrate that a listener's ability to detect a change in a statistical property of the environment depends on the time available to estimate this parameter, both for the pre- and post-change stimulus. However, how does the listener know, when to start estimating the new statistics? Since - as in real life - the change occurs at an unexpectable time, one solution would be to compare the recent statistics to a longer term estimate of the same statistics, acting as a baseline - or 'null' - distribution. A minimal implementation of this solution consists of two processes estimating the same statistical property on different timescales (Fig. 13).

For this purpose, we turned to models of statistical estimation of the drift diffusion type, used previously to account for visual and auditory decision making in paradigms where subjects were asked to choose between two alternative choices (Britten et al. [1996], Brunton et al. [2013]). In these models a dynamic variable compares the stimulus information in favor of the two alternatives, and when reaching a predefined bound, a decision is made. We extended this model to a pair of variables, estimating the statistical property on different time-scales (Fig. 13A-B and Methods). A deviation is detected if the long-term estimate (Fig. 13B, $P_{slow}$) and the short-term estimate ($P_{fast}$) differ by more than the difference between the thresholds (Fig. 13B, T). As introduced above, this was intended to capture the dual task the participants faced in our paradigm, namely to estimate the base (initial) statistics while simultaneously scanning for deviations from these statistics. The modified model is governed

by four parameters, which control the time-scales of the dynamics variables and the threshold. To make the model applicable to our auditory textures, we assume that multiple copies of it operate in parallel in different frequency channels (see Methods).

We presented an analogous stimulus to the model, exhibiting a change in the probability of tone occurrence at a random time (Fig. 13A left and 13B, gray, only one frequency bin shown) and in a random frequency location, and quantified the model's response in performance and response time. The model exhibited a comparable behavior on individual trials as humans (Fig. 13C, compare to Fig. 7C), with an initial hesitation to respond, and a mixture of false alarms (gray), correct response (black) and misses (not shown). We quantified the performance (performance, false alarms, misses) and the reaction times as a function of the change times and the change size (Fig. 13D-G). The match between the human data and the model was close, with an average residual (mean squared error) of 0.049 (in units of probability). The correlation coefficients between the real data and the fit were [0.97,0.99,0.98], for performance (Fig. 13D), false alarms (Fig. 13E) and misses (Fig. 13F), respectively.

The reaction times could be accounted for both in mean and distribution for different change sizes (r = 0.95, MSE = 0.009 (norm. prob.), Fig. 13G). For the condition with the biggest step, a certain fraction of the responses occurred very early, which may be subject-dependent and we were unable to replicate in the present model.

The parameters that best fit the average human data were $\tau_f$ = 0.2 s, $\tau_s$ = 1.1 s, $\tau_a$ = 0.65 s, and T=0.40 (in units of probability). Hence, the time constants of the fast and the slow processes differed by more than fivefold, and the threshold for detecting a step was surprisingly high. The time for eliciting a motor signal was consistent with the asymptotic times we found in the human data (see Fig. 9B, 140 %). The time constant of the transitional period represents (as the other parameters) an average over the subjects. Inspecting individual subjects revealed some variability in their propensity to react early (min median: 0.77 s; max median: 1.03 s).

The residual differences in the fit could be a consequence of the fact that the data from multiple listeners was pooled, rather than fitted individually. With the current limitation of ~1000 trials / listener, a single listener fit would be dominated by within-subject variability across trials, requiring more trials before stabilizing.

In summary, the dual timescale estimation model captures the human performance and reaction times well, suggesting that its basic principle may be implemented by the brain. The fitted time-scales of estimation suggest that a rapid estimate of the present statistics can be formed within 200 ms. While this time appears sufficient to reliably distinguish the larger steps in statistics, it is insufficient to detect

small changes in occurrence probability, which are often perceived as unchanged statistics.

## Detection of changed statistics based on spectrotemporal processing in auditory cortex

The dual time-scale model successfully captures human performance via an estimation of stimulus statistics. While this suggests a consistency with the principle of statistical estimation, it does not provide any insights into putative neural implementations. For this purpose, we turn to an established model of auditory cortical processing ('cortical model', Chi et al. [2005], Elhilali et al. [2009], Krishnan et al. [2014], Patil et al. [2012]), which we augment here with a decision stage specific to the present task. In particular, this alternative model investigates whether the cortical model (and hence the primary auditory cortex) represents the acoustic stimulus in a way that supports an account of our psychoacoustic data, i.e. supports decision making in certain statistical contexts.

The cortical model emulates the spectrotemporal response properties of neurons in primary auditory cortex, which have been extensively studied by various groups (Ahrens et al. [2008], Eggermont [2002], Kowalski et al. [1996]). Its responses are based on a filterbank-based, joint spectrotemporal modulation analysis following the output of the early stages of the auditory system (auditory spectrogram, Fig. 14A). Parameters and properties were set to approximate the responses of neurons in auditory cortex (see Methods for details) (Chi et al. [2005], Yang et al. [1992]). The spectrotemporal filters cover the experimentally observed range of 1-30 Hz and 0.5-8 cycle/oct, whose outputs are weighted in correspondence with the experimentally observed abundance of these properties in A1 (Kowalski et al. [1996], Fig. 14B).

We simulated two types of readouts from the model to account for two of the main experimental constraints. For the first, we summed all cortical outputs to simulate an effective EEG recording with limited spatial separation of sources, leading to a global response. As expected, in this case, trial onsets and offsets produced strong responses (Fig. 14B), with a plateau of sustained response for the whole duration of the stimulus. The responses due to the statistical change in the stimulus were largely diluted in the summed response and thus could not been discerned, consistent with the present EEG recordings of the auditory electrodes (Fig. 11B).

The ranges of spectral bandwidths and timescales related to the change were kept constant over the whole duration of the task. Consequently a more optimal strategy would be to focus on the temporal modulation filters in cortex that are most activated by the statistical change. Hence, we postulated that high-order areas could monitor the outputs of the task-relevant temporal filters. For example,

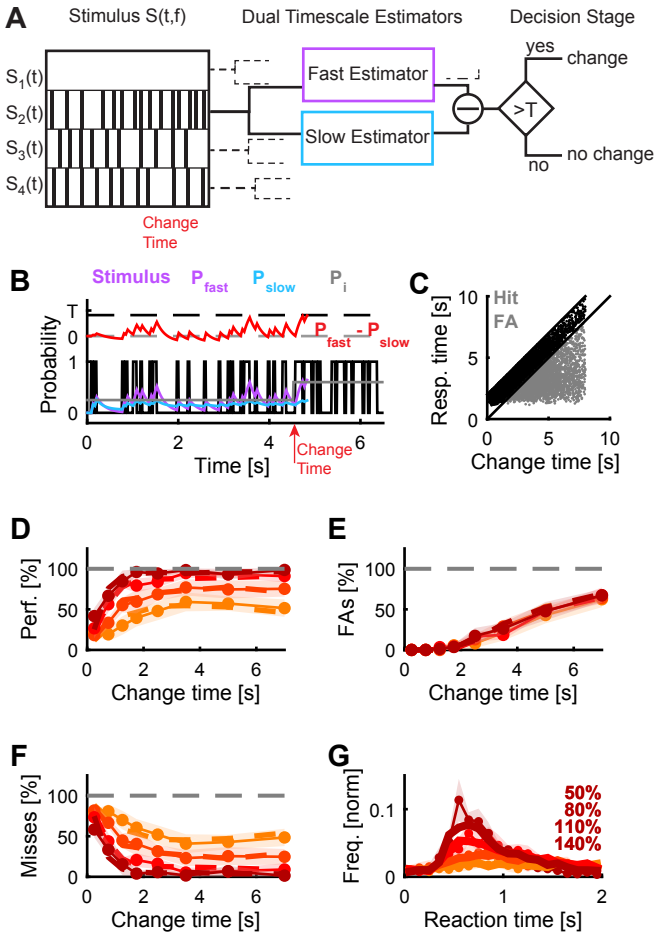


Figure 13: **Dual timescale statistical estimation replicates behavioral results.**
(A) The dual timescale model consists of two dynamical estimation processes operating with different speeds. If their estimates differ by more than a threshold T, a change in the stimulus is detected. The model was fitted to the entire set of behavioral data (D–G). (B) In a single trial the slow (P slow , blue) and the fast (P fast , purple) estimates of the actual stimulus probability (light grey) vary with the stimulus (black) on different timescales. Here, a decision. (P fast P slow >T) is detected at 300 ms after the change in the stimulus (red). (C) The distribution of response times compared with the change times exhibits a similar shape as for the real subjects (see Figure 7B). (D) Detection performance of the model (dashed lines) closely matches the human data (continuous line with 1 SEM error hull) both as a function of change time and change size (different shades see legend in G), see text for parameter values). (E) False alarm rates are also matched closely (same legend as in D). (F) Miss rates are matched equally closely (same legend as in D). (G) Response time distributions are also matched closely, which is of interest as no explicit model of response times was included in the model (same legend as in D).

subjects could make their decisions based on the largest output produced by the change. These would be sampled from the filter with the temporal dynamics and spectral modulation that roughly matched those of the stimuli. The response thus selected is shown in Fig. 14A. Aside from the strong responses at stimulus onset and offset, the responses now exhibited in addition a prominent intermediate peak due to the change in statistics (Fig. 14A). This change-induced response peak vanished in trials when the pre-change interval was very short because it became fused with the large onset peak (Fig. 14C). Change size was encoded in the amplitude of this cortical response peak (Fig. 14D). The variability in responses of the cortical outputs was solely due to the random tone-clouds preceding and following the change in the stimulus.

To quantitatively simulate the perceptual decisions of the listeners, we analyzed the cortical filter outputs for individual trials. We used a time-varying threshold that remained identical across all conditions (see Fig. 14A and Methods). The first peak exceeding this threshold (if any) was considered to be the decision point (purple arrow in Fig. 14A). This readout mechanism was fitted to the performance and false alarm rate across change sizes and change times by allowing 5 free parameters (Fig. 14E-F): the (bandwidth) scale Ω, the (temporal) rate ω, and the decision parameters (λ, a, b; see Methods). The parameters that best fitted the human dataset were Ω = 0.54 cycle/oct, ω = 0.72 Hz (a rate corresponding approximately to dynamics or an integration time-constant of the order of 1-2 s), and a = 6.2, b =10.8, and λ = 1.14 s (ρ=0.95; $p< 5.10^{-16}$; MSE=0.7%). The scale value corresponds to a full width at half-maximum for the scale filter of approximately 0.56 octave, very close to the frequency region spanned by localized changes (0.55 octave). This may indicate that subjects preferentially used a single scale value for monitoring the frequency modulation and that they estimated the most common frequency modulation across trials since half of the trials contained localized changes. Importantly, reaction times predicted by the model matched subject reaction times remarkably well both in distributional shape, mean and spread (Fig. 14G), although the fitting procedure did not make use of this information (ρ=0.90; p<5.10-13; MSE=9.1 %).

Scale filters integrate frequency modulations over a limited spectral bandwidth set by the scale factor O. As such scale filters are more prone to detect changes localized in the spectrotemporal modulation domain. It also implies that spectrally distributed changes could be missed by the decision stage as they elicit less activity in the filter outputs. This is reminiscent of the observation that listeners detected changes more efficiently if their energy was concentrated in the frequency domain (Fig. 10A). Consistent with this, we found a decrease in the model performance for non-localized changes, without fitting the model parameters to this aspect of the data (Fig. 14H).

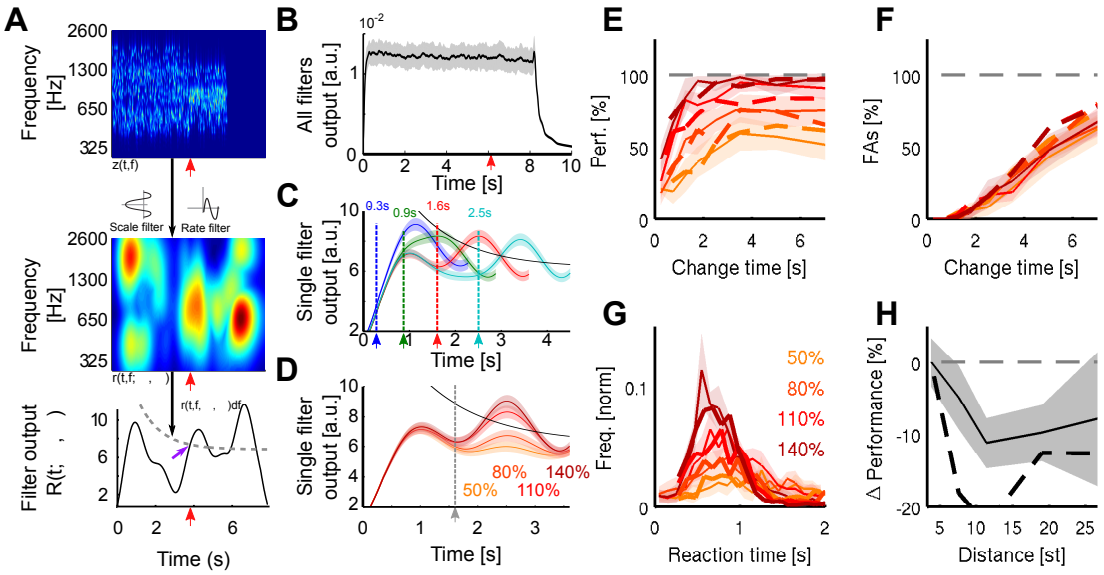


Figure 14: **A cortical filter-bank model provides an implementation consistent with the behavioral results**

(A) Conceptual structure of the model. The cochleogram (top panel) is passed through modulation filters (scale W: 0.54 cycle/oct.; rate w: 0.72 Hz) for obtaining a cortical representation of the sound (middle panel). Changes are detected with a threshold (bottom panel, grey dashed line) applied to the frequency-averaged cortical representation (collapsing threshold parameters: l = 1.14 s; b = 10.77; a = 6.23). First peak exceeding the threshold is classified as change (purple arrow). Timing of change is indicated by a red arrow in the three panels. (B) Average output of the cortical model across all modulation filters. Although trial onset elicits an overall increase in activity, the change in statistics does not lead to an average change in activity (depiction for single trial length, with change time indicated by arrow). (C) Single filter output as a function of change time (average over 100 trials for each curve). Change times are indicated by colored arrows. Notice that the change-related peak is not discernible for early changes, due to its interaction with the onset response. Same parameters than in A). (D) Single filter output as a function of change sizes (average over 100 trials for each curve). Same parameters as in A). (E) Performance for human participants (thin lines) and the decision model (dashed thick lines), as a function of change size and change time. Same colors as in D). (F) False alarm rate as a function of change size and change time. Same colors as in D). (G) Response time distributions as a function of change size. Same colors as in D). (H) Decrease in performance with respect to the distance between incremented bins. Actual data in full line, model result is depicted with a dashed black line.

Thus, the model describes a physiological mechanism that accounts for the behavioral data, as well as suggesting an implementation for the basis of statistical estimation in neural terms. Further, it provides an interpretation for the lack of change-related signal in the auditory EEG electrodes.

## Discussion

We investigated how listeners detected changes in spectrotemporally broad acoustic textures, as a model for change detection in complex auditory environments. The results demonstrated that listeners estimated the statistics of the stimulus to make their decision, as evidenced by the dependence of performance, reaction times, and the CPP response on the duration of stimulus exposure. We developed a drift-diffusion type model for estimating certain stimulus statistics, which accounted well for the response performance and dynamics in human listeners. Finally, we adapted a model of auditory cortical processing to provide a link between statistical estimation and the underlying physiology. The model accounted equally well for the human performance by exploiting a range of temporal filters, providing a potential, neurally plausible substrate for statistical decision-making.

### Relation to previous spectral detection tasks

The present experimental paradigm mimics the unexpected transformation of a sound source within a natural auditory environment. There are some relations to previous research on spectral representations of sound, e.g. profile analysis (Green et al. [1992], Green and Berg [1991], Hartmann et al. [1986], Lentz and Richards [1997], Neff and Green [1987]). Our work, however, differs in several significant ways. In profile analysis, subjects detected spectral shape changes on static spectra that were presented in isolation for short times (fraction of a second each). By comparison, our stimuli were dynamic and sustained (multiple seconds), and changes were detected in the midst of a continuous background with an explicit measure of reaction times. This enabled us to explore the dynamic acquisition of the statistical information.

Further, a series of recent studies investigated detection of change occurring in first- and second-order sound statistics (Barascud et al. [2016], Sohoglu and Chait [2016]). In particular, these authors probed the detection of appearing or disappearing regular sound sources in an acoustic scene (Sohoglu and Chait [2016]). This type of changes featured modifications of first- and second-order sound statistics, which also included an increase in the overall sound level. In comparison, our stimulus design allowed us to limit the change to the first-order statistics while keeping the overall sound level constant.

Our experimental task offers a compromise between complexity of spectrotemporal structure versus

tractability and interpretability of the changes. Furthermore, the task design and acoustic stimulus are well-suited for electrophysiological studies with behaving animals, where one can easily estimate neuronal receptive fields from the responses to tone clouds at the same time as the animal detects the changes (Ahrens et al. [2008], Wang et al. [2012]).

Another important aspect of the experiments was their interleaved (as opposed to block-based) design for change sizes and other parameters, which had several consequences. For instance, it is likely that the observed performance underestimated optimal performance, since the time, location and size of changes were variable. This also prevented subjects from using a template-match strategy on the largest change size, and provided access to reaction times, which consistently mirrored performance, and perhaps the certainty of the subjects in their decisions (Kiani et al. [2014]).

### Modeling statistical decision-making on two levels

Following the modeling steps proposed by Marr (Marr [1982]), we provided an algorithmic and a (neural) implementational model of our subjects' behavior. The algorithmic approach implemented the principle of statistical estimation, while the neural model leveraged principles of auditory cortex processing. Although both models analyzed recent inputs, and effectively detected deviations from them, they differed fundamentally in their levels of description and abstraction.

The statistical estimation model implements the principle of statistical integration in a close-to minimal form, and provides a link to classical drift diffusion models. It is a mechanistic, non-neural description of the process that performed statistical estimation in the classical sense, by representing and comparing the probability of stimuli in frequency bins, based on a lossy memory. Previous work has suggested a possible neural implementation of such a decision making process, in the form of competing neuronal populations, each corresponding to one alternative choice (reviewed in Insabato et al., 2014). While this approach can in principle be extended to the estimation of other properties of a stimulus distribution, i.e. moments or correlations, it has to be adapted more specifically to each particular task. In the present case we chose a fixed set of parameters, since the change time distribution was unchanged in a session. More generally, (temporal) integration properties can adapt to the recent statistics, as recently shown in related contexts (Ossmy et al. [2013], Raviv et al. [2012]).

The cortical model differs fundamentally in that it seeks to capture basic sensory neural responses and is inspired by physiological mechanisms. In this sense, it is agnostic to the type of stimulus, and can be readily extended to handle more complex scenarios such as changes in natural stimuli, speech and music. To create behavioral performance from its representation, we merely added a filter selection and a decision criterion. The spectrotemporal filters implemented in the cortical model

exhibit alternating excitatory (positive) and inhibitory (negative) fields (Figure 14A) that compare the spectral stimulus properties over a given time window set by a filter's temporal rate. As such, it effectively integrates the recent input with opposite signs to detect a change, which can be compared to the difference between the fast and slow estimators in the statistical estimation model.

Therefore, we may view this model as approximating a neural implementation of the statistical model, and thus as a bridge to a neural interpretation of the behavioral performance and the EEG recordings. Several limitations of human performance and properties of the neural data can be considered within each model's framework. The most relevant of these are i) reduced performance in detecting early changes, ii) longer reaction times for early changes, and iii) slow buildup of the performance and of the parietal EEG responses with respect to change times.

In the cortical model, integration time-constants of the order of 1 s (due to bandpass filters tuned at rates near ~1 Hz) appear sufficiently long to explain the decision dynamics exhibited by the subjects (Fig. 8). These time-constants, while on the slow-end of the range, are still found in the primary and secondary auditory cortical regions (Liang et al. [2002], Kowalski et al. [1996]). The reduced performance for early changes has different origins in the two models. In the cortical model, it results primarily from the large onset response masking the responses to the smaller subsequent change. In order to simulate the instructions to the subjects not to report the stimulus onset as a change, detection threshold was set to decrease from a large initial value. In the statistical model, the reduced performance is a consequence of the model's design having two estimators: one with a fast and the other with an adaptive time-constant (tf and ts). At stimulus (trial) onset, the absence of prior evidence is reflected by the equality of the two time-constants. As the trial progresses, the ts becomes longer, and the difference between the two estimator outputs builds up to reflect the buildup of evidence for a change in stimulus statistics (see Methods).

In the cortical model, the large stimulus onset response "masks" the responses to the change, rendering the peak response poorly defined, and hence less detectable and with a slower or more delayed buildup (Fig. 14D). Therefore, the dynamics of the onset response in the cortical model are intertwined with the integration time-constant, performance levels, and reaction times. By contrast, in the statistical model, the dynamics are a consequence of the time-constant dynamics (as above) as well as the not-yet converged estimate of the initial occurrence probability.

In summary, what is typically termed accumulation of evidence (and its associated performance and dynamics) could be explained by the dynamics of the onset response in the cortical model intertwined with its integration time-constants. Future experiments need to further test the validity of this neural interpretation, given the ubiquity of such "sudden" events in natural stimuli due to saccades (in vision),

attentional switches, or trial onsets, which could also influence the detectability of changes (as e.g. in change blindness, Levin and Simons [1997], Rensink et al. [2000]).

### EEG recordings and the site of decision-making

As discussed above, recognizing a change in the statistics of a complex spectrotemporal sound requires the extraction and accumulation of evidence from the stimulus to estimate decision-relevant properties. This transition from a stimulus-related to a task-related representation needs to occur along several stations of the auditory system. Our EEG recordings provide partial evidence regarding their putative location. Specifically, we found a clear difference in the representation of the stimulus at the central electrodes (estimated to originate from auditory cortex activity) and at the parieto-occipital electrodes (estimated to reflect parietal activity): while the central electrodes exhibited a sharp onset response at stimulus onset and offset (Fig. 11A), they showed little evidence of the change response or of the presumed accumulation of evidence for a change (Fig. 11B).

In sharp contrast, the centro-parietal electrodes displayed no response to the onset (Figure 11D), and a clear evidence of the sensory evidence accumulation after the change aligned to response (Figure 11E2). This predominance of decision-related signals in the parieto-occipital electrodes is consistent with decades of research in the accumulation of task-related visual information in the parietal cortex, more specifically in decision-making with saccades in the lateral intraparietal (LIP) cortex (Huk [2005], Roitman and Shadlen [2002], Shadlen and Newsome [2001]). Neurons in LIP have been shown to exhibit activity correlated with the accumulation of visual evidence coming from MT (Huk [2005], Mazurek et al. [2003]). Their firing rate usually exhibits a linear increase until the animal makes a decision (Shadlen and Newsome [2001]). In these studies, typically a fixed threshold on neural firing rate is used to relate neural activity to decision making. A set of related EEG studies termed the corresponding potential the centro-parietal positivity (CPP, Kelly and O'Connell [2013], O'Connell et al. [2012]). The location of the CPP was presently found slightly more occipital, which may depend on details of the task and the subjects (see e.g. Twomey et al. [2015]).

It has recently been suggested that individual neurons change their firing rate instantaneously at the single trial level (Latimer et al. [2015]). We presently observed gradual, rather than step-wise changes in our across-trial averages. However, we predict that even single trial EEG signals would be gradual as these step-changes occur randomly, and hence are unlikely to be synchronized at the population-level. Due to the large ensemble of neural responses contributing to a single scalp location's potential, this instead results in the commonly seen ramping activity on the EEG level, as observed in our data. The lack of evidence for a change-related signal in the auditory EEG potentials can, however, not fully

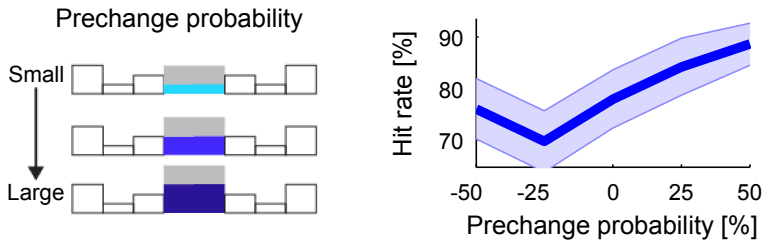


Figure 15: **Change detection improves with base probability**
The prechange marginal probability of a frequency bin significantly influences the performance in the same trial (~10% increase, p=0.005, only 110% condition considered here). Prechange probability is relative to the flat marginal probability (pinit = 0.125), i.e. the absolute amount of change in probability is equalized This suggests that large prechange probabilities allow a faster or more accurate estimate, possibly due to a higher rate of tones sampled up to the change time.

rule out the presence of a change-related signal in auditory cortex in the present stimulus context. The representation of the change could be diverse and distributed, which may average out in the non-selective, coarse averaging on the EEG level (see Fig. 14B). This is also consistent with recent work, demonstrating choice-related signal in auditory cortex (e.g. Bizley et al. [2013], Tsunada et al. [2016]). Our cortical modeling suggests that the representation in auditory cortex provides a good substrate for initial accumulation of sensory information about changes in stimulus statistics, which is then selected and amplified in parietal cortex, leading up to the sustained parietal activity and a full representation of accumulated evidence and choice (Shadlen and Newsome [2001]). This interpretation is supported by the match in performance, reaction times (Fig. 14E-G), and in the progression of activity between specific filters of the cortical model (Fig. 14C) and neural data (Fig. 11E).

In conclusion, as with many other cognitive functions, it is likely that higher-order areas such as the LIP and PFC select and potentially amplify task-relevant outputs of the auditory cortex. To test this hypothesis and the value of the proposed models, it will be necessary to extend change detection tasks to more natural and complex stimuli. As shown previously (Lewicki [2002], Smith and Lewicki [2006]), natural statistics shape neural processing, and in a similar way should be informative about which changes to focus on in research. Furthermore, the models should be extended to include the effects of cognitive functions in modulating this process, such as attention or expectations.

## Supplementary

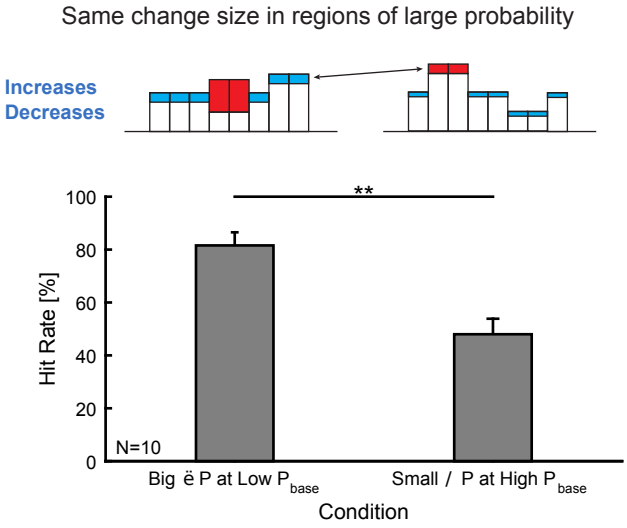


Figure 16: **Change detection is not focused on high probability bins**
Subjects could adopt a strategy to listen to salient, high probability bins. We tested this hypothesis by comparing equal changes in high probability bins, with differential changes in other bins (top, compare left and right example frequency marginals where red indicates the increase in a frequency region and blue a decrease. These patterns arise from the local change (increase) together with the decrease due to normalization). If listener's focused on high probability bins, very similar performance should be expected. In contrast we find a strong dependence on the surrounding bins (bottom), with hit rates substantially higher ($p<0.01$, Wilcoxon signed ranks, $N = 10$) for the case of a strong increase in a low probability region (left) than smaller changes in low frequency regions (right), although change in high probability bins was kept roughly the same.

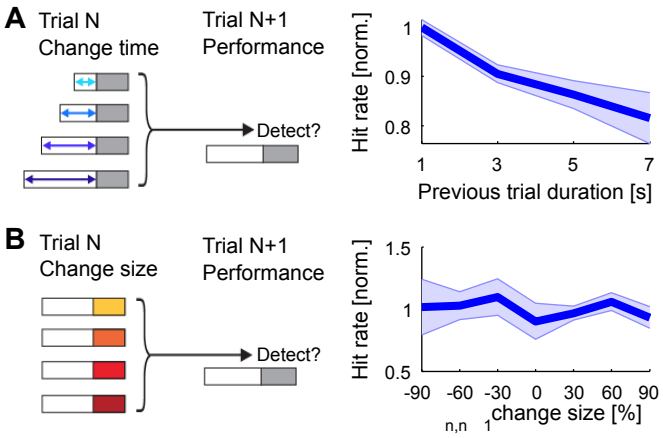


Figure 17: **Listening duration in the previous trial significantly reduces detectability in the current trial**
(A) Listening duration in the previous trial significantly reduces detectability in the current trial (~15% decrease, p=0.008, Friedman test). A very similar result was obtained in comparison with change time in the previous trial. Performance in the current trial was normalized to the average performance within each change size. This suggests that the estimate of the previous trial is more stable for longer exposure, which interferes with the estimation in the current trial. Performance in the previous trial was not predictive of performance in the current trial (data not shown). (B) Change size of the previous trial has no influence on the detectability in the current trial (p=0.12, Kruskal-Wallis). Change size in the previous trial was evaluated both absolute and relative to the current trial's change size (the latter is depicted). Performance in the current trial was normalized as in A). Together, these results suggest that 'what' is estimated is less influential on performance, than 'how well' it has been estimated.

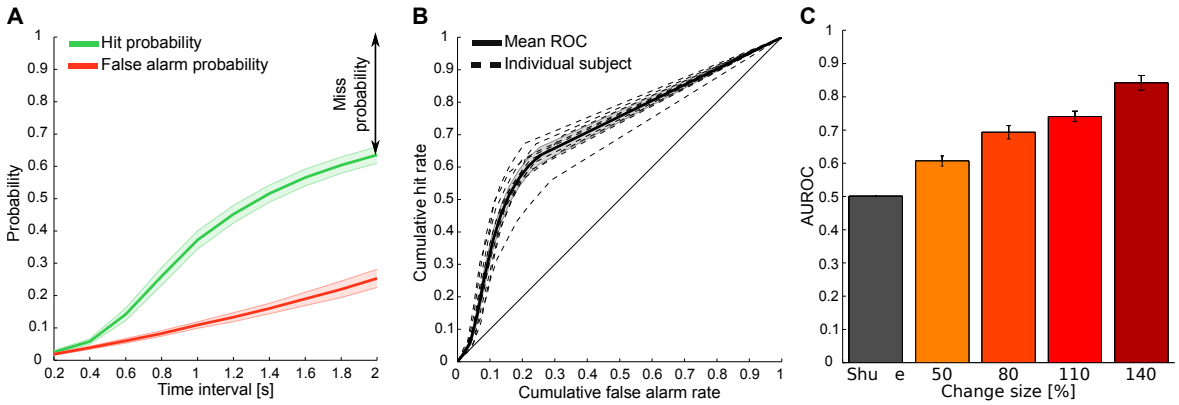


Figure 18: **Change sizes ROC analysis**
(A) The probabilities for hits and false alarms were independently computed from their respective reaction time (RT) distributions at each time intervals from 0.2 to 2 s with 0.2 s increments (see details in the d' Analysis paragraph of the Methods and Yin et al. [2010]). (B) The false alarm probability function was plotted against hit probability function to construct the receiver operating curve (ROC). The area under the ROC (AUROC) is a measure of discriminative performance of the task. (C) The AUROC was significantly different across change sizes and chance level ($p<10^{-7}$; Friedman).

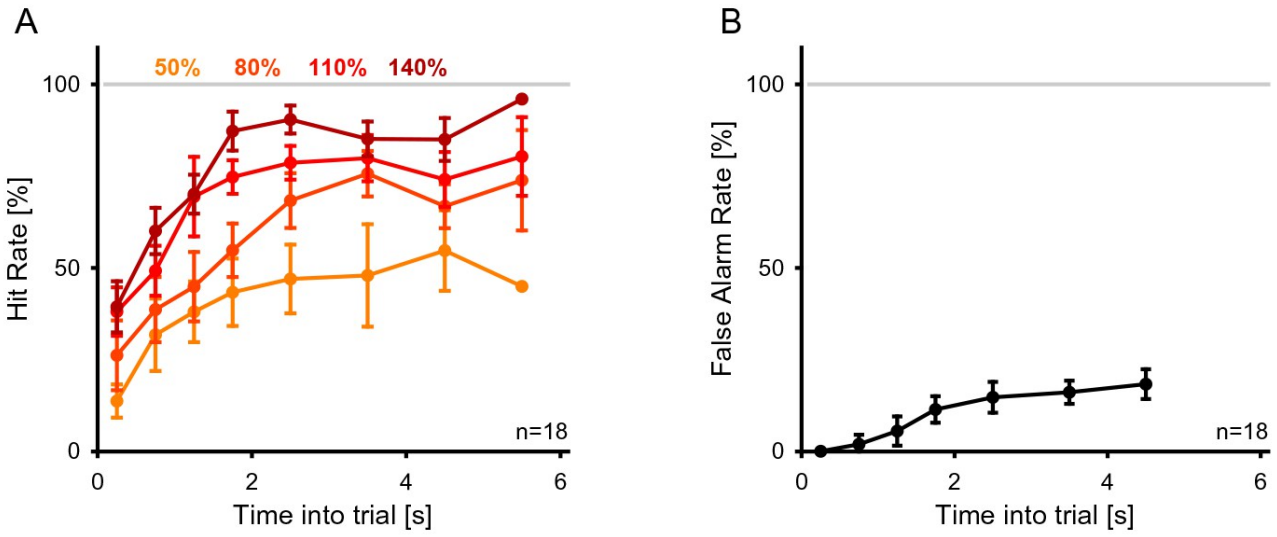


Figure 19: **The detection rate of subjects during EEG**
(A) The detection rate of subjects in the EEG version of the task was quite comparable to the one in the psychophysics only task (see Figure 8A). (B) The false alarm rate stayed approximately constant after the initial 2 s, corresponding to the available response period. Precisely, the false alarm rate given here is the instantaneous rate per second as a fraction of all trials with a change time greater than the current time bin.

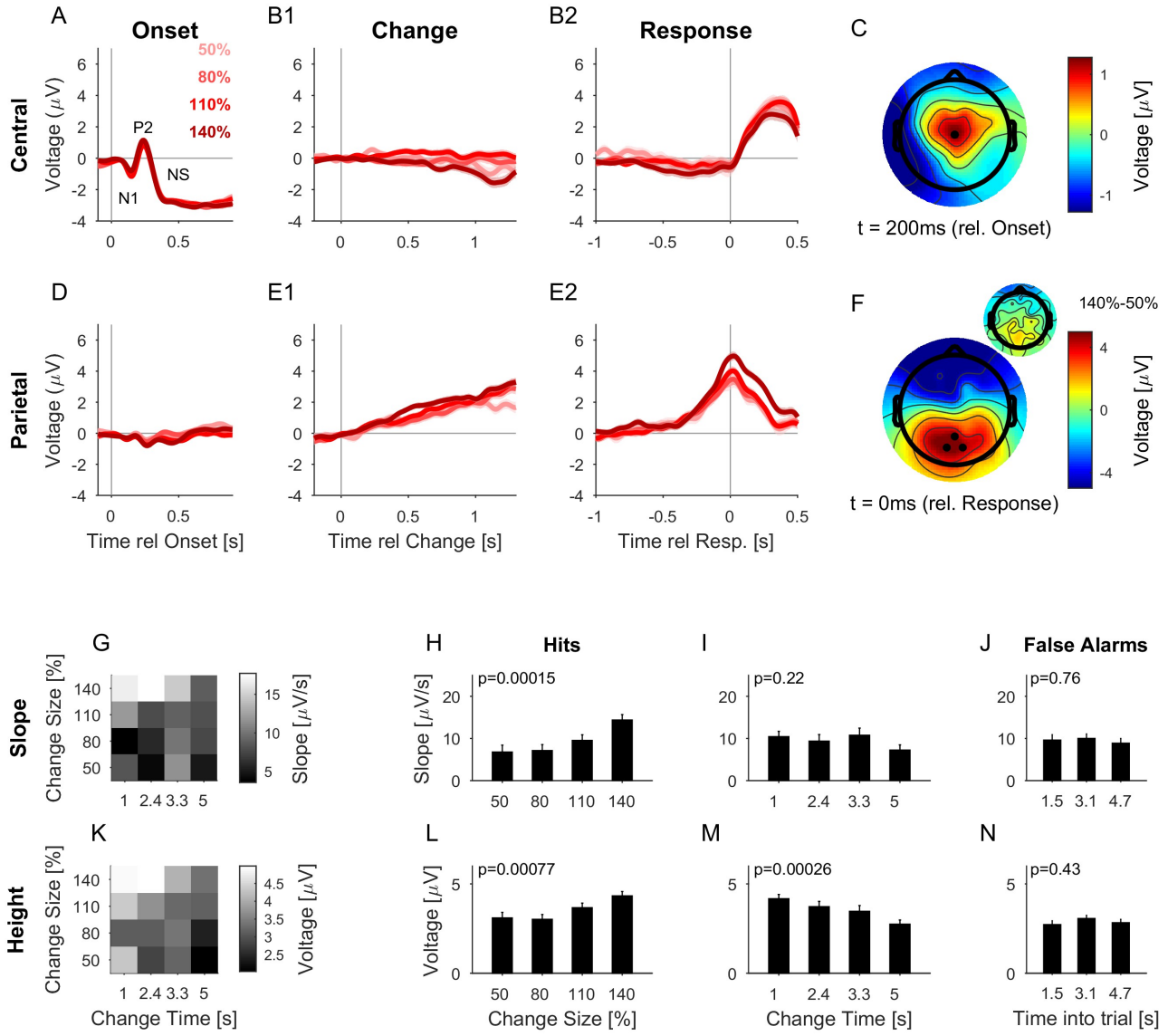


Figure 20: **EEG detrented with classic high-pass filter**
Same data and analysis as in Figure 5, however, detrended with a classical high-pass filter (Matlab: filtfilt, 0.1 Hz, 15th order, 50 dB attenuation in the stop band).

# Chapter 3: The representation of changes is generalised along the cortical pathway


## Abstract

Complex, cluttered acoustic environment, such as a busy street, are characterised by their ever-changing dynamics. Despite their complexity, listeners can readily detect changes in continuous acoustic streams. However, the neural basis of the extraction of relevant information in complex streams during goal-directed behavior is currently not well understood. As a model for change detection in complex auditory environments, we designed spectrotemporally broad tone clouds whose statistics change at a random time. Ferrets were trained to detect these changes within continuous sound. Hence, they are faced with the dual-task of estimating the baseline statistics and detecting a potential change in those statistics at any moment, mimicking real-life challenges. To characterize the extraction of relevant sensory information performed between sensory cortices and frontal areas, we performed electrophysiological recordings in the primary auditory cortex (A1), secondary auditory cortex (PEG) and frontal cortex (FC) of the behaving ferret. A1 neurons exhibited strong onset responses and smaller amplitude frequency-tuned change-related discharges. PEG population showed reduced onset-related responses, but enhanced and broader change-related modulations. Finally, FC neurons presented an enhanced response to all change-related events in a behavior-dependent manner. In addition, PEG and FC population dynamics showed a time-dependent evolution within trials and before the change occurred, possibly reflecting an initial sensory process, necessary in this dual-estimation task. All together, these area-specific responses suggests a behavior-dependent mechanism of sensory extraction and amplification of task-relevant event.

## Introduction

Detecting and reacting appropriately to changes in a complex environment requires adapting to the available sensory inputs while constantly monitoring for deviations and converting the relevant ones into discrete motor acts. Perceptual decisions are thought to be composed by three main operating stages (Sternberg [1969]): sensory encoding, decision formation and motor execution. In such decisions, sensory information are thought to be processed in a bottom-up fashion by the brain, i.e. along a hierarchy from the periphery, through cortical sensory areas and up to higher integrated areas.

Most decisions involve more than one stream of information even within a modality. Therefore processing and selecting the relevant information is crucial to produce the adequate behavioral output. In the ferret, dorso-lateral frontal cortex has been associated with the enhancement of the representation of both visual and auditory targets compared to reference task-irrelevant stimuli in categorical tasks (Fritz et al. [2010]). The emergence of task-relevant selectivity is also reported in higher auditory area (Atiani et al. [2014]), suggesting that stimulus meaning is already encoded at the sensory processing stage. Recently, even primary auditory cortex population activity has been shown to carry information about stimulus meaning during behavior (Bagur et al. [2018]). In all those areas, the enhancement of the target stimuli depends on task engagement. Thus, the selection of relevant information starts early on at the sensory processing stage and is behaviorally-gated.

In natural scene, the pertinent information is rarely presented in isolation and in a token-based manner, but is rather embedded in a continuous, dynamic flow (Thura and Cisek [2014]). The propagation of the relevant information embedded in a continuous stream leading up to formation of a perceptual decision are poorly described. To investigate the underlying mechanisms of decision-making in complex ongoing sounds along the cortical pathway, we use the task described in chapter 2 in combination with electrophysiological recordings in the awake behaving ferret. Extracellular recordings were performed at three target cortical locations previously implicated in auditory sensory processing and decision formation: primary auditory cortex (A1), belt auditory area (Pseudo Ectosylvian gyrus, PEG) and frontal cortex (FC, dorso-lateral/premotor). The following chapter focuses on three main questions: How are subtle changes in sound statistics selected? Is the cortical representation of these changes generic and independent from stimulus acoustic property? Does this extraction process depend on the behavioral context?

We report that change-related neural correlates become stimulus independent along the cortical pathway in a behaviorally-gated fashion. In addition, population-level dimensionality reduction techniques reveal time-dependent modulations of activity before the change arises and correlating with behavioral performance.

# Materials and Methods

## Ethics

Experiments were approved by the French Ministry of Agriculture (protocol authorization: 01236.02) and strictly comply with the European directives on the protection of animals used for scientific purposes (2010/63/EU). All of the surgeries were performed under anesthesia, and every effort was made to minimise suffering.

## Experimental set-up

Adult female ferrets (n = 3, Marshall Farms) were trained using positive reinforcement on a reaction-time change detection task with a Go/No-Go paradigm, closely resembling the psychophysics task described in chapter 2 and detailed below. Animals were placed in a custom-made horizontal cylindrical holder inside a acoustically-sealed booth (Industrial Acoustics Company GmbH). One animal was trained neck-fixed prior to head post implantation. All the animals were then trained head-fixed after implantation. Acoustic stimulus presentation and behavioral control were performed using custom-written software in MATLAB (BAPHY, from the Neural Systems Laboratory, University of Maryland, College Park; available upon request). The acoustic stimulus was sampled at 100 kHz, and converted to an analog signal using an IO board (National Instruments, PCIe-6353) before being sent to through an amplifier (Sennheiser HDVA600) and finally presented at 65dB SPL diotichally to the restrained animal using high-fidelity earphones (Sennheiser IE800, calibrated flat, i.e. ±5 dB, within 100–20000 Hz). Animals reported the detection of a change by licking a water-spout placed in front of them. A piezoelectric actuator glued to the water-spout transformed the mechanical stress associated with a lick into an electric potential that was recorded by a data acquisition card (National Instruments, PCIe-6353).

## Change detection task

### Stimulus

Ferrets were trained on a Go/No-Go reaction time task in which they had to detect changes in first-order statistics of ongoing sounds. A tone cloud, closely resembling the stimulus described in chapter 2 was presented on every trial (see Figure 21). An extensive description of the stimulus design can be found in chapter 2, only the differences will be detailed thereafter. An initial marginal distribution composed of 6 equally distributed frequency bins over 5.3 octaves (see Fig. 21 left panel, the example

marginal is in grey), ranging from 500 to 20000Hz, was drawn on each trial. On 90% of the trials (10% catch trials) a change consisting in an increase in the tone occurrence probability in two adjacent frequency bins (see Fig. 21 right panel, change indicated in orange) was introduced at a varying but discrete change times (see 21B). Change spectral locations were limited to 3: low frequency (see Fig. 21 stimulus example; 500-1700Hz), middle frequency (1700-5800Hz) and high frequency (5800-20000Hz). Two change sizes were chosen (small and big changes), based on Ferret M's performance and kept constant throughout all the recordings. Ferrets had 0.85s (Ferret M & T) or 1s (ferret B) to detect a change.

As a result of the initial delay period in the stimulus used to enable training (see next section), the timing of the change (see Fig. 21) always exceeds 1.75s. Therefore, the effect of change time on performance reported in chapter 2 are absent for this study.

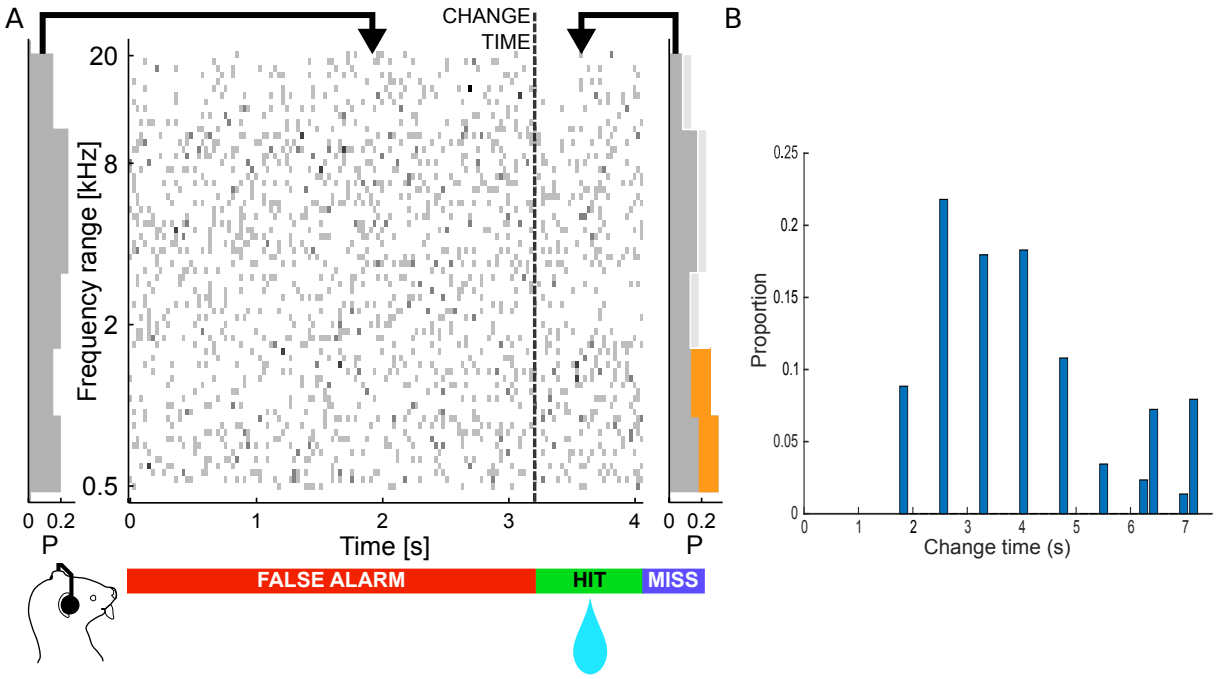


Figure 21: **Example stimulus: statistically defined tone cloud and change time distribution** (A) The tone occurrence probability was governed by its marginal frequency distribution (grey curve, left panel). Tones in individual frequency bins were drawn independently consistent with the marginal (middle panel). The frequency marginal was modified (indicated in orange in the right panel distribution) after a randomly chosen point in time (change time). Animals were trained to report a change by licking a water-spout placed in front of them. (B) Change time distribution.

### Procedure

Ferrets were placed and head-fixed in the custom-designed in the above-mentionned custom designed setup. Once isolated units were found, stimulus presentation coupled with data acquisition

began (BAPHY and MANTA). Every trial consisted of a 0.3s pre-stimulus silence followed by the presentation of the stimulus. Each behavioral session was composed of at least 180 trials, which corresponds to a minimum 6 repetitions of each combination of conditions (change size$\times$change location). Stimulus sound offset occurred either at the end of the response window for passive session and miss trials, or concomitantly at the first lick outside of the initial delay period for false alarm and hit trials.

Change size presentations over a session were as follow: 10% catch trials (no change), 30% small change and 60% large change. Change locations were typically distributed equally over a session. In order to investigate attentional effects and characterise target selection further, some sessions were biased towards one of the three change locations in all behavioral epochs and with a proportion of 2/3.

### Behavioral paradigm

Adult female ferrets (n = 3), housed in pairs in normal light cycle, were trained using positive reinforcement on a change detection task over period of 12 months on average prior to recording (Ferret M: 12 months, Ferret B: 16 months, Ferret T: 10 months). Animals were trained to lick a water spout placed in front of them during a response window (0.85s- or 1s-long) whenever they detected a change in stimulus first-order statistics. Correct responses were rewarded by 0.1mL of water. False alarms and misses were punished by a 1s timeout.

At the start of the training, the dimensions of the stimulus were reduced to only big changes in one change spectrum localization (Ferret M: high frequency, Ferret B: low frequency, Ferret T: low frequency), and a loudness cue was added by decreasing the level of the pre-change sound. None of the animal started training on the middle frequency because saliency of changes in the middle portion of a broad spectrum has been shown to be lower than on the edges (Catz and Noreña [2013]). Loudness cue was then slowly reduced and the other parameters (including reward amount) were adjusted according to the animal's behavior. Once animal's performance (based on the hit rate, d' , sharpness of hit reaction time distribution) was deemed satisfactory, a second change localization was added, and then a third one.

One of the challenging aspects of a reaction time task is the high hazard rate. It is especially detrimental during training as false alarms prevent animals from hearing the change to detect. In order to decrease the number of early licks related to the animal's thirstiness (Berditchevskaia et al. [2016]), the nature of our task (Boubenec et al. [2017], Johnson et al. [2017]) and the animal's impulsivity, we introduced a fixed pre-change period of 1.5s. If a lick was detected during that period, the change

time was delayed by another 1.5s and so on, until no lick was detected for at least 1.2s. On average this initial delay period is high at the beginning of the session, then decreases and stabilizes in about 20 trials (Fig. 25).

#### Water restriction procedure

Animals were water-deprived on the night preceding a training or recording session. At least 15 minutes after a session involving behavior (training or recording) , water was given ad libidum for roughly 1 hour or more to ensure a sufficient daily water intake. Both training and recording sessions typically took place during the weekdays. A two day break was ensured (usually during the weekend), where water was given freely. The animal's weight was monitored carefully and training was interrupted if a threshold of 75% of the initial weight was reached.

### Extracellular electrophysiological recordings

#### Surgery

To enable head-fixed electrophysiological recordings, a stainless steel headpost was surgically implanted on the skull and target cortical location was determined using stereotaxy. Anesthesia was induced with a combination of Ketamine-Medetomidine and maintained with isoflurane (1%) throughout the rest of the procedure. Masticatory muscles covering the skull were removed and the skull was exposed to allow for the headpost fixation and stereotactic measures. The auditory and frontal cortex regions were located using approximate stereotaxic coordinates. The implant was then build using bone cement, encasing the headpost but leaving the target locations accessible. Antibiotics and analgesics were administered following surgery. A two week recovery period was enforced. For a detailed surgery protocol see Appendix.

Primary auditory cortex: the approximate location of the center of the primary auditory cortex (A1) was 16 mm anterior to the occipital midline crest and 12 mm lateral to the midline. For single electrode recordings the target location was ascertained by following the tonotopic axis from one day to the next and observing characteristic physiological features such as short latencies and well defined tuning.

Secondary auditory regions: The location of the Pseudo Ectosylvian Gyrus (PEG) in ferret M was ascertained using the tonotopy reversal reported in Bizley et al. [2005]. For ferret T secondary areas were identified using characteristic physiological features such as latencies.

Frontal Cortex: Forntal cortex (FC) location was determined with the following coordinates: 25-29mm antero-posterior and 1.5-5mm medio-lateral. The antero-posterior origin is defined as the nuchal crest

5mm medial, as this location can be reliably measured in ferrets.

**Single electrode recordings set-up**

Experiments were conducted inside an acoustically-sealed booth (Industrial Acoustics Company GmbH). Small craniotomies (~1 mm diameter) were made over auditory cortex (primary or secondary) or frontal cortex prior to recording sessions that lasted 6–8 hr. Electrodes were lowered into the same craniotomy until enough data was collected from that specific brain region, this required maintaining the craniotomies by removing the cicatricial tissue forming onto their surface typically the evening preceding a recording session. We used four high impedance (2–6 MΩ), tungsten, independently moveable recording electrodes (Alpha-Omega) separated by 500 µm for the neurophysiological recordings. Electrodes were lowered into the brain of the awake animal using an Electrode Positioning System (Alpha-Omega) until a majority of channels displayed isolated spontaneous activity.

**Mutli-array implantation**

32-channels (Platinum/Iridium, 1-6 MΩ, separated by 500µm) microelectrode arrays (MicroProbes) mounted on a micro-drive were implanted in two fully trained female ferrets. For ferret T, one array was first implanted in the left auditory area, a second one was implanted 3 months later in the ipsilateral frontal cortex. For ferret B, only one array was implanted in the left frontal cortex. The A1 and FC regions were located with approximate stereotaxic coordinates during surgery and then further identified physiologically. Arrays' location and angle were constrained by the implant shape and the position of the surgical screws, orthogonality to the brain could not therefore be ascertain. For each implantation site, a craniotomy (5x6mm) matching the size of the array (2.5x5mm) in the target location was made under anesthesia (isoflurane 1% and topical application of lidocaïne), followed by a duratomy. Once the brain was exposed, the mounted array was lowered onto the craniotomy and attached to the implant using UV dental cement (M+W Dental). Electric signal was displayed to ensure that the electrodes' penetration was successful (using the presence of spikes as a marker) and the ferret was woken up under careful monitoring of any sign of putative seizures. The connector and the cables were protected with shrink cable and cemented to the implant. For a detailed multi-array implantation protocol see the Appendix.

Antibiotics and analgesics were administered following the implantation. A week recovery period was enforced but the signal was monitored everyday and the electrodes lowered as needed since we suspect that the brain bulging observed after the duratomy decreases in the days following the procedure.

### Recording sessions

Every recording session was composed of an epoch of passive stimulus presentation, followed by an active behavioral epoch and usually another passive presentation period (about 1.5 to 2 hours of stimulus presentation). The ferret was cued to the passive condition by the absence of the water-spout and to the active condition by the presence of the water-spout (Atiani et al. [2014], Fritz et al. [2010], Schwartz and David [2018]). For recordings of auditory areas, additional passive sounds presentation preceded the first passive epoch, in order to characterise cells tuning properties and derive the tonotopy (TORCS and random pure tones).

Recordings were established as being in A1 and PEG according to the presence of characteristic physiological features (short latency, localized tuning for A1 and longer latency and coarser tuning for PEG) and the position of the neural recording relative to the cortical tonotopic map in A1 and PEG, especially for semi-acute recordings.

All electrodes were connected to an Omnetics 36-channels connector and data acquisition was controlled using MANTA (Englitz et al. [2013]).

### Single electrode recordings specificity

Typically, recordings involving single tungsten electrodes lasted all day (a maximum of 8 hours in the tube for the ferret) and included multiple behavioral sessions (up to 3). Between each sequence of passive/active/post-passive stimulus presentation, electrodes were lowered by a minimum of 150µm to ensure recording of different units.

### MEA recordings specificity

After implantation, arrays were gradually lowered, until clear spontaneous activity was found again on subset of channels. Recordings comprised one sequence of passive/active/post-passive stimulus presentation and were therefore shorter (about 2-3 hours). In between recordings, the arrays were lowered according to the amount of previous recordings in a depth. If the arrays were lowered just prior to recording, stimulus presentation was delayed by at least 30min until neural activity was deemed stable.

### Spike sorting

For all recordings, the raw signal was digitized and bandpass filtered between 300 and 6000 Hz. Spiking events were then extracted from the signal using principal components analysis and k-means

clustering (Fritz et al. [2003], Atiani et al. [2014], Bagur et al. [2018]). Clusters were grouped by hand for an entire session. Unstable units that either appeared or disappeared during a recording session were discarded. Every identified unit is present at least during the prepassive and the active epochs.

## Analysis

**Behavioral analysis** Behavior is analysed under the Signal Detection Theory framework (DM Green et al. [1966]). A dynamical d' described in chapter 2 (Boubenec et al. [2017], Johnson et al. [2017]) captures the detection sensitivity. Correct rejections are defined all pre-change segments corresponding to the response window length. In order to report performance and sensitivity linked to perception and not external factors, periods of drowsiness during behavior are identified as a minimum of 6 consecutive misses and are removed from the behavioral analysis. In accordance with previous perceptual change detection studies in which responses with a reaction time shorter than 200ms in a 2AFC paradigm were found to be no different than chance level (Drugowitsch et al. [2012]), hits with a reaction time shorter than 250ms are categorised as false alarms.

Significance is mostly assessed by comparison with chance level for specific conditions, obtained by shuffling reaction time across trials. Significance level is displayed on the figures, one star corresponds to a pvalue<0.05, two stars to a pvalue<0.01 and three stars to a p-value<0.001.

### Neural activity analysis

**Neural data preprocessing** Spike-sorted units with an average firing rate lower than 2spk/s were removed from analysis, to avoid numerical instability for dimensionality reduction methods (Castranova et al. [2016]). In addition, raw spikes were binned into 30ms bin.

Middle frequency changes were removed from analysis for ferret M (see **Performance is similar for all change spectral location**).

**Auditory tuning properties** Units' receptive fields can be obtained using the pre-change tone clouds and a spike triggered averaged method. However, the changes are spectrally broader (> 1 octave) than typical A1 neurons tuning properties (< 1 octave Kowalski et al. [1996], Fritz et al. [2003], Bizley et al. [2005], Fritz [2005]). As a consequence, the best-frequency and the associated lateral inhibition positions within the spectrum have to be taken into account to assess the influence of units' selectivity on change-related firing rate modulations. It is possible, that a unit might not modulate its firing rate for a change location even if its BF is within that location because the lateral inhibition could also be in the same change location. A unit could also respond differentially to two change

locations because the BF and lateral inhibition are positioned at the edge of two frequency bins (see receptive field A1 example cell: Fig. 28A and its response to middle and low frequency changes Fig. 28B). We therefore specified units' tuning properties using their responses to the 3 different change locations. For that purpose we computed the area under the receiver-operating curve (AUROC) per unit (van Vugt et al. [2018]) and per frequency bins after the change (A1 window: 0-90ms , Belt window: 0-90ms, FC window: 120-280ms). If a response for a change location was significantly different than the AUROC obtained by shuffling the unit firing rate, the unit is considered to respond to the frequency location.

**PSTHs** The average firing rate per unit was z-scored by the mean and the standard deviation of average spontaneous rate (300ms of silence preceding each trial) within a behavioral epoch (passive/active). Single units and multi-units PSTHs are separated and displayed below (Fig. 27and Fig. 34). For A1 and PEG/Belt units that respond selectively to a specific change location, only the trials containing this change are considered. Normalised firing rate is then averaged across units and conditions and locked to an acoustic or a task-related event.

**Linear discriminant classifier performance** Differences in cortical representation of the different acoustic events and subsequent effects along the cortical hierarchy were computed by training and testing cross-validated linear discriminant classifiers per time bin (Bishop [2006], Bagur et al. [2018]) to specify the events encoding dynamics.

Pseudo-population firing rate vectors were constructed for each 30s ms time bin relative to the event using units from all sessions per animal per behavioral epoch and cortical area. Training and testing sets were constructed by randomly selecting equal numbers of event and non-event 30ms time bin for each unit (limited by the session with the smallest trial number for a specific condition, with a cut-off at 20 trials). The classifier was trained for each time bin using the average pseudo-population vectors $c_{R,t}$ and $c_{T,t}$ calculated from a random selection of an equal number of event and non-event snippet. These vectors define at time bin t the decoding vector $w_t$ given by

$$w = c_{T,t} - c_{R,t}$$

end the bias $b_t$

$$b_t = \frac{(c_{R,t} \times w_t + c_{T,t} \times w_t)}{2}$$

The decision rule for a population activity vector $x$ is defined by its projection onto the decoding vector and the bias:

$$y(x) = w_t^T \times x + b_t$$

where $y(x) < 0$ is classified as an event and $y(x) > 0$ as a non-event.

The decoding accuracy corresponds to proportion of correctly classified snippets drawn from the remaining snippets that were not used for training the classifier. To estimate the average and the variance accuracy per time bin, 300 cross-validations were computed by randomly selecting the training and the testing set of snippets.

Chance level and its confidence interval was computed for each time bin by using the same population while shuffling the labels ("event" and "non-event"), and 300 cross-validations. Average chance level corresponds to the average accuracy for this shuffled dataset and the confidence interval to the standard deviation obtained from the cross-validations.

**Decoding the change**

Non-change snippets had to match the timing distribution of change snippets because of time-related modulations present before the change, particularly in FC data (see Fig.30). This balance in the two distributions was obtained by matching each change snippet with a non-change snippet taken from another trial with a longer pre-change time. In addition, we attempted to remove possible motor contribution by discarding the activity just preceding the lick for hit trials (90ms).

In order to compare the accuracy in all the cortical areas, both miss and hit trials were included in this analysis and the number of units was limited to the smallest number of units recorded for one cortical area (in ferret M A1 with 79 units) to avoid increasing the accuracy by the sheer increase of cell number (Bagur et al. [2018], Fig. zS4). This penalized decoding in FC where activity is modulated by the outcome (see 40C in chapter 4).

To ascertain how generalised (i.e. frequency-independent) the encoding of the change is along the cortical pathway, we first computed the accuracy using all change possible locations (except middle frequency change for ferret M's FC , see **Performance is similar for all change spectral location**) and compared it to a "localised" decoding accuracy that takes into account units selectivity measured with the ROC analysis (see **Auditory tuning properties**). The "localized" decoding incorporated only trials containing the selected change location. If A1 or PEG/Belt units responded differentially to two change locations (see example cells in Fig. 28A & B) , they were split into two "units" with each their set of change location trials.

**Decoding the sound onset**

The sound onset was decoded against the spontaneous firing rate from a randomly drawn trial from the same unit.

**Principal component analysis** To describe the population dynamics in all cortical areas, we first reduced the dimensionality of the dataset using a principal component analysis on the averaged activity per unit but separated by outcome before the change (Machens et al. [2010], Sun et al. [2017], Wohrer et al. [2013], Bartho et al. [2009]). The averaged population activity before the change and after the change (separated by outcome) was then projected onto the two top principal components per cortical area.

**Assessing the correlation between the decoder and the population activity before the change** The angle between the decoding vector at peak decoding accuracy and PC1 or PC2 was computed to assess the relationship between the two vectors (Carnevale et al. [2015]):

$$\Theta = \arccos\left(\frac{(w \bullet pc1)}{(||\, w \,|| \bullet ||pc1\,||)}\right)$$

Where w is the decoder vector over a window after the change and pc1 is the weights of the first principal component of the population activity before the change (same for pc2).

Significance was tested with permutation of “event”/”non-event” labels and creating 500 “shuffled” decoding vectors.

## Results

To characterize the extraction and the encoding of relevant sensory information performed between sensory cortices and frontal areas, we designed a task in which animals have to constantly monitor a continuous acoustic stream to detect a change in its first-order statistics. We then performed electrophysiological recordings in the primary auditory cortex (A1), secondary auditory cortex (PEG and more generally belt areas) and frontal cortex (FC) of behaving ferrets. Neural activity was recorded during behavior and during passive presentation of the tone cloud stimuli, before and after behavior. Three ferrets were successfully trained on a reaction-time change detection task. A first set of data was successively collected in ferret M using high impedance tungsten single electrodes in the three target areas and in both hemispheres. Those results are currently being replicated using MEAs in two other ferrets. The following section will focus on the neural activity associated with the change detection in one ferret, with supporting evidence from other ferrets when available.

## Task performance

### Performance and reaction time confirm a dual estimation strategy

Three ferrets were successfully trained on the change detection task (Fig. 21). d' (dynamical, same method as in chapter 2) values range in between 1 and 2 (Fig. 22A, C & E). The low d' values attest task difficulty. However, for all conditions, d' (Fig. 22A, C & E, Fig. 24A, C & D) is always significantly above chance (permutation test, $p<0.001$). Other measures reflecting performance such as hit rate or AUROC are consistent with those findings (Fig. 33).

Similarly to human subjects performance reported in chapter 2, the observed performance cannot be explained by a timing or a pattern recognition strategy. Both of these explanations can be rejected based on the data and the paradigm: if ferrets had used a timing strategy, their instantaneous false alarm rate should never reach a constant value. However, after an initial increase, the false alarm rate remains constant as a function of time within the trial (Fig. 23A, C & E). The stochastic nature of the stimulus does not allow for a pattern recognition strategy as the change is an alteration of a randomly drawn marginal distribution. In addition, performance depends on the baseline probability (significant for ferret M: Fig. 26 A), indicating that the initial statistics are not ignored. All together these results are inconsistent with both strategies.

**Performance improves with change size** To assess the effect of change size on its detection, change size was varied. Large changes were presented on 60% of the trials, and small changes on 30% (10% catch trials, with no change presentation). Large changes consisted of an increase in one of the three frequency bins equal to 130% of the uniform distribution and a subsequent decrease of 65% in the remaining frequency bins. Small changes correspond to a 60% increase. Performance improves with change size (Fig. 22A, C & E), as signified by an increase in d'. Reaction time distributions changed shape and peak as a function of change size (Fig. 33C, D & E). Median reaction time decreased with larger change sizes (Fig. 22B, D & F), in accordance with an increase in performance. Change detection is therefore dependent on the size of deviation from baseline.

**Performance is similar for all spectral locations** To perform effectively on the task, ferrets had to pay attention to the three frequency channels prone to a change in their first-order statistics. We checked whether the animals equally performed on these three frequency location. For ferret M d' is lower for the middle frequency change (Fig. 24A). As ferret M was the first ferret undergoing experiments and trained last on the middle frequency, we wondered if this decrease in performance was due to a perceptual effect (Catz and Noreña [2013]) or was a consequence of training. To investigate

this effect, middle frequency changes were introduced in second and not last for the two remaining ferrets. There is no significant difference in behavioral results as a function of change's spectral location for ferret T (see 24 C) and a significant difference for ferret B (see Fig. 24 D) for the high frequency, suggesting that ferrets are able to perform equally well on all three changes. In addition, the performance of ferret M on middle frequency improved over time over recording sessions (Fig. 24 B) and eventually reached a level of performance identical to the two other locations. Overall, those results suggests that middle frequency changes are not more difficult to detect but that the ferret was not fully trained when the electrophysiological experiment started. Therefore, trials containing middle frequency changes are removed from analysis for recording sessions with a significantly lower performance for middle frequency changes (specifically, for left FC recordings).

**Performance does not improve with a longer estimation period** A necessary property for statistical decision-making reported in chapter 2 is the improvement of the estimation with time. Change detection improves and then saturates with the length of the pre-change interval in the psychophysics study, where changes could arise from 0 up to 8s (8). Here, we do not report any significant effects of the estimation period on performance (Fig. 23A, B, C). However, in the current study, a fixed pre-change interval of 1.5s was added for training purposes, shifting the change time distribution. As a result, the shortest change time is 1.75s and behavior in the three animals suggest that the estimation of the initial distribution has already saturated.

**Performance depends on baseline first-order statistics** Performance significantly improves with the base probability in the bin containing the change in at least one ferret (Fig. 26A). This effect was also reported in chapter 2 and is consistent with the idea of an estimation of the initial distribution to allow detection of the deviations defined as the change. The effect is currently not significant for the two other ferrets (Fig. 26B & Fig. 26C) but even with a lower number of recording sessions for ferret T, a trend is already present (Fig. 26B).

**Performance on biased sessions** Attention was manipulated in "biased" sessions, where a spectral location was preferentially presented in two thirds of the changes. Independently of its identity, performance improves for the dominant spectral location in ferret M (see right side of Fig. 33A). The same tendency is observed in ferret T's behavior (see right side of Fig. 33B), it is however not significant. For both ferrets T and B, the number of biased behavioral sessions is low (respectively, n: 11 and n: 8).

**Performance within a session** Contrary to human psychophysics where clear instructions can be given, animal behavioral studies suffer from a number of shortcomings associated with non-sensory processes, such as changes in motivation during sessions (Stüttgen et al. [2011],Berditchevskaia et al. [2016]). In the case of water-deprivation, discrimination in a Go/NoGo perceptual task is initially poor, until the initial thirst is quenched (Berditchevskaia et al. [2016]). For all ferrets, the initial delay period decreases within the first 20 trials (Fig. 25A, B & C), indicating a higher number of licks after sound onset for trials located early in the session. Such effects are not directly considered or included in the following study, their impact on the neural activity variability has been reported (Renart and Machens [2014]).

**Conclusion** In summary, these findings indicate that change detection improves with change size and depends on the initial stimulus statistics, even if stimulus estimation has already saturated. These properties are consistent with a dual estimation strategy, where a decision arises if the deviation (change) from the initial estimated statistics corresponds to the animal's threshold. Statistical decision making involves reducing uncertainty by collecting more stimulus information over time and using larger differences in the stimulus property to overcome the uncertainty more rapidly.

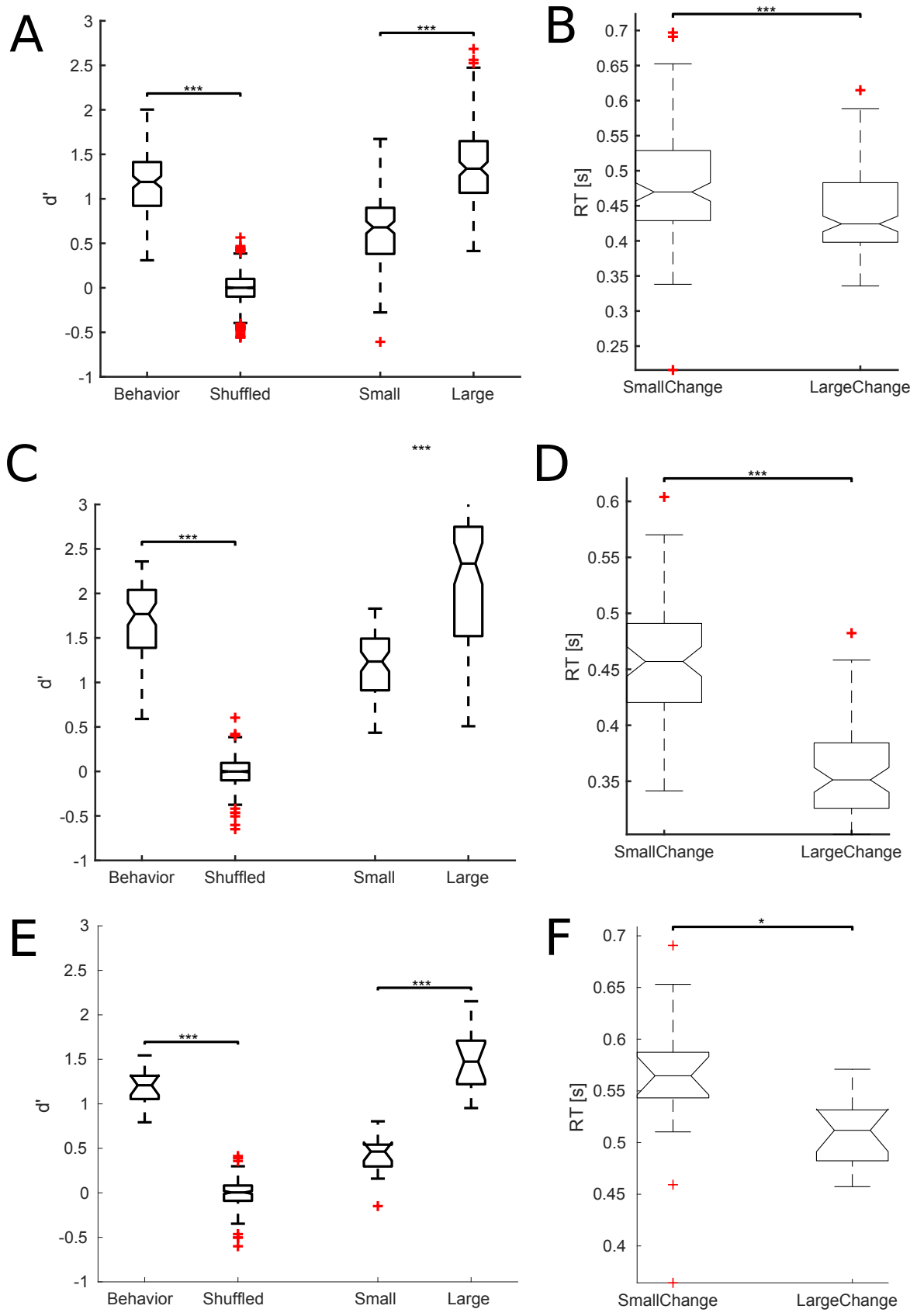


Figure 22: **d' and RT as a function of change size**
(A) Averaged d' is significantly different from chance level for ferret M. d' increases with change size ($p<0.001$). (B) Median reaction time decreases with change size for ferret M ($p<0.001$). (C,E) Similar to A for ferrets T and B, respectively ($p<0.001$). (D,F) Similar to B for ferrets T and B, respectively ($p<0.001$ and $p<0.05$).

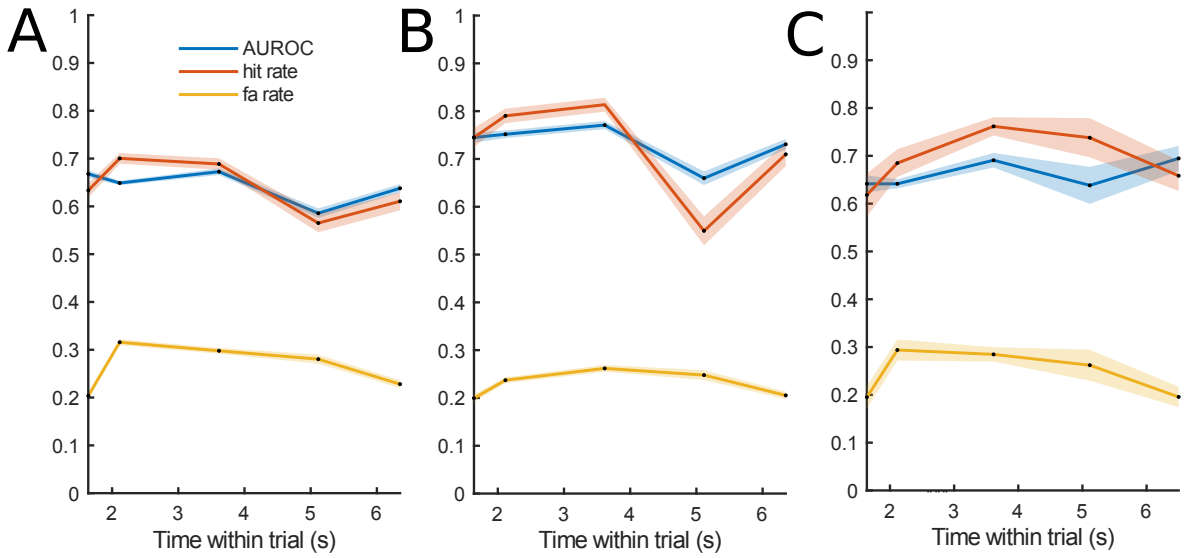


Figure 23: **Effect of change time on behavior**
(A) Behavior as a function of time within trial (d', AUROC, hit rate and false arlam rate) for ferret M does not show any significant differences.(B) Behavior as a function of time within trial (d', AUROC, hit rate and false arlam rate) for ferret T does not show any significant differences. (C) Behavior as a function of time within trial (d', AUROC, hit rate and false arlam rate) for ferret B does not show any significant differences.

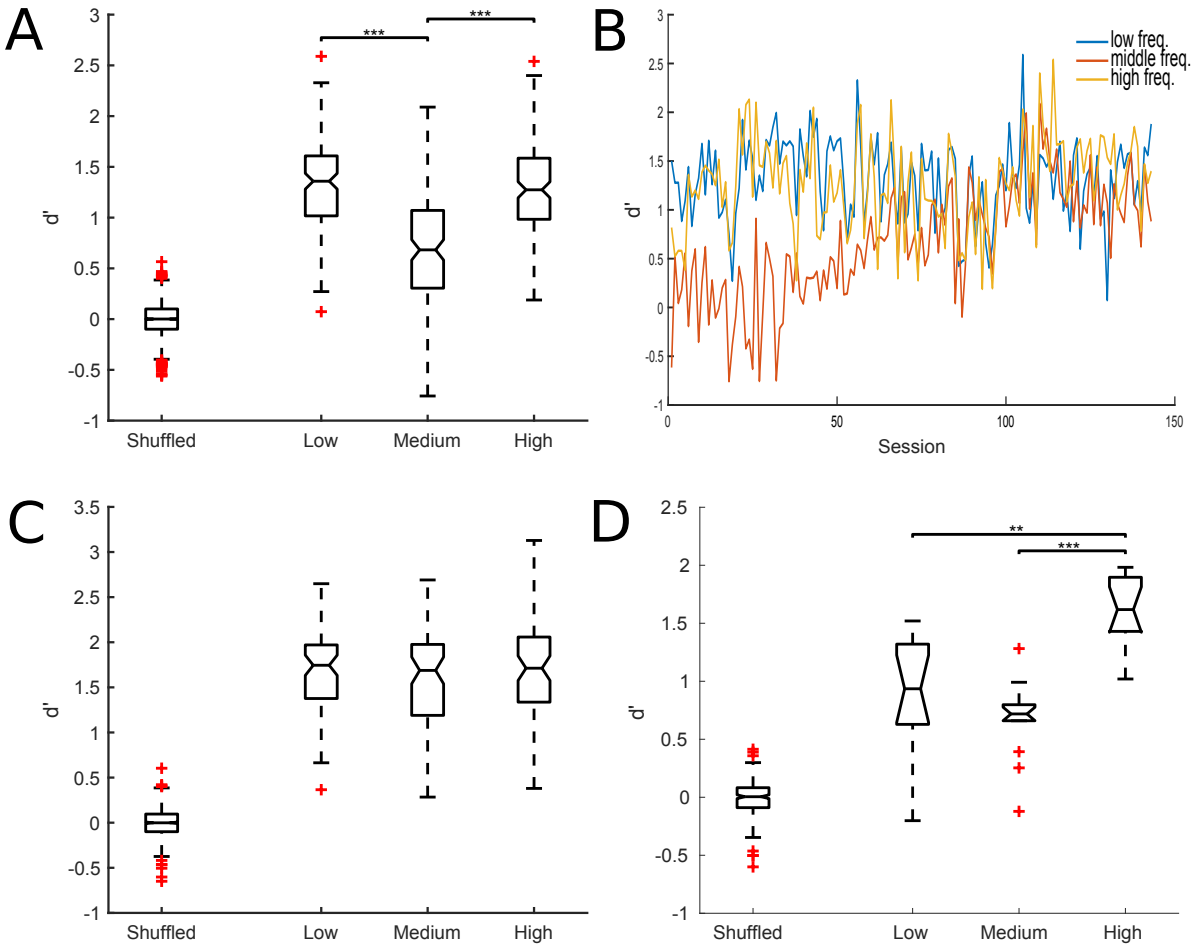


Figure 24: **d' as a function of change spectral location**
(A) d' as a function of change spectral location for ferret M. All three change locations are significantly different from chance level (left), however d' for middle frequency changes is lower. (B) Performance for middle frequency change location is initially lower than for the two other spectral locations. After 60 sessions, the performance is equal for all change locations, suggesting that the initial poor performance on middle frequency is due to the training and is therefore not a perceptual effect. (C) d' as a function of change spectral location for ferret T. All three change locations are significantly different from chance level (left) and performance is similar across frequency bins. (D) d' as a function of change spectral location for ferret B. All three change locations are significantly different from chance level (left) and performance is higher for high frequency changes.

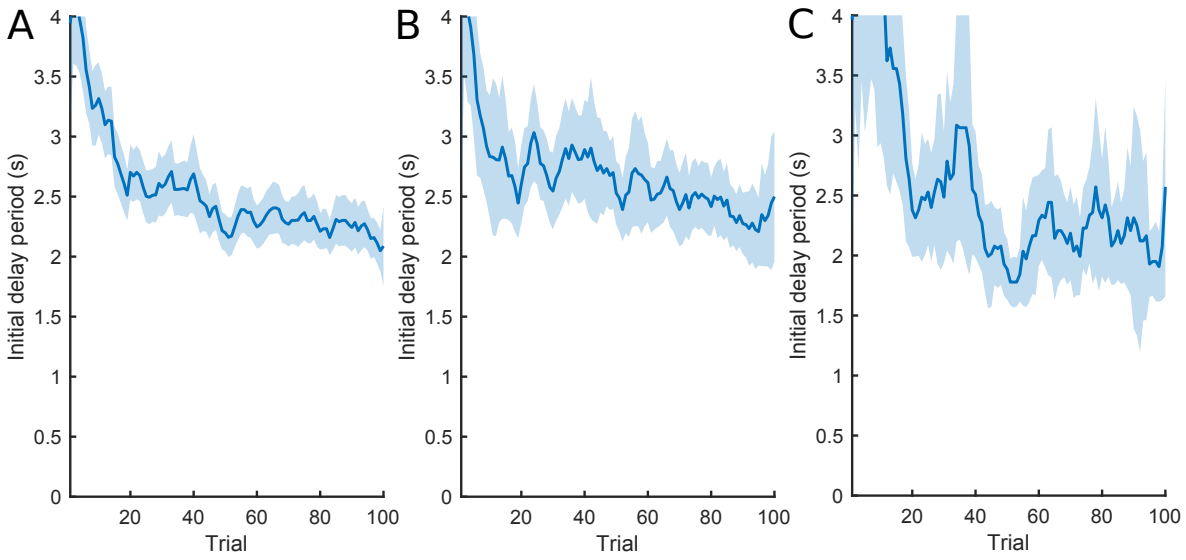


Figure 25: **Average** duration of the initial delay period **as a function of trial number**
(A) Duration of the initial delay period for ferret M as a function of trial number. Delay duration decreases at the beginning of the session and remains constant after roughly 20 trials. (B-C) Similar to A for ferrets T and B respectively.

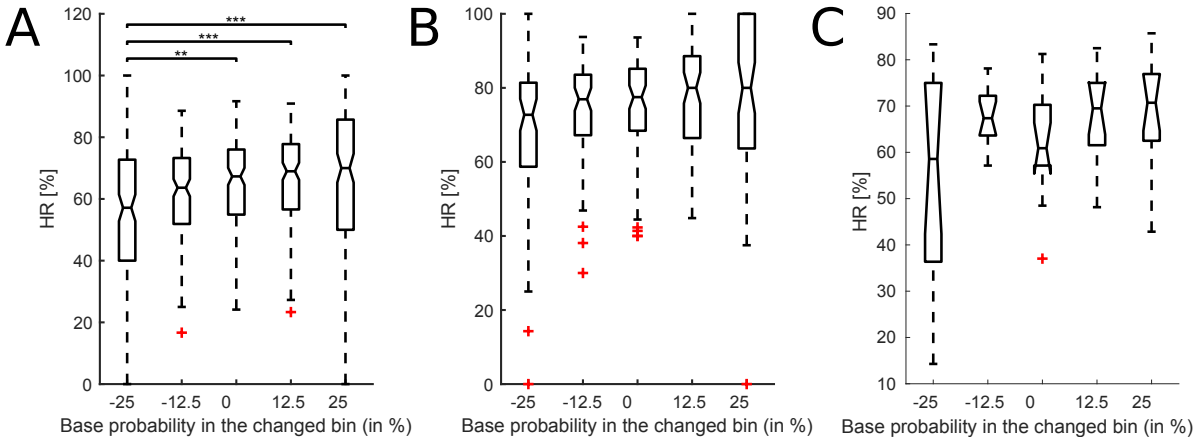


Figure 26: **Hit rate as a function of base probability**
(A) Hit rate increases with base probability for ferret M (n: 143) (B) Hit rate tends to increase with base probability for ferret T. (n: 69) (C) Hit rate tends to increase with base probability for ferret B. (n: 14)

## Behaviorally-gated selection of relevant auditory event along the cortical hierarchy

To describe the selection and amplification of relevant auditory information embedded in a continuous stream at different cortical stages, we recorded the neural activity in three cortical areas previously implicated in auditory target selection and enhancement (Fritz et al. [2003, 2010], Atiani et al. [2014],

Scott et al. [2017]). We then contrasted the population activity in response to two types of acoustic events, the sound onset and the subsequent change in first-order statistics, and investigated how change-evoked response becomes less specific to spectral location along the auditory pathway.

**Behaviorally-gated selection of the relevant auditory event along the cortical hierarchy**

To shed light on the selection of relevant information we contrast the activity associated with different acoustic events: sound onset and change. Sound onsets are salient acoustic changes but are behaviorally irrelevant, whereas change in first-order statistics are more subtle acoustic event but if detected will lead to a water reward during the active epoch. To ascertain the effect of task engagement, similarly to Fritz et al. [2003] and following studies, we contrast also the activity of the same populations recorded during behavior and during the first passive presentation of the stimuli.

**Task-irrelevant sound onset is filtered out at the level of frontal cortex** The magnitude of sound onset-related responses decreases along the cortical pathway independently of the behavioral context (Fig. 27A, B & C, left panels). Because sound-evoked responses can result in decrease or increase of neuronal firing rate, we further quantified this effect using a linear discriminant classification method (Fig. 38) over time. This decoding was done with the same number of units in each area (roughly 80) for passive and engaged conditions in all three cortical regions of ferret M (Fig. 27E). Decoding performance for other ferrets are displayed in the supplementary. Peak decoding accuracy displayed in Fig. 27D allows for the comparison of task engagement effects on the event cortical encoding. Not surprisingly, sound onset can be reliably decoded in A1 for both active and passive conditions. Decoding accuracy is significantely smaller in PEG during passive state compared to the engaged condition. This effect is, however, not present in ferret T auditory belt population (Fig. 35A, left panel). In both A1 and PEG decoding accuracy is still above chance level. In FC, sound-onset can no longer be decoded in both ferrets, irrespective of task-engagement. Overall, those results indicate that the task-irrelevant acoustic event is filtered out at the level of frontal cortex.

**Task-relevant change event is amplified along the cortical hierarchy** In contrast, task-relevant changes, though variable in spectral location and subtle in amplitude, are propagated and amplified along the cortical pathway during task engagement (Fig. 27, middle panels). Accuracy for decoding change events without taking into account units tuning properties (Fig. 27E for ferret M) is only significantly different from chance level in PEG and FC. As expected from the responses displayed in (Fig. 27B,C, right panels), decoding accuracy improved significantly with task engagement in these two

areas. These results are consistent with an emergence of task-relevant selectivity along the auditory pathway related in Atiani et al. [2014] and Fritz et al. [2010], extending this finding in the context of change detection in a continuous acoustic stream.

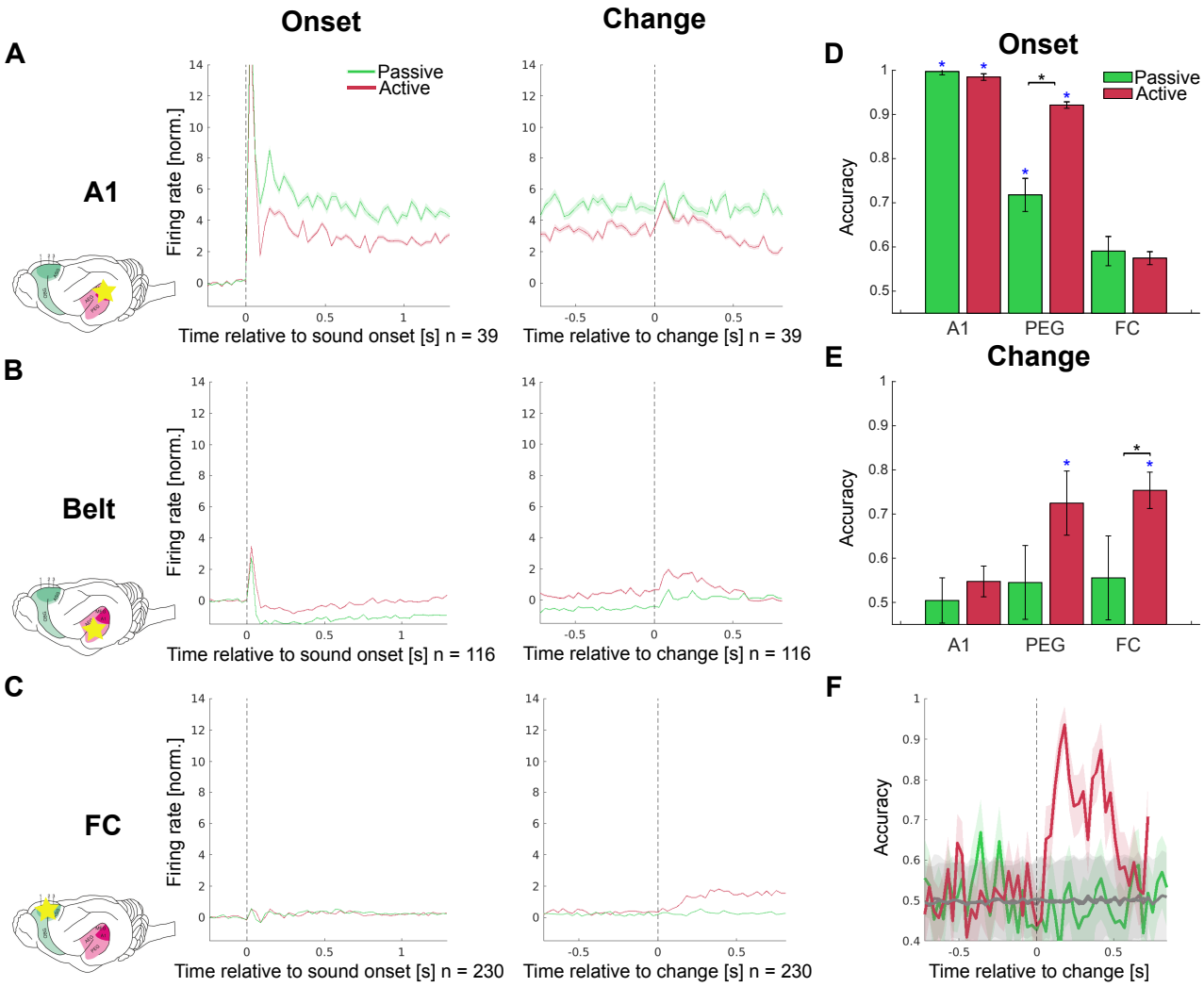


Figure 27: **Average acoustic event-related single-unit activity in A1, auditory belt and FC** (A) Average single-unit z-scored activity in A1 relative to sound onset and change (ferret: 1) (B) Average single-unit z-scored activity in belt auditory cortex relative to sound onset and change (ferret: 2) (C) Average single-unit z-scored activity in FC relative to sound onset and change (ferret: 3) (D) Sound onset peak decoding accuracy for each cortical area and behavioral state (number of units 79, limited by A1 unit number). (E) Change peak decoding accuracy for each cortical area and behavioral state (number of units 80, limited by A1 unit number). (F) Change decoding accuracy in ferret M FC (282 units) for active (red) and passive state (green) per 30ms bins. Chance level in grey from permutation of labels ('Change', 'No change'). Standard deviation is computed over 100 cross-validation.

**Change representation is generalised along the cortical pathway**

Frequency tuning is narrower in primary than secondary auditory regions (e.g. Fig 2B in Atiani et al. [2014]). Because we pooled change events across spectral locations (low, middle, and high frequencies), it could be that the discrepancy in change-evoked response between A1 and PEG is due to broader tuning in PEG or opposite-signed response type from A1 unit (example in Fig. 28A,B). We therefore performed change decoding while keeping only trials in which change was localized at the unit's best frequency ('localized' condition in Fig. 35). In doing so, decoding accuracy in A1 and PEG increases in the passive condition (passive localized compared to passive all trials in Fig. 28C). However, this effect was observed only in A1 during task-engagement. During behavior, PEG shows a non-frequency selective response pattern. This results is replicated in the belt area of a second ferret (see Fig. 35A). All together, this suggests that PEG stimulus representation becomes less feature-based in a context-dependent fashion. In FC the decoding accuracy is high for all changes during behavior indicating a generic response to task-relevant changes specific to task-engagement.The drop in accuracy 'localized' in FC in mainly due to a poor description of FC responses by the ROC analysis, since the the population dynamics are heterogeneous (i.e, it is hard to define a good window). In only one of the three ferrets change can be decoded above chance in FC, due to a small number of change responsive units in the two other animals (as well as a smaller number of recordings so far). This was caused by lack of flexibility in recording location associated with the arrays implantation (see Fig. 35 A). Similar activity was however found in the three ferrets as the example units in Fig. 35B & C show.

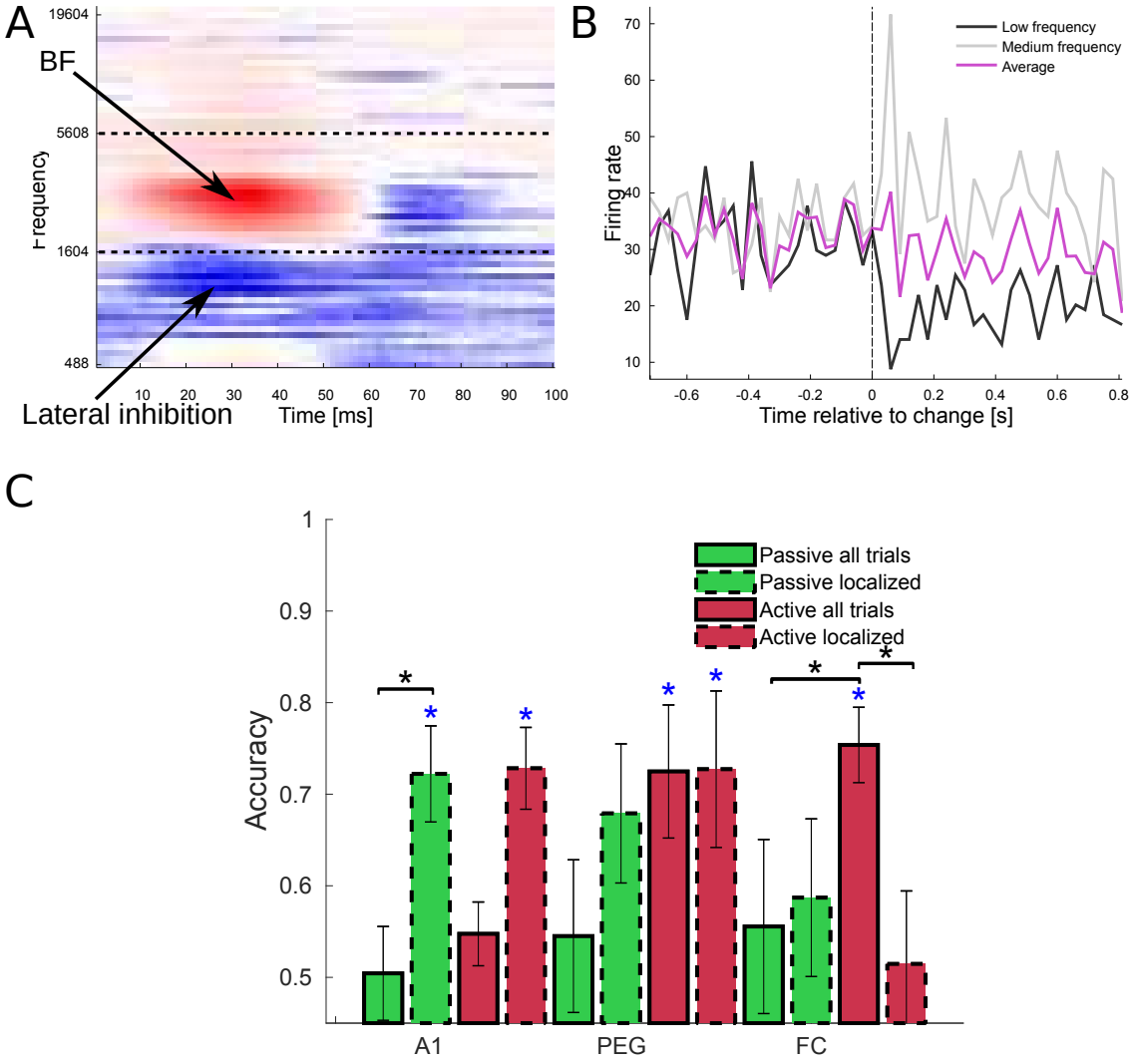


Figure 28: **Behavior-dependent and tuning-dependent decoding accuracy along the cortical pathways**
(A) Receptive field: A1 example cell. BF is located in the middle frequency band and lateral inhibition in the low frequency band. (B) Change-related PSTH for A1 example cell, as predicted by receptive field shape, change-related modulations are of opposite signs for low and medium frequency changes. (C) Change peak decoding accuracy for each cortical area and behavioral state, either taking into account tuning ('localized') and selecting the appropriate trials, or not. All trials bars are identical to the data showed in Fig. 27. Decoding accuracy improves in A1 when taking into account tuning in both behavioral states. For PEG, tuning only improves decoding accuracy in the passive condition and does not in FC (ferret M).

Overall, those results suggest a scenario in which secondary auditory regions respond more vigorously to any type of acoustic event similar to the target to detect, be it sound onset or change in first-order statistics. In a second time, frontal cortex is gating task-irrelevant event such as the sound event to exhibit a target-specific response. This leads to a step-wise abstraction of the change representation along the auditory hierarchy that is dependent on the task-engagement, even in fully trained

animals.

## Population dynamics before the change

### Population activity is time-modulated before change

Activity in a large variety of brain areas, such as monkey primary motor cortex (M1) and premotor cortex (PMd) (Thura and Cisek [2014]), rat frontal orienting field (FOF) and posterior parietal cortex (PPC) (Scott et al. [2017] Fig 3F), varies as a function of time in perceptual decision-making tasks over seconds. While some of those slowly modulated pattern of neuronal activity are clearly related to accumulation of sensory evidence (see also parietal EEG signal in Chapter 1 and O'Connell et al. [2012]), others have been related to various types of signals such as urgency to respond or contextual information about the task structure. This urgency signal was described in a task where monkeys are free to respond at any time in face of growing sensory evidence (Thura and Cisek [2014], Thura et al. [2012]). Prior information about target stimulus timing, can also be reflected in population activity Carnevale et al. [2015].

In our paradigm, these different factors can affect population dynamics in the pre-change period. First urgency can play a role, but its contribution should be limited to the very first 2 seconds of trials, since false alarm then stabilizes (Fig. 23). Because of the 1.75s-long minimal duration of the pre-change period, ferrets could refrain from licking during this duration. Last, temporal integration of the initial baseline statistics are another phenomenon that could occur during this initial trial phase.

We thus displayed averaged single-unit activity in the three cortices are displayed as a function of time within trial and before appearance of change (or before initiation of motor response for false alarms, taken as 90ms) in Fig. 29 (MU: Fig. 36). Both FC and PEG averaged activity changes slowly over multiple seconds (also see example cells in Fig. 30). Those examples cells are not isolated cases, the population of cells in FC shows a variety of dynamics (Fig. 30).

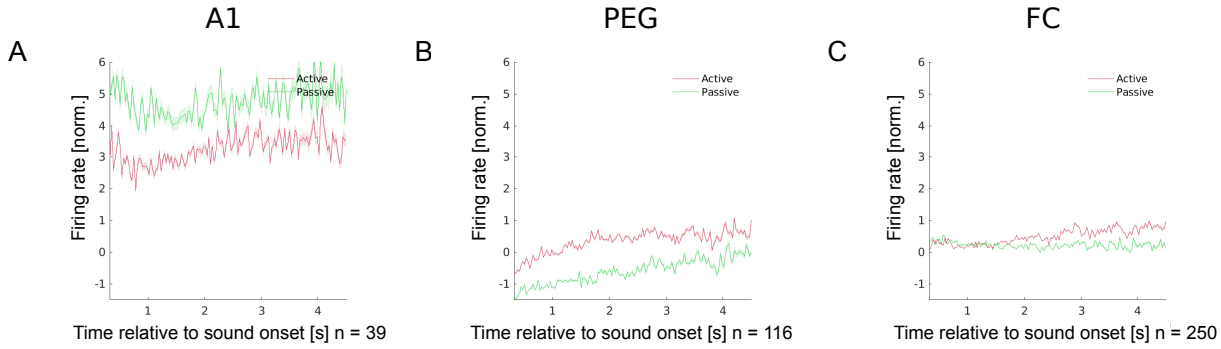


Figure 29: **Average single-unit activity within trial and before the change in A1, auditory belt and FC**
(A) Average single-unit z-scored activity in A1 300ms after the sound-onset and up to change or 90ms before a false alarm (ferret: 1). (B) Average single-unit z-scored activity in PEG 300ms after the sound-onset and up to change or 90ms before a false alarm (ferret: 2). (C) Average single-unit z-scored activity in FC 300ms after the sound-onset and up to change or 90ms before a false alarm (ferret: 3).

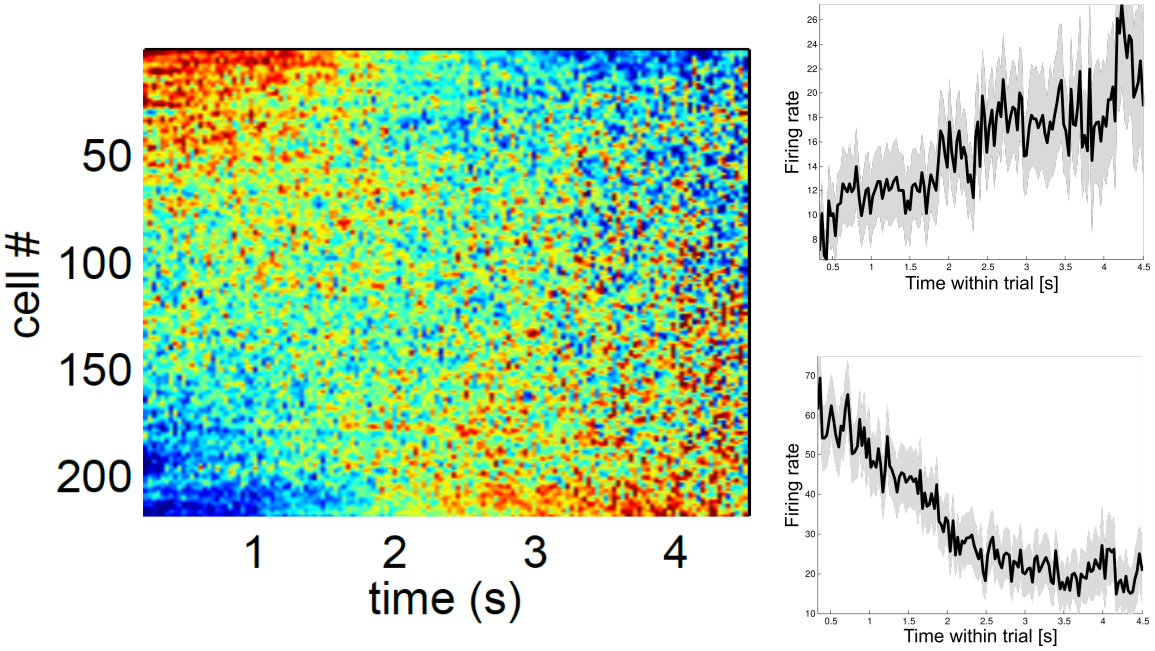


Figure 30: **Population activity within trial and before the change in ferret M FC shows temporal scaling**
Firing rate for FC units from locations 1&7 in ferret M during the pre-change period organised by weights on PC1. Some units increase of decrease their firing rate slowly over the range of seconds, as illustrated in both example cells (right).

**PCA captures time varying dynamics before the change in FC and PEG**

We used a PCA approach to visualize in a reduced space population dynamics in the period preceding change and its relationship with outcomes and post-change activity. The first two principal

components for ferret M captured respectively 16%, 10% and 21% of variance in A1, PEG and FC. For FC and to a lesser extent PEG, pre-change activity evolves over the first component (Fig. 31, black circles growing in size with time), whereas it is clustered in A1, consistent with the activity in Fig. 30. Interestingly, the second component mainly captured population activity related to the final behavioral outcome of the ongoing trial, and this even before the trial started (see pre-trial epoch symbolized in Fig. 30) (see Fig. 31C & 37A, pre-stimulus marker per outcome: filled square). In FC time-dependent population dynamics on PC1 did not show differences depending on the future outcome of the ongoing trial (Fig. 32A). Therefore outcome-independent population dynamics along PC1 cannot be driven by an urgency signal, which would otherwise translate in a *growing* discrepancy in between the miss and false alarm curves (see Fig. 32A).

Because the first 1.75s of each trial did not contain any change, slow fluctuations in FC population could be a contextual signal matching this fixed pre-change. In particular, one would expect these dynamics to reflect a distance to decision criterion Carnevale et al. [2015]. As the trial progresses, the time-varying population activity would facilitate crossing of a decision threshold in the neural space. We therefore wanted to test the hypothesis that time-varying dynamics along PC1 (computed only from pre-change activity) are aligned in the neural space with post-change activity. For this, we projected into the space formed by the first two components the post-change activity from all three cortical areas. We took up to 450ms for hit and miss trials and the last 450ms before the first lick for false alarm trials, excluding the last 90ms before the lick for hits and false alarms. In FC, projections of hits and misses evolve in the PC1/PC2 subspace as a function of time (see Fig. 31C). Hit trial trajectory are similar to pre-change dynamics in the PC1/PC2 space. Surprisingly, the same dynamics can also be found in ferret T, even if the number of change-related cells is to low to decode above chance (see Fig. 32B and Fig. 37B).

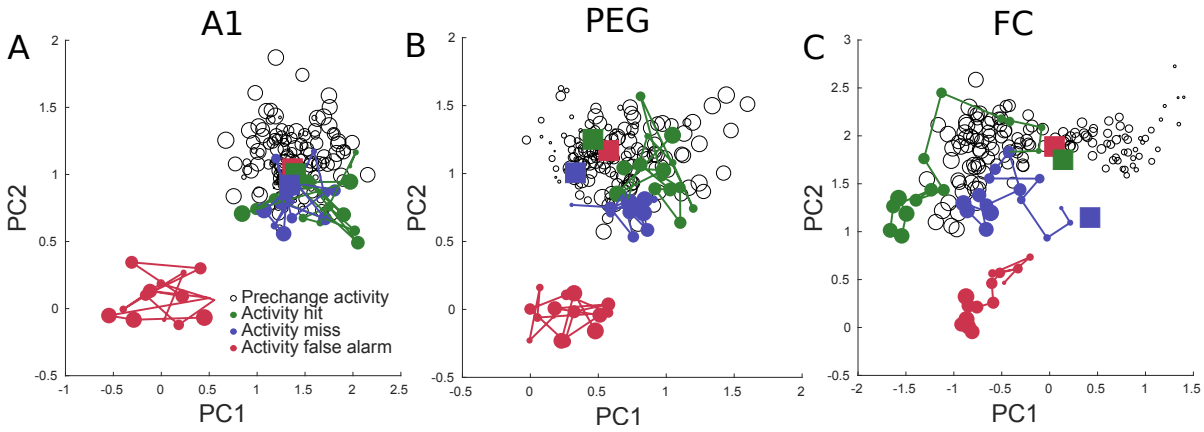


Figure 31: **Population dynamics in PC1/PC2 space before the change and per outcome after the change**
(A) Mean population activity pre-change and outcome related activity for 450ms after the change or from 450ms before of false alarm in PC1/PC2 space in ferret M A1. The size of the dot corresponds to time within the trial or after the event. Both activity pre- and post-change are clustered along PC1. Post-change outcome is separated along PC2. Pre-stimulus marker per outcome: filled square (B) Mean population activity pre-change and outcome related activity for 450ms after the change or from 450s before of false alarm in PC1/PC2 space in ferret M PEG. Before the change population varies with time along PC1. Post-change outcome is separated along PC2.(C) Mean population activity pre-change and outcome related activity for 450ms after the change or from 450s before of false alarm in PC1/PC2 space in ferret M FC. Before the change population varies with time along PC1. The post-change outcome is separated along PC2. The trajectories are similar for the activity pre-change and post-change hits.

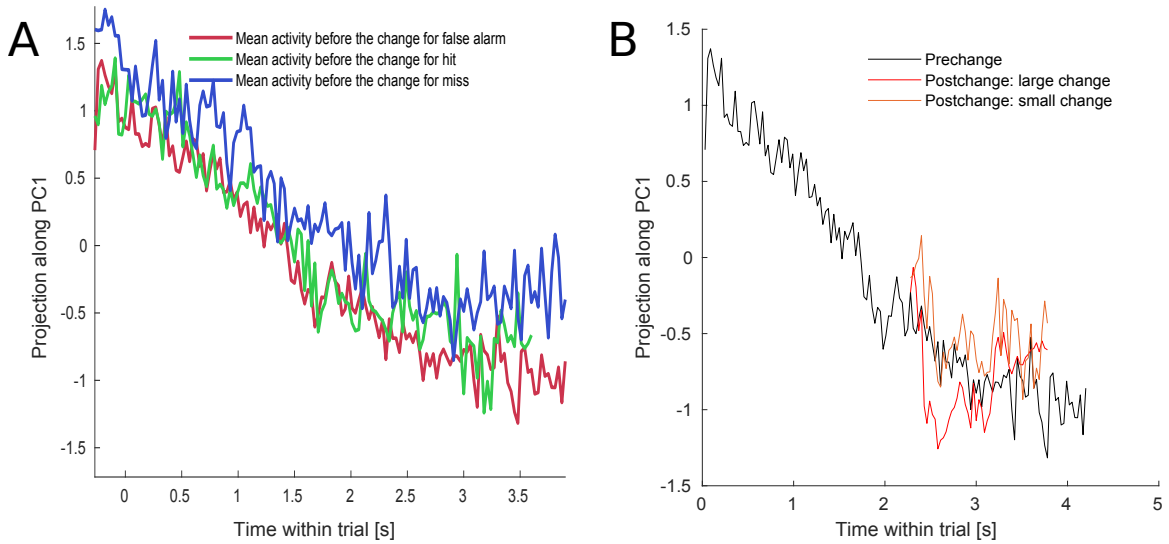


Figure 32: **Population dynamics projection on PC1 per outcome for FC**
(A) Projection of the mean activity before the change per outcome in ferret M FC. Overall outcome activity evolve over time along PC1 and the dynamic for hits and false alarm is similar for all outcome, suggesting that this activity is not relating to urgency. (B) Projection of averaged pre-change and hits post-change activity per change size in ferret M FC. The post-change activity follows a similar trajectory that the prechange one. In addition, the projection is scaled by the change size, indicating that those projections are not orthogonal.

We wanted to ascertain the relationship between the projections before and after the change. We thus computed the angle (Carnevale et al. [2015]) between each PC and the average change decoding vector that independently provided the axis along which change are encoded. PC1 and the decoding vector in FC are correlated in ferret M (101°, $p<0.05$). PC2 and the decoding vector in FC are not orthogonal in ferret M (78°, $p<0.05$). In ferret T only PC1/decoding vector (67°, $p<0.05$) . The activity preceding the event is not only time-varying but captures some aspect of the post-change activity. This indicates that a subset of the cell population in FC that encode for the change (high weights on the decoder) show a firing rate modulation as a function if time preceding the change. Overall, those observations are consistent with time-varying population activity facilitating crossing of a decision threshold in the neural space (note that the time varying activity is not present in the passive state in FC, see Fig. 29C).

## Discussion

Ferrets were able to constantly monitor an acoustic stream and detect changes in its first-order statistics, achieving a dual estimation strategy similarly to human subjects in Chapter 2. Even if the stimulus presented to the ferret is simplified (reduced number of possible spectral location, stimulus spectrum is wider and change timing distribution is narrower), the reaction-time design leads to relatively high false alarm rates. Also, change spectral locations' multiplicity renders the task more challenging. False alarms are useful to disentangle the motor contribution to a signal recorded in the FC (see next Chapter, 40) because a motor event is produced without the signal being present. However, their definition is problematic in our experiment as early responses and false alarms are manifested in the same way. And because our stimuli are probabilistics, a subset of false alarms are linked to deviations in the tone cloud that resemble changes. In addition, results from Berditchevskaia et al. [2016] indicate that in the case of positive reinforcement with water reward, the first part of the session is driven by the animal initial thirst and higher false alarms rates. The actual performance of the ferrets is consequently underestimated.

Along the auditory pathway the representation of changes became abstracted from stimulus features (Rossi-Pool et al. [2016], Fritz et al. [2010] and Brincat et al. [2018]). At the level of the primary auditory cortex, and contrary to the frontal cortex, task-engagement does not impact how well one can decode the change from the population activity (Fritz et al. [2010], Atiani et al. [2014]). Both abstraction and gating seem to take place in a step-wise fashion, since at auditory belt areas level the abstraction is itself gated. In addition both auditory events in the belt area are more represented

during behavior. Effects of task-engagement on auditory representation of a target are well described (Fritz et al. [2003], David et al. [2012], Atiani et al. [2009]). However, in most of those studies the target is a specific frequency and changes in the receptive fields based are predictable (with respect to the target frequency). In the current task, target events, i.e. change, exhibit some uncertainty (apart for biased session) about their spectral location. It is therefore unclear how the receptive fields in the belt area adapt to achieve better change (and the onset) representation during behavior. Further investigations, using the biased sessions (with mostly one change spectral location) could shed light on this issue (Biased sessions and Belt recordings exist for ferret T).

We do not report significant differences in decoding accuracy between active and passive in A1. This however, does not allow to conclude that the change representation is identical in between behavioral state, suggesting that A1 acts simply as an acoustical filter. The hierarchical view under which sensory cortices merely extract and represent stimulus features is currently being challenged (Bizley et al. [2013], Zhou et al. [2014], Petreanu et al. [2012], Bagur et al. [2018]).

FC activity preceding the change varies a a function of time. What role this signal plays in the decision process is still unclear, although our evidence rejects urgency and argues for a facilitation of the decision process because it is somewhat related to the post-change activity. Whether, this process reflects confidence, a better representation of the stimulus baseline, or simply time can not be determined with the current form of the experiment. Dissociating the start of the trial from sound onset could enable this distinction.

The traditional view under which both evidence accumulation and decision formation take place in higher-order cortical areas (parietal and frontal) is being reformulated. Experiments combining behavior, pharmacology, electrophysiology and optogenetics have demonstrated that LIP is not causally implicated in decision-making and that the striatum could be responsible for evidence accumulation Yartsev et al. [2018], Katz et al. [2016]. Together those results, call for a more systematic description of functional role of different cortical and subcortical areas in perceptual decision-making.

## Supplementary

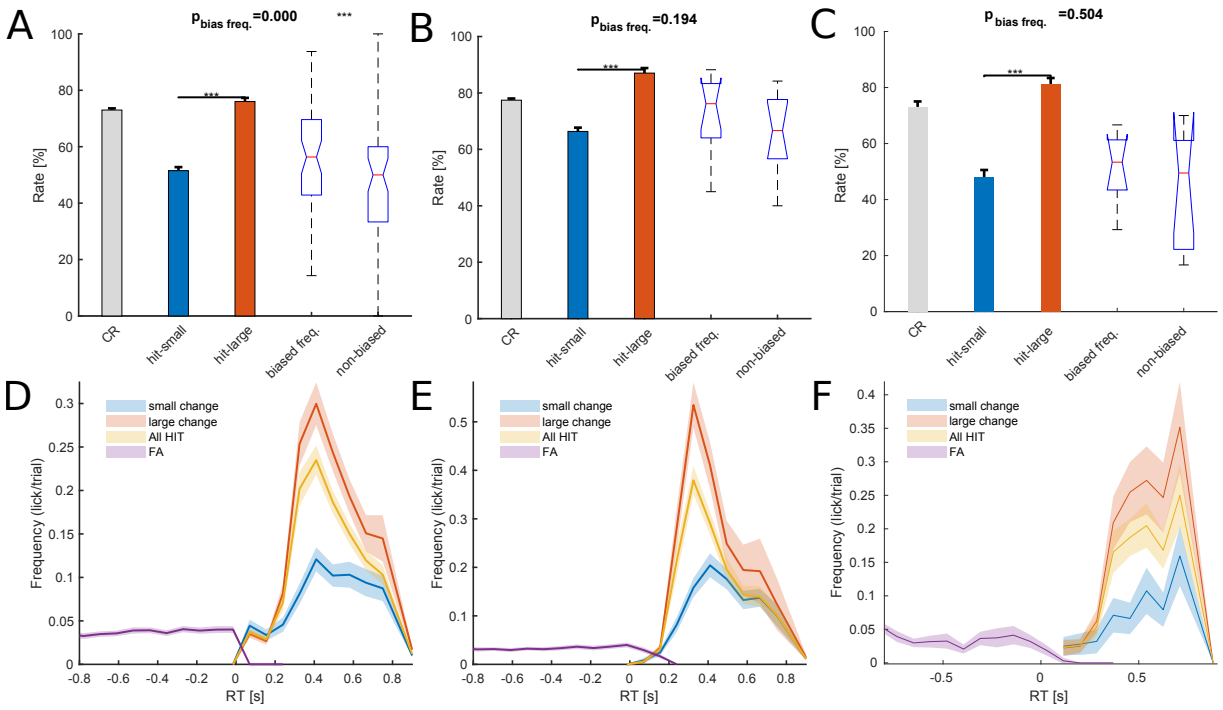


Figure 33: **Supplementary behavior**
frequency and non biased frequency. Detection improves with change size and presentation frequency (biased, n: 52). (B) Ferret T. average hit rate for CR, small changes, large changes, biased frequency (n: 11) and non biased frequency. Detection improves with change size. (C) Ferret B. average hit rate for CR, small changes, large changes, biased frequency (n: 8) and non biased frequency. Detection improves with change size. (D) Ferret M reaction time distribution per outcome. False alarm distribution is uniform, whereas hit RT distribution is peaked. The peak value and spread of the distribution is change size dependent. (E) Ferret T. reaction time distribution per outcome. False alarm distribution is uniform, whereas hit RT distribution is peaked. The peak value and spread of the distribution is change size dependent. (F) Ferret B. reaction time distribution per outcome. False alarm distribution is uniform, whereas hit RT distribution is peaked. The peak value and spread of the distribution is change size dependent.

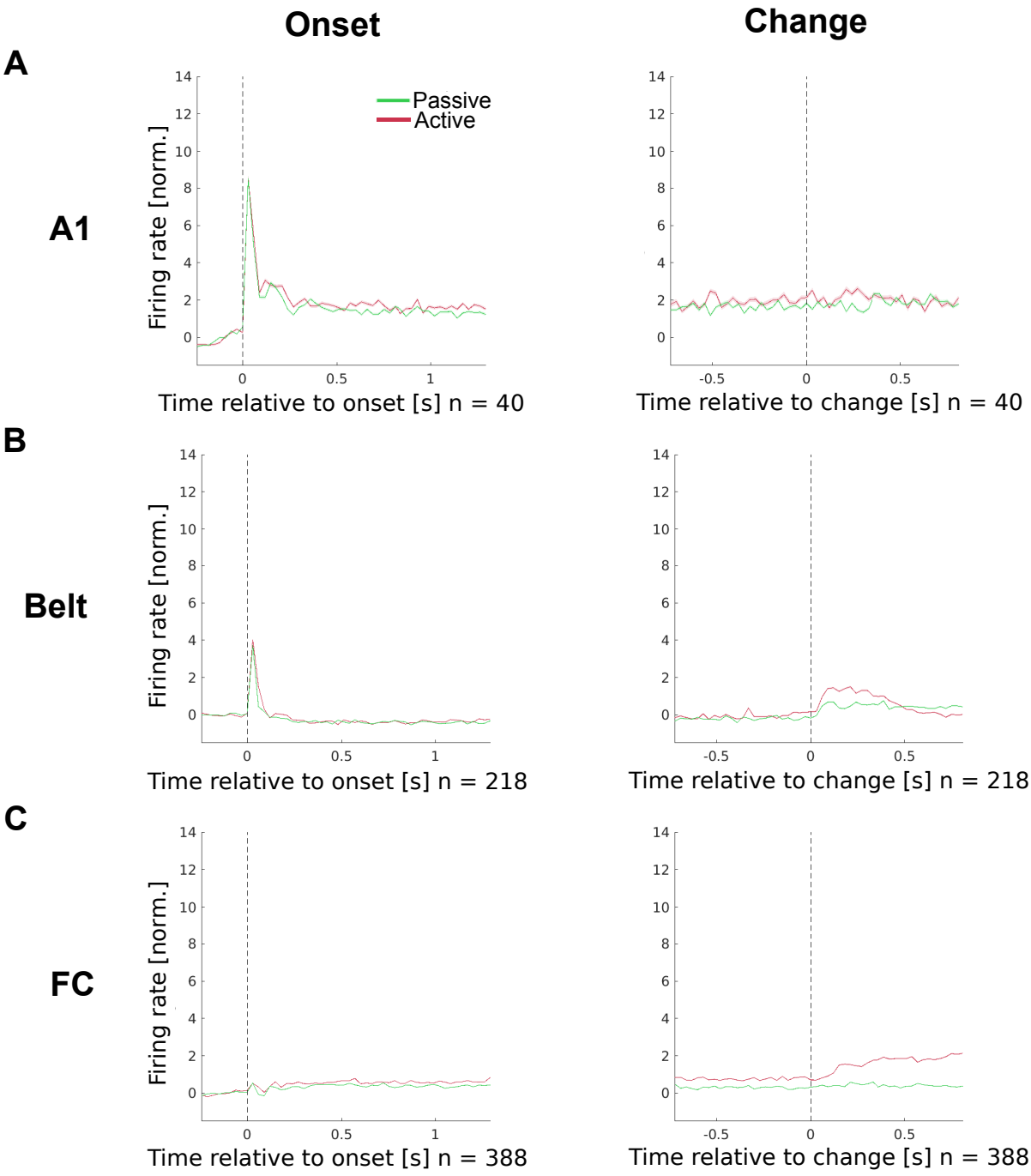


Figure 34: **Average acoustic events-related multi-unit activity in A1, auditory belt and FC** (A) Average multi-unit z-scored activity in A1 relative to sound onset and change (ferret: 1). (B) Average multi-unit z-scored activity in belt auditory cortex relative to sound onset and change (ferret: 2). (C) Average multi-unit z-scored activity in FC relative to sound onset and change (ferret: 3).

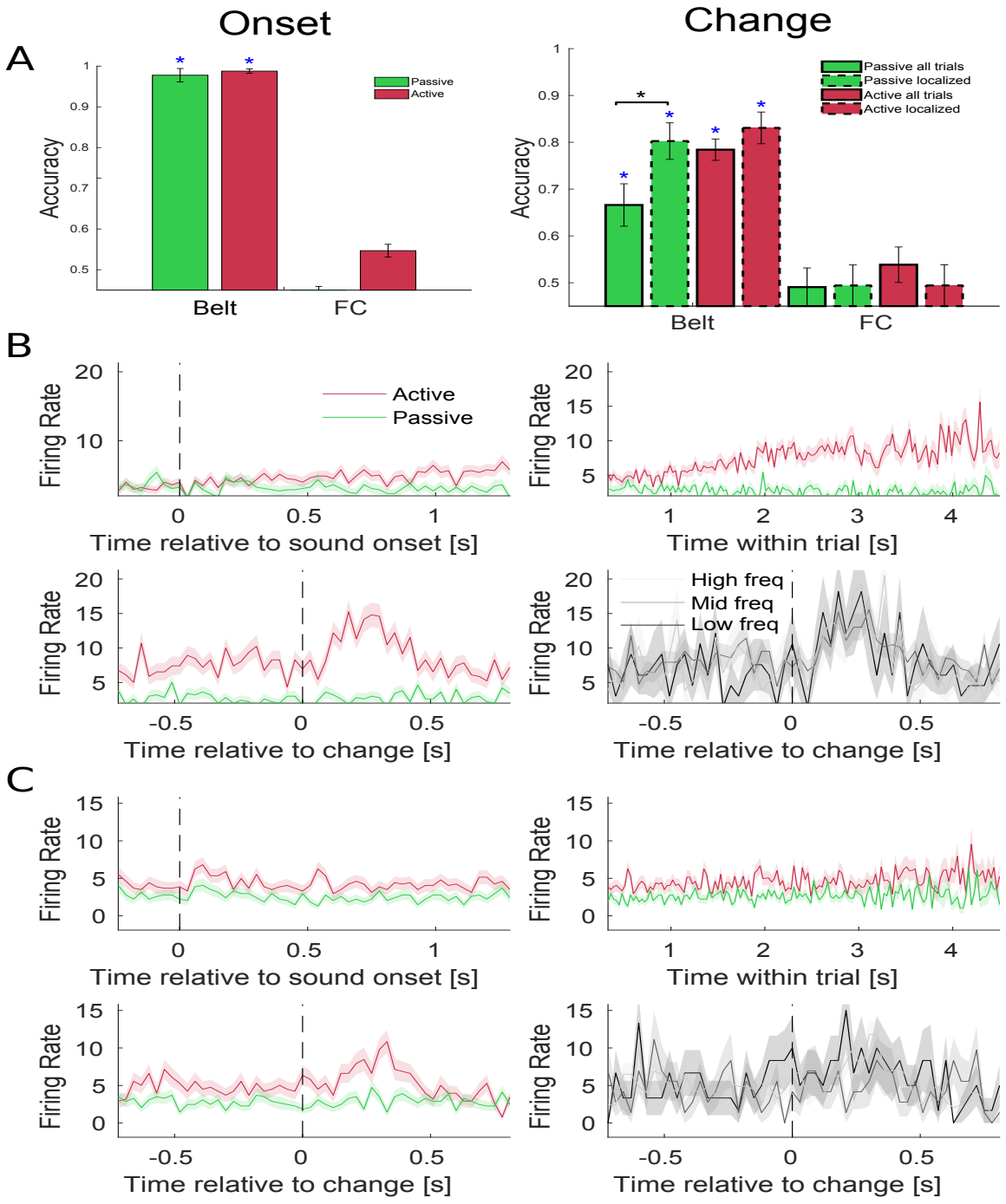


Figure 35: **Average multi-unit activity within trial and before the change in A1, auditory belt and FC**

(A) Change peak decoding accuracy for each cortical area and behavioral state, either taking into account tuning ('localized') and selecting the appropriate trials, or not. For the auditory belt area, tuning only improves decoding accuracy in the passive condition. Peak accuracy is at chance level for FC (ferret: 1). (B) Task-event PSTHs summarising the activity of a FC multi-unit recorded in ferret T Similar to what we found in ferret M, the activity of this unit increases with time and is strongly modulated after the change for all change spectral location. Those effects are only present during behavior. (C) Task-event PSTHs summarising the activity of a FC single-unit recorded in ferret B Similar to what we found in ferret M with a change-related modulation during behavior. The low frequency change response seems to capture most of the change-related modulation, this is due to the cell being recorded during a low frequency biased session.

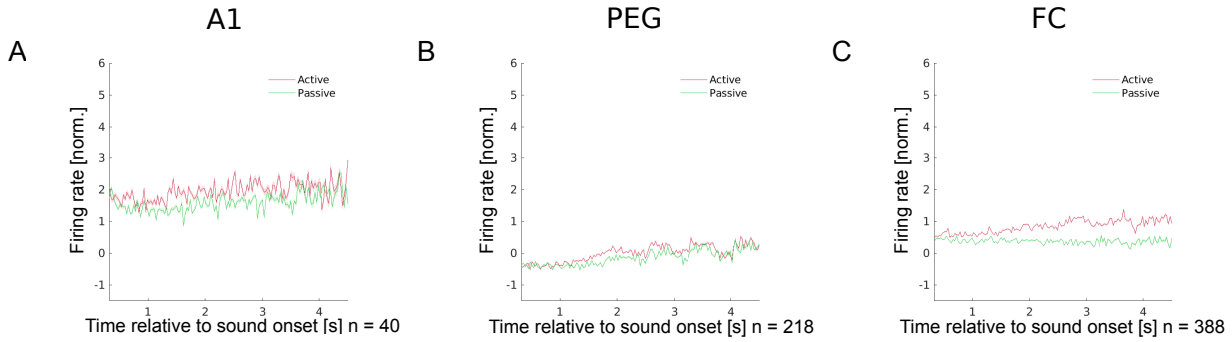


Figure 36: **Average multi-unit activity within trial and before the change in A1, auditory belt and FC**
(A) Average multi-unit z-scored activity in A1 300ms after the sound-onset and up to change or 90ms before a false alarm (ferret: 1). (B) Same in Belt (ferret: 2). (C) Same in FC (ferret: 3).

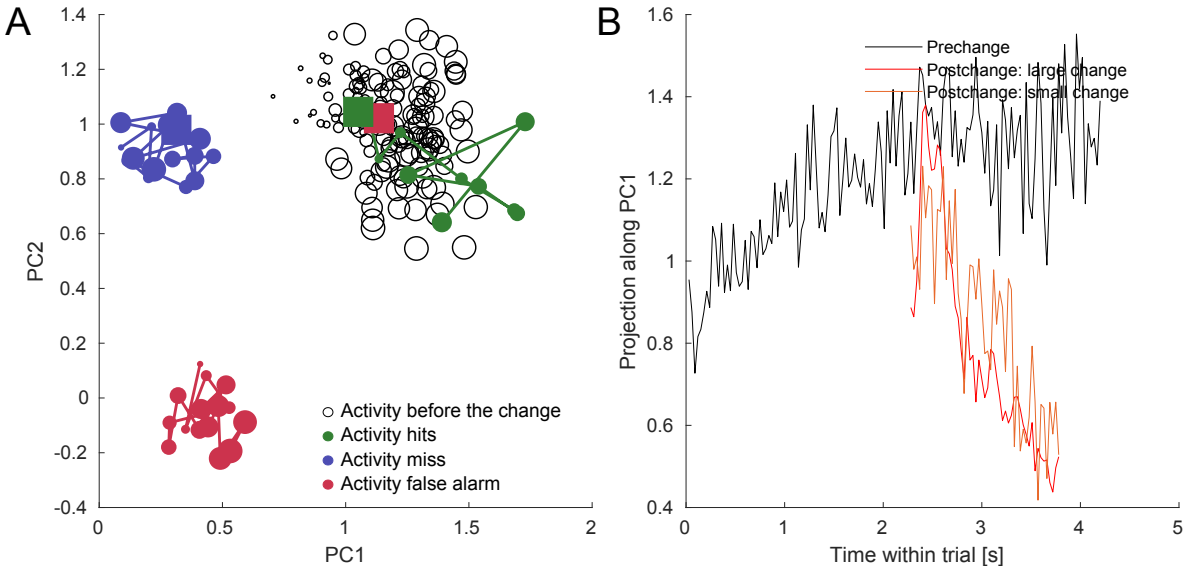


Figure 37: **Population dynamics in PC1/PC2 space before the change and per outcome after the change for ferret T**
(A) Mean population activity before the change and outcome related activity for 450ms after the change or from 450ms before of false alarm in PC1/PC2 space in ferret T FC. Post-change outcome is separated along PC2 and PC1. T (B) Projection of averaged activity for hits post-change per change size in ferret M FC. Post-change projection is scaled by the change size, similarly to ferret M (see Fig. 32B).

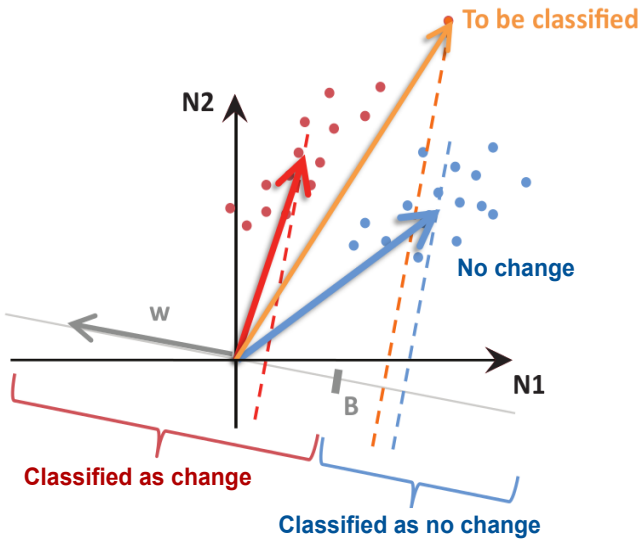


Figure 38: **Illustration decoding**Illustration of binary classifier (from Bagur et al. [2018]).

# Chapter 4: From sensory evidence to categorical decision in ferret frontal cortex


## Abstract

The frontal cortex is often associated with enhancement of relevant information for goal-directed behavior. In particular, frontal cortex (FC) neurons of the behaving ferret have been shown to respond selectively to target auditory stimuli during discrimination tasks (Fritz et al. [2010]). However, in natural and cluttered environments, sounds are not necessarily presented in token-based sequences (Thura and Cisek [2014]). Instead relevant events are embedded in continuous sound streams and their detection demands to dynamically update the representation of incoming stimuli (Boubenec et al. [2017]). Here, we attempt at characterizing the extraction of relevant sensory information from complex continuous sounds performed at the level of frontal areas. To address this question, we trained ferrets on a change detection paradigm where animals have to constantly monitor a stochastic and continuous acoustic stream to detect subtle statistical changes. We then gathered electrophysiological data in the dorso-lateral FC of the behaving ferret. Because modulations in FC neurons' firing rate can be correlated with a large variety of (sometimes overlapping) task-relevant and irrelevant events, we used a Linear Non-Linear Poisson model to disentangle the contribution of different task events (sound onset, change in stimulus statistics, decision, motor activity and sound offset) to those modulations. Our model allowed us to orthogonalize the responses to each predictor and quantified their specific contribution to the firing rate of individual neurons. By contrasting responses of neurons for different behavioral outcomes (hit vs. miss and small vs. big changes) in combination with a demixed PCA, we found that neurons encoded both stimulus changes in a stimulus-dependent manner and perceptual decisions in a categorical stimulus-independent fashion. In addition, a fraction of the neurons displayed a dual encoding of these two types of events, suggesting that conversion from sensory

evidence towards a decision signal may take place in the FC.

## Introduction

One of the fundamental problem of the perceptual decision-making field is how the brain processes the sensory evidence and converts it into a decision. The functions attributed to the prefrontal cortex range from emotions to rule representation and selection, it is thought to be highly involved in cognitive functions (Carlen [2017]). FC and more specifically the dorso-lateral and premotor cortices have been implicated by a number of studies in target selection, accumulation of evidence, and decision process (Rossi-Pool et al. [2016], Romo and de Lafuente [2013], Romo et al. [2004], Zhou et al. [2016b], Fritz et al. [2010]). A number of task-specific information for action selection have been associated with these areas (Kim and Shadlen [1999], Wallis and Miller [2003], Thura and Cisek [2014]), and it is likely that, in our task, FC is amongst the regions contributing decision formation given change-related signals described in Chapter 3. The prefrontal cortex has been known for representing a wide number of task-related variables such as target enhancement, outcome, reward and having decision-related activity, as well as premotor activity in a number of species (Mante et al. [2013], Rigotti et al. [2013], Machens et al. [2010], Kobak et al. [2016], Fritz et al. [2010], Zhou et al. [2016b], Romo and de Lafuente [2013]). The heterogeneity in the responses and dynamics of individual cells can not be simply captured by averaging the responses (Kobak et al. [2016] and see Fig. 40). The reaction-time design allowed us to have a precise end point to the decision process. However, the period during which the decision evolves is short as median reaction time are about 500ms and Drugowitsch et al. [2012] suggest a 200ms without a decision process. Thus, it is hard to differentiate the contribution of different components. In the present chapter we present two approaches to characterize the variety of responses to different task-events in the recorded population of cells. First, we use a generalized linear model to tease apart the different contribution of these events: sound onset, change, decision, licks (motor command), and sound offset. Second, we use a demixed PCA to specifically look at the interaction between sensory and decision encoding in FC.

# Materials and Methods

## Analysis

### Linear-Non linear Poisson Model

To characterize the population activity we use regression-based generalized linear model (Paninski et al. [2011], Lawhern et al. [2010]).

We describe the firing rate of the neurons as an in-homogeneous Poisson model with instantaneous rate:

$$\lambda(t) = f(\beta_0 + \sum_{i=1}^{N} + \sum_{j=1}^{T_i} \beta_i^j P_i(t - t_j))$$

where $P_i(t) = 1$ if predictor i occurs at time t (and 0 otherwise). $f$ is chosen as exp and $\beta_i^j$ are the weights attributed to each predictor (shifted by time $t_j$). $\beta_i^j$ are estimated by maximizing the log-likelihood of a Poisson process with instantaneous firing rate $\lambda(t)$, given a real firing rate $r(t)$.

We model spike trains of the population directly using the following explanatory variables (see Fig. 39C, predictors): sound onset, change, decision defined as the first post-change lick, lick and sound offset. The underlying hypothesis is illustrated in Fig. 39B, where jitter in RT correlates with variability in neuronal responses on a trial basis. Cell example in Fig. 39A scaling of firing by one of the predictors, the change. Increase in firing rate after the change occurs around 100ms and is scale by the change size. Predictor strength is taken into account for the change ($P_i(t)$ is not categorical). In addition, $P_i(t) = 1$ throughout the trial for onset and offset predictor.

### Demixed PCA

To ascertain the relationship between decision and stimulus representation we used a demixed PCA analysis. The demixed principal component analysis (Kobak et al. [2016]) is a modified version of PCA that demixes the task parameter dependencies of the population, where demixed principal axes are not constrained to be orthogonal. For methods details see (Kobak et al. [2016]). A toolbox developed by the Machens' Lab and available online was used to highlight the tuning of the ferret M FC population to the different task parameters. Here three parameters were considered, stimulus, decision and the interaction between those two parameters.

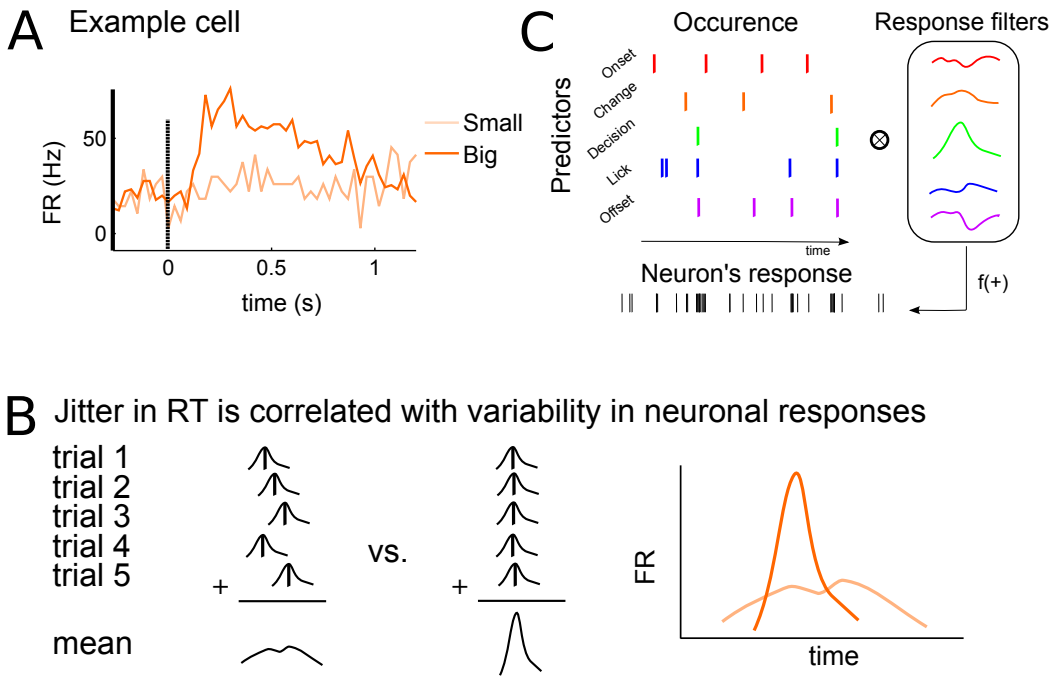


Figure 39: **Methods for the Generalised Linear Model (GLM)**
(A) PSTHs locked to the change of FC example cell for hit trials. Firing rate increases after the change for large changes, not for small changes (B) Illustrating the correlation between reaction time and and neural response (C) Principles underlying GLM. Five chosen predictors: sound onset, change, decision defined as the first lick after the change (after 250ms), licks (including the decision one) and sound offset.

### Selected data

Data used for GLM and dPCA came from ferret M most posterior recording sessions (see Appendix 54) thought to be premotor/dlPFC.

## Results

#### Neuronal responses in dorso-lateral FC reflect sensory evidence & behavioral output

Variability in behavioral outputs help separate contribution of different processes in the ferret. Hit and miss trials both contained sensory-related information, while hit and early trials both end with a motor output. Comparing the averaged population activity while separating the outcome can then lead to a few conclusions. If hits and miss modulations both show similar modulations (see Fig. 40, left panels and for MU Fig. 43), it is likely that the population encodes the sensory input faithfully. If a modulation before the lick exists for both early and hit trials, then population can be related to the motor command (see Fig. 40, right panels and for MU Fig. 43). In addition, if pre-lick activity is scaled by the outcome (between hits and early trials), one can postulate that the population encodes non-motor additional information, like decision formation for example. In ferret M, it is true for PEG and FC.

#### Firing rate decomposition

We predict neurons' firing rate reliably using a GLM (see **Materials & Methods**). However, our model predicts similar modulations for all change locations (Fig. 41E), while encoding of middle spectral location in ferret M FC is poor (see Chapter 3, **Results/Performance is similar for all change spectral location**). When removing middle frequency changes, dependencies on the outcome and change size is reproduced (Fig. 41A, B, C and D). Modulation scaling of the response by the strength of the change is present for both hit and miss, indicating sensory encoding. Trial outcome also scaled population response, suggesting poorer sensory encoding for miss and absence of decision-related modulations. Recently van Vugt et al. [2018] linked weaker activity in dlPFC for miss trials with loss of sensory information in downstream areas. Our results are consistent with this hypothesis, especially considering outcome already scaled change-related discharges in the PEG of the same ferret (see Fig. 40B).

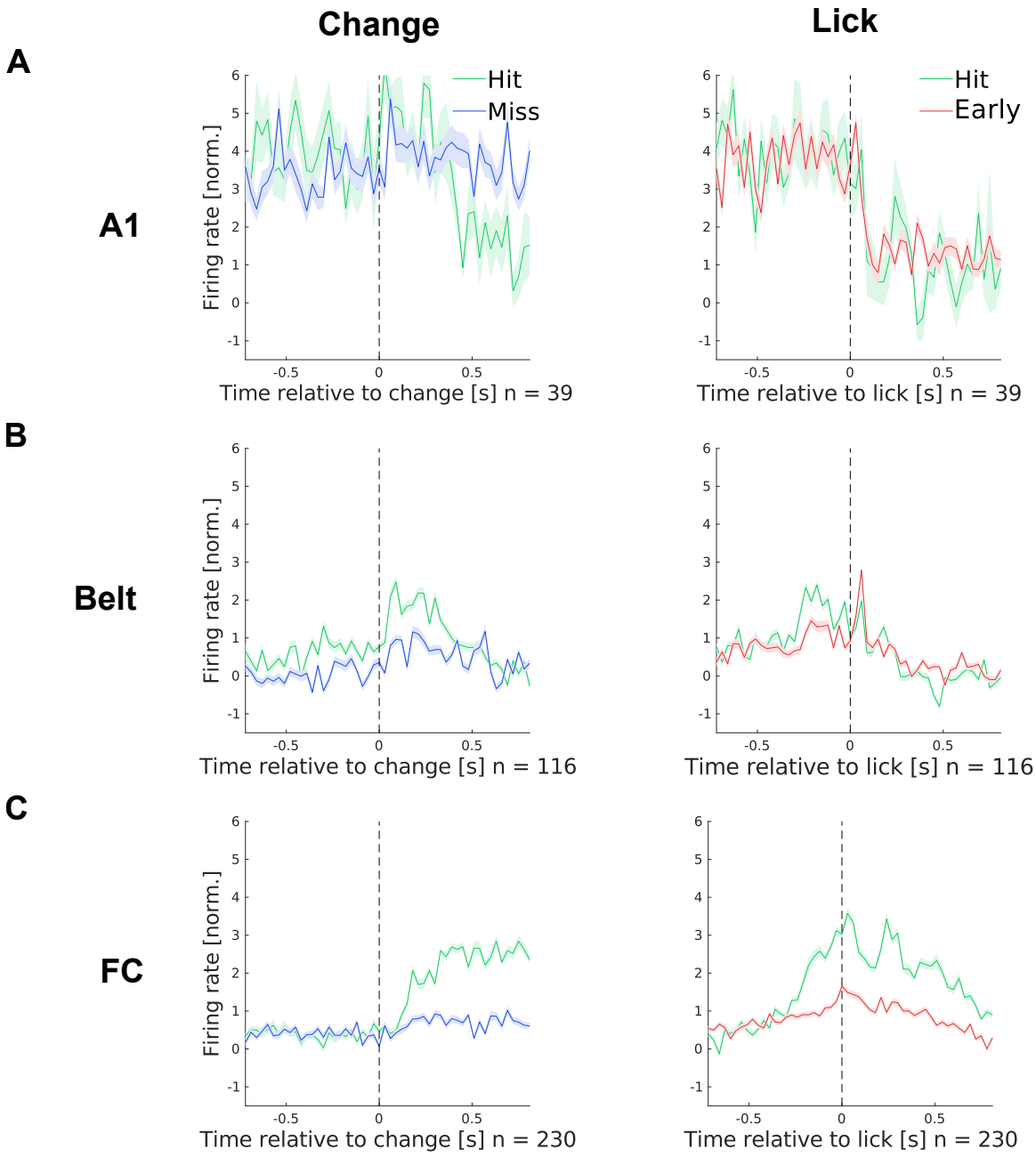


Figure 40: **Average task events-related single-unit activity in A1, auditory belt and FC** (A) Average single-unit z-scored activity in A1 relative to change and decision lick (ferret: 1). (B) Average single-unit z-scored activity in belt auditory cortex relative to change and decision lick (ferret: 2). (C) Average single-unit z-scored activity in FC relative to change and decision lick (ferret: 3).

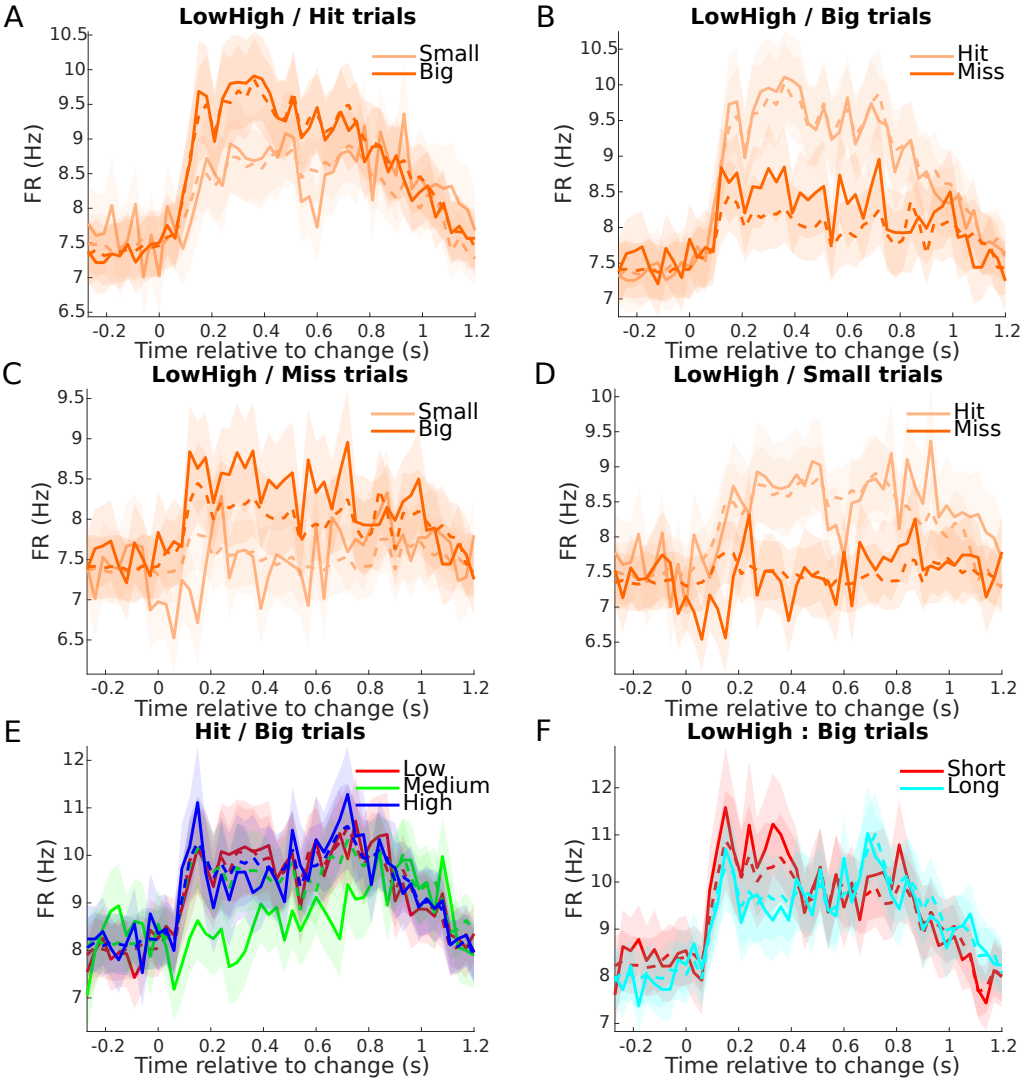


Figure 41: **Averaged and GLM predicted firing rate relative to change time in ferret M FC**
(A) Averaged population (plain lines) and predicted averaged population firing rate (dotted lines) for small and large changes (low and high frequency) relative to change time. The model predicts the change size dependency well (B) Averaged population and predicted averaged population firing rate (dotted lines) for hit and miss trials (low and high frequency) relative to change time. The model also captures the dependency on outcome (C) Averaged population and predicted averaged population firing rate (dotted lines) for miss trials ((low and high frequency) as a function of change size relative to change time. The change-related activity is scale d by change size even for misses (D) Averaged population and predicted averaged population firing rate (dotted lines) for small changes (low and high frequency) as a function of trial outcome relative to change time. The change-related activity is scale d by the outcome even for small changes (E) Averaged population and predicted averaged population firing rate (dotted lines) for hits as a function of change location relative to change time. Our model predicts the response to be independent of change location, however the encoding of middle frequency changes is poorer. (F) Averaged population and predicted averaged population firing rate (dotted lines) for large changes as a function of RT (short vs. long). Initial response and its prediction is similar in the two RT categories, supporting a sensory encoding in FC.

**Convergence of sensory and decision process**

Using the GLM and the averaged population response we show that ferret M FC encodes sensory yet abstracted signal (see Chapter 3 and Fig. 27), similarly to what has been reported in a number of studies on the dlPFC and premotor (Romo and de Lafuente [2013], Romo et al. [2004], Rossi-Pool et al. [2016], Fritz et al. [2010], Hanks et al. [2015]). The heterogeneity of cells responses in the FC and their dynamics are well known (Machens et al. [2010]). For large population, dimensionality reduction methods have been successfully applied (Cunningham and Yu [2014]). But we also want to describe the recorded activity while taking into account task parameters. Kobak et al. [2016] have modified their earlier demixed PCA method and developed an approach that reduces dimensionality while keeping the dependence of each component to the task parameters segregated. Here, we specifically look at the relationship between the sensory and decision parameters. Fig. 42C displays components ordered by explained variance and their identity in a bar plot. The fact that bars are mostly single-colored indicates a good demixing. The largest explained variance (9.2%) is condition-independent, but the second component (5.8% explained variance) (see Fig. 42A third row) is decision related and shows an opposite relationship between hit and miss independent of the change size. Stimulus related components (see Fig. 42A second row) show scaling with change size independent of trial's outcome. Overall, decision (defined as the first post-change lick) represents 22% of total variance, while stimulus 27% (see Fig. 42C). A smaller portion of the variance is explained by the interaction between stimulus and decision (see Fig. 42A fourth row). Furthermore, the significant correlations between component 2 (decision) and 4 (stimulus), and 5 (decision) and 4 (stimulus) (see Fig. 42D) suggest that a subset of cells encode both stimulus and decision, suggesting convergence of the two processes.

## Discussion

Temporally overlapping sensory, decision and motor signals are hard to disentangle, especially in PFC given the heterogeneity of cells responses (Machens et al. [2010], Kobak et al. [2016]). Classical approach based on averaged population results does not capture the diversity in dynamics at the trial level. Computational approaches enabled us to disentangle the influence of the task-related parameters on the activity and deduce how they are encoded. However, both the GLM and the demixed PCA required us to define those components and that can be problematic but will be further discussed in the **General discussion**.

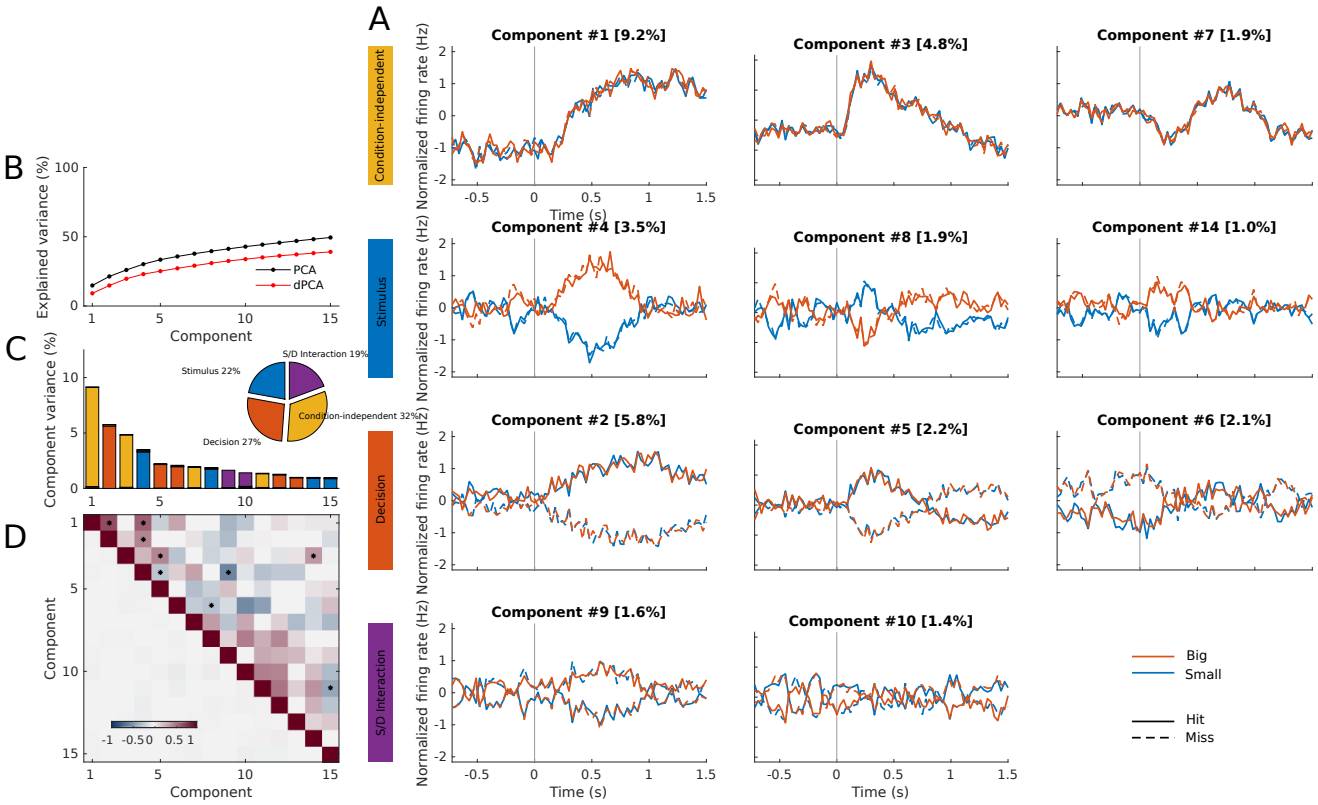


Figure 42: **Demixed PCA applied to recordings from ferret M FC**
(A) Demixed principal components (Kobak et al. [2016]). Top row: first three condition-independent components; second row: first three stimulus components; third row: first three decision components; last row: first stimulus/decision interaction component. In each subplot, the full data are projected onto the respective dPCA decoder axis, so that there are 4 lines corresponding to 4 conditions (see legend, bottom right). Ordinal number of each component is displayed above the plot; explained variances are shown as percentages. (B) Cumulative variance explained by PCA (black) and dPCA (red). Demixed PCA explains less variance as standard PCA. Dashed line shows an estimate of the fraction of 'signal variance' in the data, the remaining variance is due to noise in the PSTH estimates. (C) Variance of the individual demixed principal components. Each bar shows the proportion of total variance, and is composed out of four stacked bars of different color: yellow for condition-independent variance, blue for stimulus variance, red for decision variance, and purple for variance due to stimulus-decision interactions. Each bar appears to be single-colored, which signifies nearly perfect demixing. Pie chart shows how the total signal variance is split among parameters. (D) Upper-right triangle shows dot products between all pairs of the first 15 demixed principal axes. Stars mark the pairs that are significantly and robustly non-orthogonal.

# Supplementary

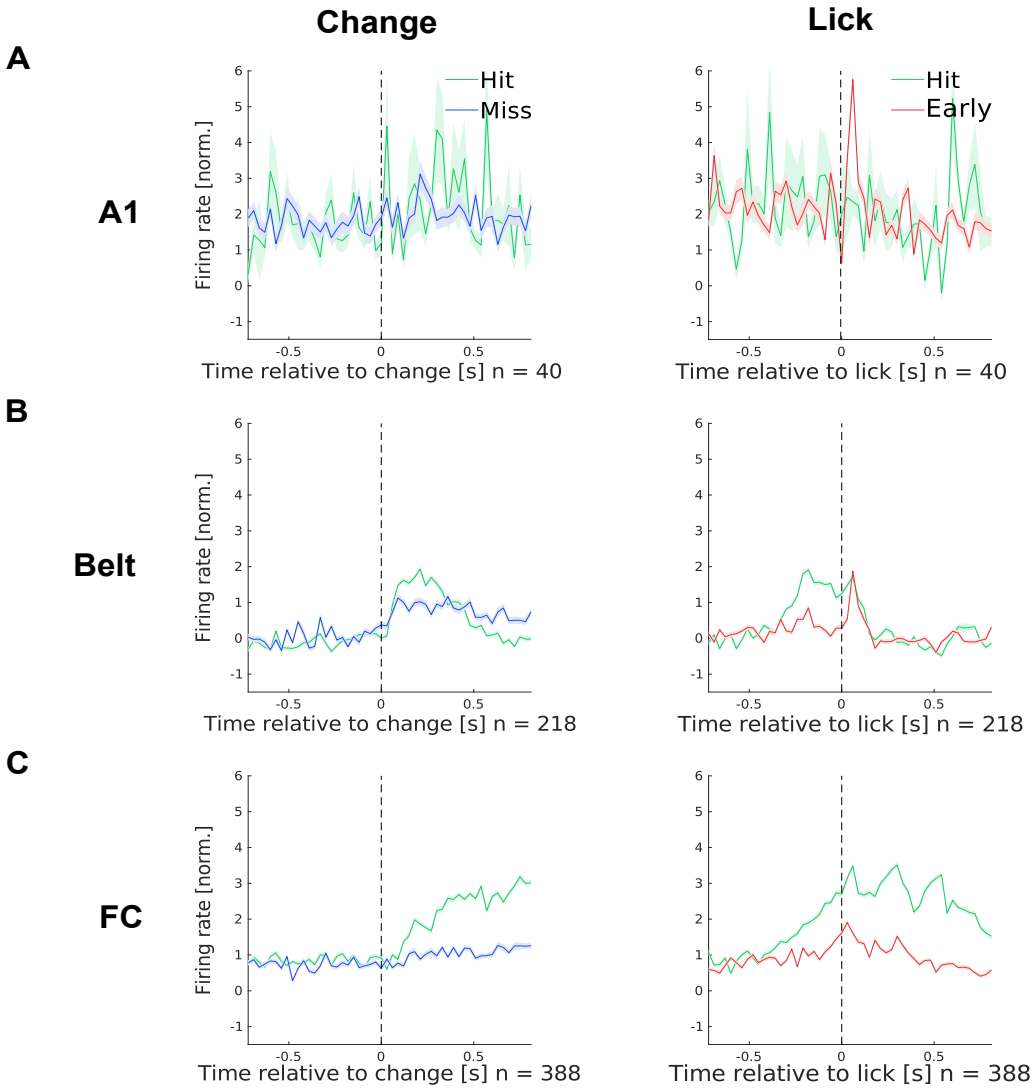


Figure 43: **Average task events-related multi-unit activity in A1, auditory belt and FC**
(A) Average multi-unit z-scored activity in A1 relative to change and decision lick (ferret: 1). (B) Average multi-unit z-scored activity in belt auditory cortex relative to change and decision lick (ferret: 2). (C) Average multi-unit z-scored activity in FC relative to change and decision lick (ferret: 3).

# Chapter 5: Contextual influence of target event temporal distribution on behavioral expectation and evoked pupil responses


## Abstract

In humans, pupil dilation has been associated with a number of underlying cognitive processes, such as decision-making and attentional load. Here, we want to test how modulation of pupil diameter can reflect subject's temporal expectation during a perceptual decision-making task. For this purpose we recorded pupil diameter of 18 individuals performing a change detection reaction time task. Subjects had to monitor a continuous and complex acoustic scene and detect a change in its statistical properties. Unbeknownst to the subjects, change time blocks were introduced. In each of these blocks, the change could arise only after a fixed pre-change period (0s, 1.5s and 3s from sound onset). We found a decrease in false alarm rate during these fixed pre-change periods, indicating that subjects implicitly incorporated the contextual information available at the block level into their decision strategy . Task-related pupil response was reduced with increasing pre-change period durations, correlating with subjects' decreased false alarm rate during this time period. Altogether, this suggests that the pupil-related modulation can reflect time-dependent adaptation of the decision threshold.


## Introduction

Perceptual decisions are often made under conditions of uncertainty, either because sensory inputs are noisy and embedded in a more complex scene, or because they unfold over time and need to be monitored to achieve a good representation. Detecting changes in a dynamic environment therefore

induces a trade off between tracking rapid changes and estimating over longer periods. In the case of signals that require time-averaging to be properly estimated, subjects need to decide when it is beneficial to start the process of evidence accumulation. It has been reported that human observers delay their decision onset when asked to emphasize speed over accuracy (Teichert et al. [2014]), suggesting that the decision process is not necessarily initiated as soon as the evidence is available. In addition, subjects may adapt their integration timescale to optimize behavior (Ossmy et al. [2013], Piet et al. [2017]).

The adaptive nature of decision-making requires selection of task-relevant information and suppression of irrelevant signals. In the previous chapters we demonstrated selection of information over mutliple scales in our task. In the hope of identifying differences in arousal level in our ferrets during behavior, we recorded pupil diameter and analysed it as a function of behavioral outcome (see Fig. 44 A & B). An inverted U-shaped relationship between performance and baseline pupil size has been reported in human and animal studies (Van Den Brink et al. [2016], McGinley et al. [2015a]). A similar relationship between performance and locus coeruleus (LC) activity has also been reported during tonic state (Aston-Jones and Cohen [2005], Aston-Jones et al. [1999]). Period of elevated tonic activity correlated with higher false alarm rate and lower response criterion. Here again, good performance is associated with an intermediate level of activity. The adaptive gain theory of LC relates the LC activity to both task performance and task engagement. At constant luminance pupil dilation is thought to be driven by neuromodulatory network involved in the control of arousal. Microstimulation of the LC (also inferior and superior colliculus) triggers pupil dilation Joshi et al. [2016] and in general changes in arousal state are linked with changes in pupil diameter (McGinley et al. [2015a,b], Reimer et al. [2015]). In addition to a classical U-shaped relationship between pupil size and performance (Van Den Brink et al. [2016], McGinley et al. [2015a]), we report similar dynamics for all outcomes within a trial with a slow dilation after a faster initial constriction. We noticed that the constriction coincide with the initial delay period of 1.75s (see Fig. 44 A). It has been known that subjects anticipate timing of behavioral-relevant events' onset (Tsunoda and Kakei [2008], Janssen and Shadlen [2005], Oswal et al. [2007]), we sought to test the hypothesis that pupil modulations captured ferret M's estimation of the change time distribution. Because we did not want to change parameters during electrophysiological recordings, we decided to test the effect of change time expectation in humans.

Pupil size modulations under constant luminance have been associated with numerous cognitive processes, such as cognitive load, attention, decision bias, and meta-confidence (Murphy et al. [2014], Urai and Pfeffer [2014], Krishnamurthy et al. [2017], de Gee et al. [2014], Einhauser et al. [2008], Einhäuser [2010], Van Den Brink et al. [2016], Kahneman and Beatty [1966]). The exact ef-

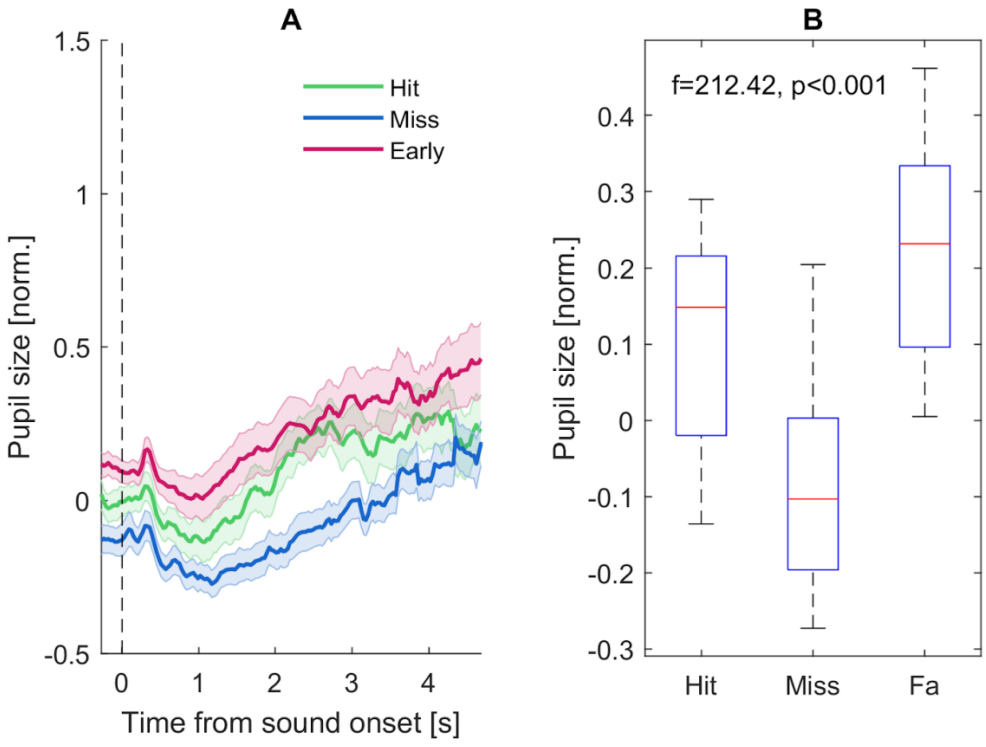


Figure 44: **Normalized pupil size as a function of outcome for ferret M**
(A) Pupil diameter within a trial for ferret M before the change per outcome. Pupil dynamics after sound onset are similar across outcome, however pupil baseline is scaled by the outcome. Early trials (red) have a larger pupil diameter, hit trials (green) have an intermediate pupil size and miss (blue) have a smaller pupil size before the start of the trial. (B) U-shaped relationship between baseline pupil diameter and performance ($p<0.001$, ANOVA)

fects of the neuromodulatory activity from different nuclei on behavior and pupil dilation are not well described. Most of the studies exploring how pupil diameter evolves with desicion-making reported effects associated with terminating the process (Einhauser et al. [2008], Einhäuser [2010], Lempert et al. [2015]). However, de Gee et al. [2014] showed a sustained dilation throughout the decision process relating to both subjects' bias and choices.

To determine if subjects' pupil size reflects their expectation, the task structure of our change detection paradigm (Fig. 45) was modified to specifically manipulate subjects' change time expectation. Trials were divided into 3 blocks defined by their fixed pre-change period (early, intermediate and late change time blocks) (Fig. 46). Each subject performed the change detection task described in Chapter 2 and was unaware of the block design. We hypothesised that subjects would update their estimation of the change time distribution after each block and that they would adapt their behavior accordingly (online shift in criterion (de Gee et al. [2014])). We expect pupil size to vary in between blocks and reflect behavioral adaptation. More specifically, we expect a delayed pupil evoked dilation and an decreased pupil baseline with longer pre-change period.

## Materials and Methods

### Ethics

See **Ethics** Chapter 2.

### Experimental set-up

We recorded the pupil diameter (ISCAN, sampling rate: 1000 Hz) of 18 subjects performing a change detection task. Subjects placed their head on a chin-rest 90cm away from a gray screen (31.6 cd/m$^2$) with a central fixation cross, which they were instructed to fixate during trials. Luminance was kept constant, black curtains occluded the window of the acoustic chamber. The auditory stimuli were delivered via HD Seinheiser 380 headphones at a 100,000 Hz sampling rate, from a NI card. Behavioral response entered via a button on a response box was recorded with the same device. Subjects were instructed to press the button placed in front a them whenever they heard a change. Feedback was displayed on the gray screen after subjects entered their response, and matched the fixation cross in size and color.

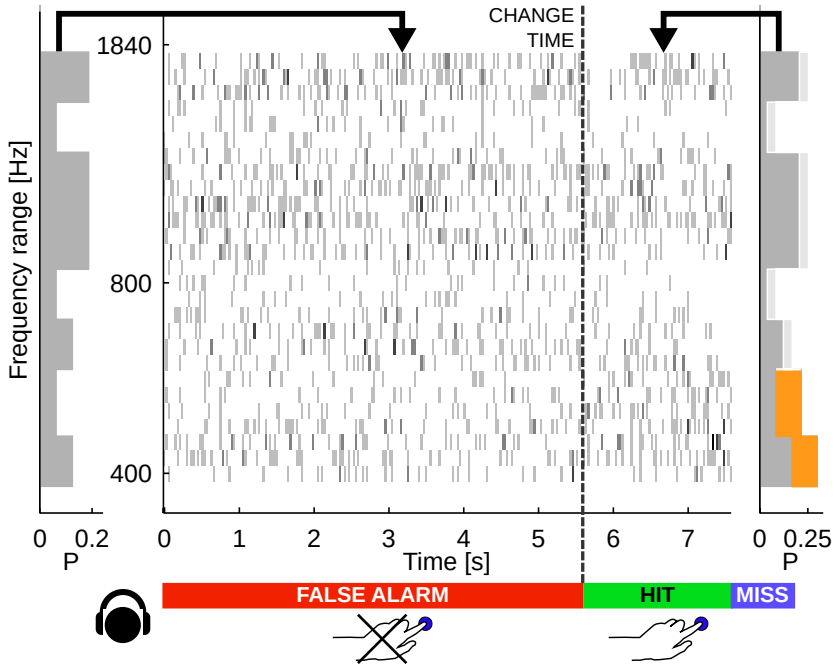


Figure 45: **Statistically defined tone cloud**
The tone occurrence probability was governed by its marginal frequency distribution (grey curve, left panel). Tones in individual frequency bins were drawn independently consistent with the marginal (middle panel). The frequency marginal was modified (indicated in orange in the right panel distribution) after a randomly chosen point in time (change time). Subjects were instructed to report a change by a button-press.

### Change detection task

### Stimulus

On every trial, the subjects were presented with a tone cloud governed by a marginal distribution (see Fig. 45 and Chapter 2). Stimulus design is similar to the stimulus design presented in Chapter 2. Change sizes were limited to 3: 60%, 95% and 130% and changes always consisted of two adjacent frequency bins (see Fig. 10A). Other parameters were kept constant. Unbeknownst to the subjects, change time blocks were introduced. In each of these blocks, a change could arise only after a fixed pre-change period (0s, 1.5s and 3s from trial onset, see Fig. 46). Before the start of each trial, an 800 ms period of silence was introduced, to allow the estimation of pupil diameter baseline before sound onset.

## Procedure

The procedure is based on the procedure presented in Chapter 2 (see Chapter 2 **Procedure**). Each subject performed a total of 360 trials, divided into 3 blocks of 120 trials each. Block presentation order was randomised across subjects. In order to avoid changes in the measured pupil size due

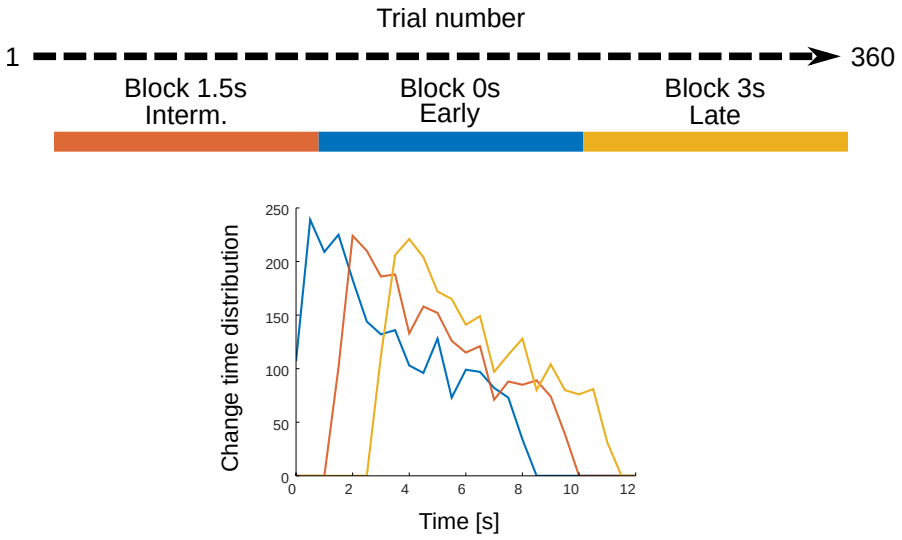


Figure 46: **Change time block design**
Subjects performed a total of 360 trials, separated in three change time blocks of 120 trials and presented in a randomised order. Frequency histogram defined by drawing change times from a Poisson distribution per block. Early (in blue) from 0s to 8s, intermediary (in orange) from 1.5s to 9s, late (in yellow) from 3s to 11s.

to shifts in gaze, we asked participants to fixate a cross placed in the centre of the screen in front of them. Feedback was given at the end of every trial, in the form of a check ('v') for correct trials and a cross ('x') for incorrect trials. The fixation cross and the feedback objects were the same size and color (white over a grey background) insuring a constant luminance over the entire experiment. Feedback was displayed after the button press, and subjects were instructed to preferentially blink during feedback presentation. After being displayed for 1 s feedback was replaced by the fixation cross for another second before the start of the next trial.

## Analysis

### Pre-processing of pupil data

The pupil time series were first low-pass filtered (third order Butterworth, cutoff, 10 Hz)(same filter,de Gee et al. [2014] but at 4 Hz). Periods of blinks were detected as any signal outside of a 1.5 standard deviation window around the mean pupil diameter for the entire session for one subject. Every identified blink point and adjacent data points over a 350ms asymmetric window (150ms on the left, 200ms on the right) were then replaced by NaNs so as to excluded this period from further analysis.

One subject was excluded from all analyses because pupil diameter was not recorded properly (software threshold were not respected, leading to only one value for pupil diameter) , leaving a total

of 17 subjects for the analysis.

#### Pupil data z-score

In order to compare subjects' pupil diameter and because the output from the eye-tracker is an arbitrary value, we z-scored each subject's pupil time series (Van Den Brink et al. [2016]) ($p(t)$) by the mean ($\mu_b$) and the standard deviation ($\sigma_b$) of the computed baseline: $s(t) = \frac{p(t)-\mu_b}{\sigma_b}$ . To investigate effects of parameters on the task-evoked pupil response (EPR), baseline was computed per trial over the the last 500ms of the 800ms silence preceding sound onset. For effects of blocks on pupil diameter before the trial, baseline was computed over the same window but over a block (120 trials). In both cases, trials with less than 15 non-NaN points during the silence preceding the trial were excluded from analysis.

#### Slope of task-evoked pupil response

To compare the task-evoked pupil responses across blocks and outcome, the slope of the pupil response was computed over a specific time window using a simple linear regression (polyfit, MATLAB). The window was chosen after the small initial constriction and before the asymptote (see Fig. 49) from 1 s to 3 s.

#### Behavior analysis

Behavioral analysis is described in Chapter 2 (see Chapter 2 **Performance**, **d' Analysis**, **Reaction time**).

#### Statistical analysis

Pairwise parametric tests were used for all statistical analysis, ANOVA, either 2 or 3 way depending on the number of conditions. All shaded areas in the following figures are SEMs.

## Results

### Behavioral results

Performance measured by hit rate and d' is matched per block (47B & E). Change time distribution did not affect performance or reaction times, as hit rate, d' and median rt are matched across blocks (47C). However, false alarm rate decreases with the length of the fixed pre-change period (47A).

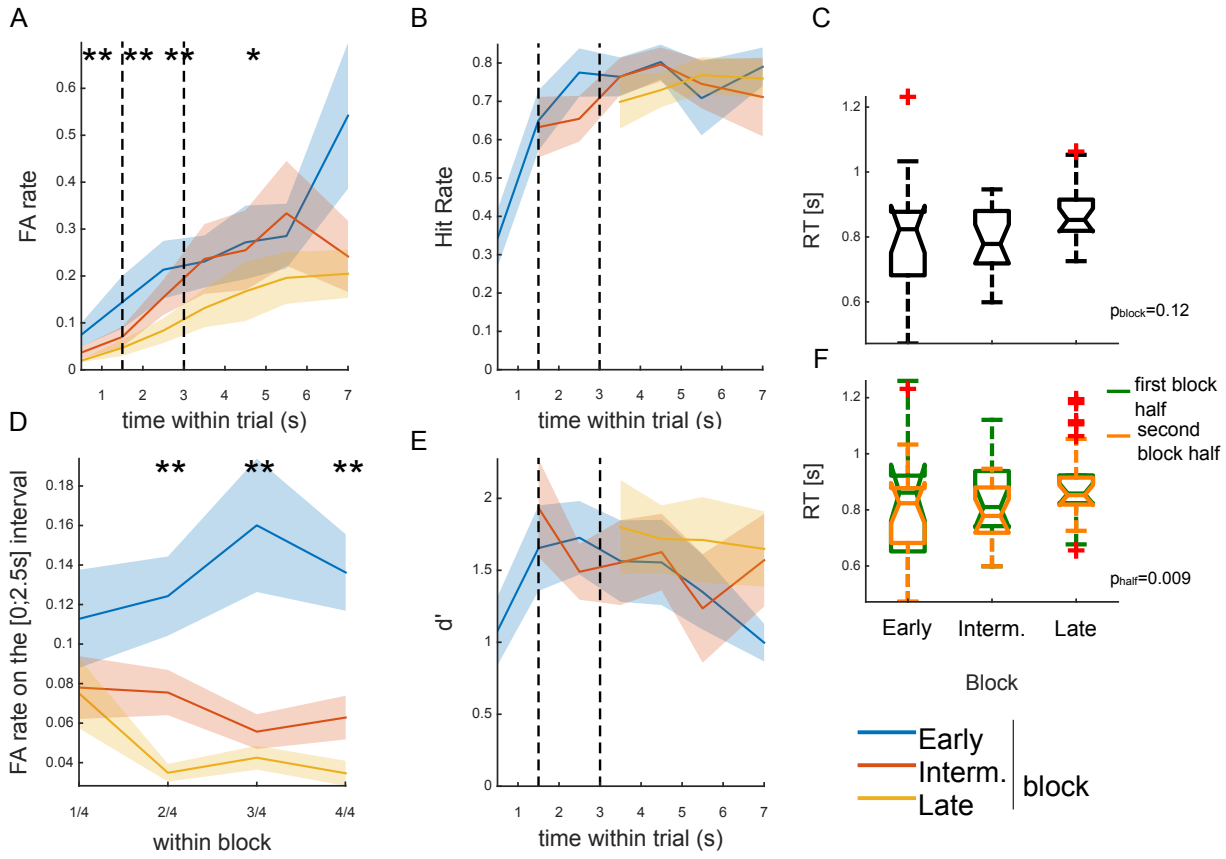


Figure 47: **Behavior depends on block identity**
(A) Average false alarm rate per block. False alarm rate increases with shorter fixed pre-change time within the 0-3s window. This suggests subjects' adapt their strategy to the block design. (B) Average hit rate rate per block as a function of time within trial. After an initial increase (see performance in Chapter 3) for the early block, hit rate is similar across blocks. (C) Median reaction time per block. Change detection speed is similar across blocks. (D) Evolution of false alarm rate in between 0s and 2.5s within a block: after 30 trials (1/4), difference across block is significant. (E) D' per block as a function of time within trial is similar across blocks, after the initial increase in the early block. (F) Median reaction time decreases within the block for early and intermediary blocks (p=0.009), mirroring the increase in false alarm rate.

This adaptation to change timing is significant after 30 trials (a forth of a block), which suggests an adaptation to the block in under 30 trials (47D).

## Outcome influences pupil diameter within a trial

Pupil size differs significantly for the 3 outcomes before the change arises (ANOVA, p <0.001) and follows the previously reported U shape relationship in baseline pupil diameter in animals (McGinley et al. [2015a] and see Fig. 44A), humans (Van Den Brink et al. [2016]) and is consistent with the adaptive gain theory of LC-NE function (Aston-Jones and Cohen [2005]), where intermediate levels of activity are correlated with optimal performance. In addition, choices that lead to 'yes' response, i.e. false alarm and hit, elicit a higher EPR that the 'no' responses (de Gee et al. [2014]) before the

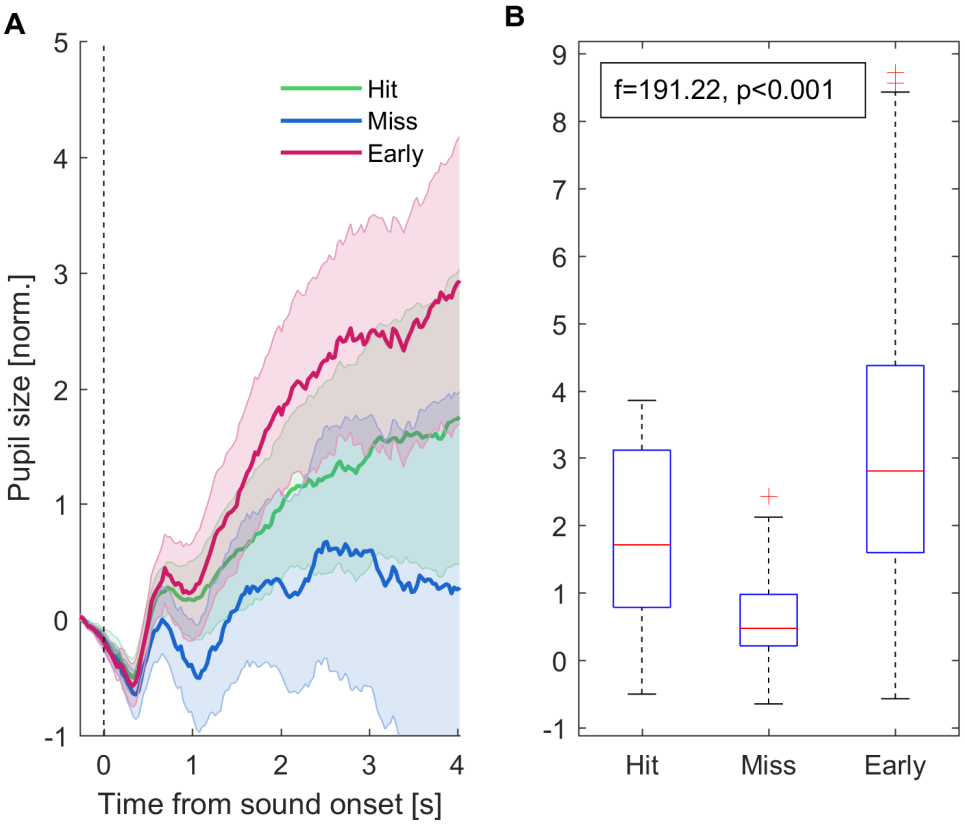


Figure 48: **Inverted U-shape relationship between task-evoked pupil size and trial outcome** (A) Sound-onset evoked pupil is modulated by the outcome of the trial, with a previously reported inverted U shape relationship (McGinley et al. [2015a]), where the modulation is strongest for false alarms, intermediate for hits and low for misses. (B) This relationship is significant ($p<0.001$, ANOVA).

change or the button press (for false alarms). This indicates that pupil diameter reflects trial outcome before the end of the decision process.

### Evoked pupil modulation reflects subjects' strategy adaptation

If pupil diameter reflects subjects' expectation of change timing, we expect a reduced onset-related pupil dilation for longer pre-change periods after the adaptation period. Blocks are split in half and compared the second half (after behavioral adaptation) across blocks (see 49). We expect to observe a smaller slope for the late block, intermediate for the intermediate block and larger for the early block. There is a significant difference between the slopes of evoked pupil response across blocks (ANOVA, $p<0.01$) and across subjects (ANOVA, $p<0.01$).

To quantify the relationship between the context and the pupil diameter, we correlate the false alarm rate with the slope of evoked pupil response computed over the last 90 trials of a block (Fig.

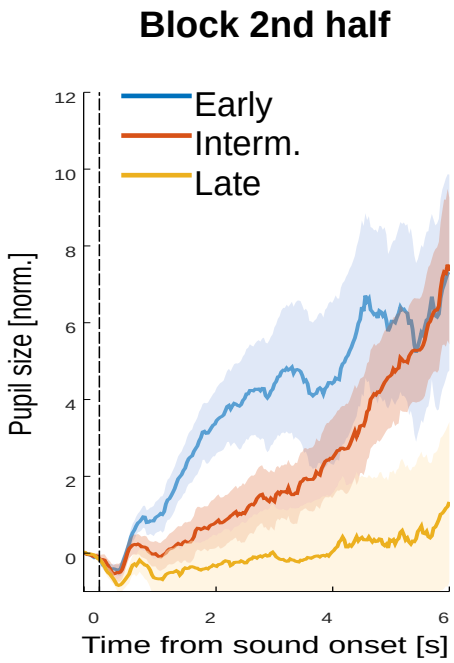


Figure 49: **Average task-evoked pupil response after sound onset and before the change per block**
Sound-onset evoked pupil (z-scored per trial) modulation reflects subjects' adaptation to block bias: pupil evoked dilation varies as a function of block identity during the second half of the block. It is stronger for the early block and suppressed for the late block, mirroring false alarm rate dependence on block identity.

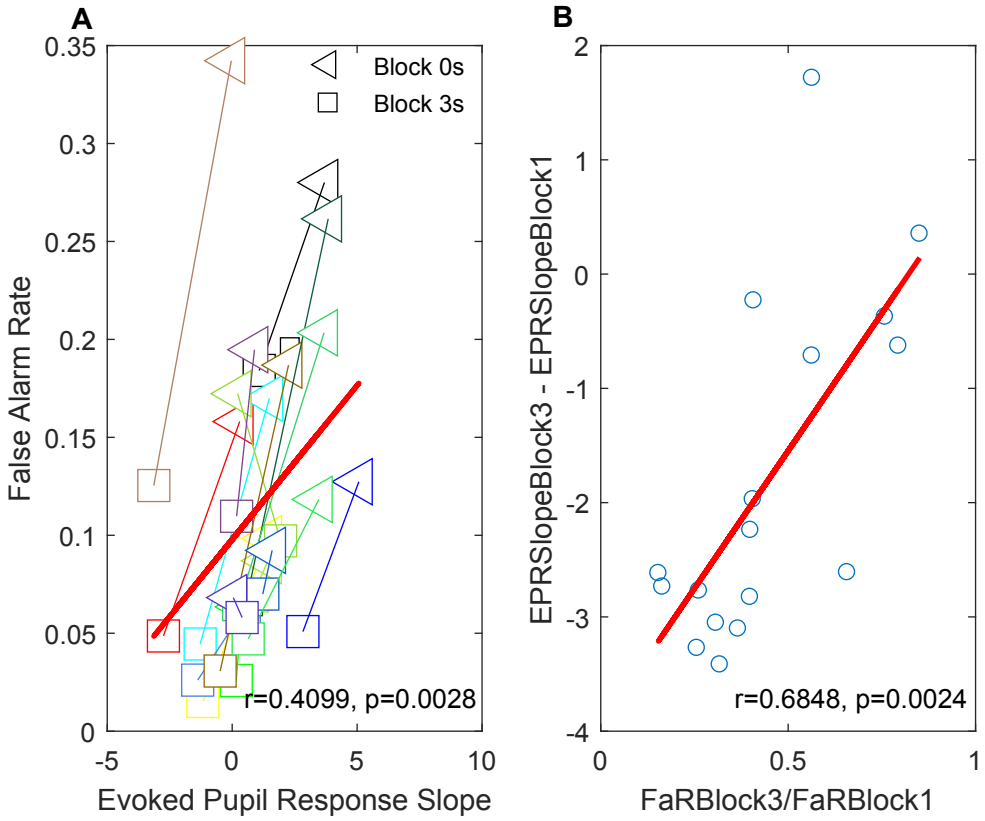


Figure 50: **Evoked pupil size slope correlates with blocks' false alarm rate**
(A) False alarm rate and pupil evoked response slope per subject for early and late blocks. False alarm rate decreases with fixed pre-change time and so does EPRs, as signified by the positive correlation (r = 0.4099, p=0.0028). One color per subject and each one marker per block (only late and early block presented) (B) Linear regression between false alarm rate ratio in early and late block and pupil evoked response slope difference for early and late block per subjects (r =0.6848, p=0.0024). Each dot is a subject, red line correspond to the linear regression.

50A). To further quantify that effect the false alarm ratio and the EPRs slope difference between the early and the late block are computed per subject (Fig. 50B). The difference between block slopes was chosen instead of the ratio because some subjects show a constriction instead of the more common dilation after sound onset. A positive correlation is reported (Linear regression, p=0.0024), suggesting that subjects' pupil diameter and false alarm rate decrease with the length of the fixed pre-change period.

## Pupil diameter is both scaled by context temporal expectation and future outcome

The relationship described in the previous section leads to two concurrent hypotheses. The first possible explanation for the positive correlation between EPR and false alarm rate is that pupil diameter

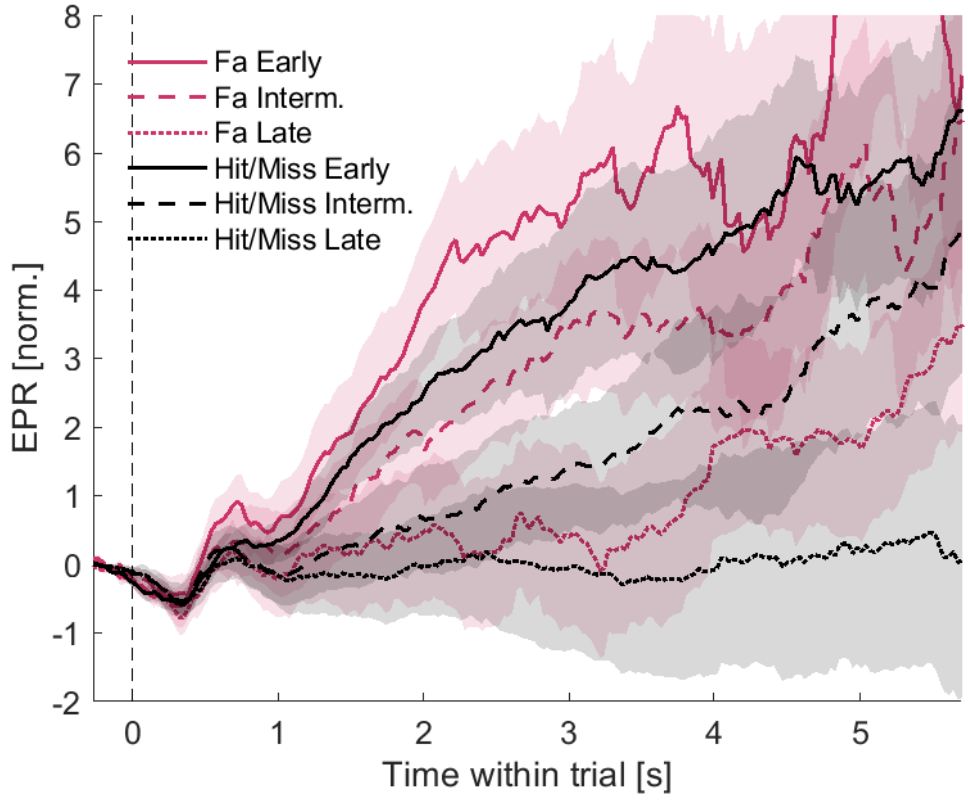


Figure 51: **Evoked pupil size varies a function of outcome and is scaled by the context**
False alarm EPRs' slopes (computed over 1-2s) are larger than Hit and Miss per block ($p < 0.05$, ANOVA). EPRs' slopes irrespective of the outcome is scaled by the block identity ($p < 10e\text{-}04$, ANOVA). The interaction between the two effects is not significant ($p = 0.45$, ANOVA).

varies with the context. The second is is that the decreased pupil diameter is due to the decrease in false alarm rate in between block (see **Outcome influences pupil diameter within a trial**). To disentangle the two effects, we computed the EPRs and their respective slope per outcome (false alarm vs. hit and miss) and per block (see Fig. 51). False alarm EPRs tend to be larger than the hit/miss EPRs across blocks (ANOVA, $p < 0.05$). However, both EPRs are scaled by the block identity (ANOVA, $p < 10^{-4}$). The effects are independent (ANOVA, $p = 0.45$). In conclusion, we show that task-evoked pupil diameter depends on the outcome of the trial and is also influenced by the temporal contextual information at the level of the block.

### Baseline pupil diameter

Baseline pupil size and behavior have been correlated (McGinley et al. [2015a], Van Den Brink et al. [2016]). We expected that the estimation of change time distribution has the same effect on baseline

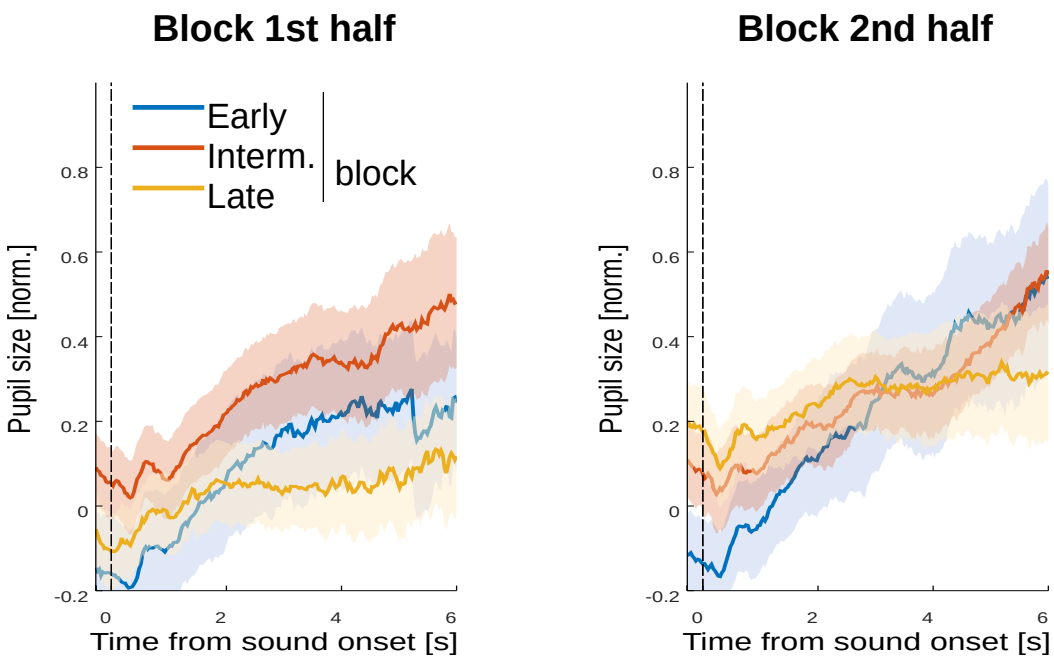


Figure 52: **Baseline pupil size per block as a function of temporal context**
Baseline pupil size (z-scored per block) contrary to our hypothesis, increases in the late block (ANOVA, $p < 0.05$). This effect might be related to confidence within block.

pupil size as the EPR. But contrary to EPR the baseline pupil size in late block increased (Fig. 52). The random block presentation order per subject excludes a fatigue related explanation. This result could be explained by the influence of trial n-1 on the baseline of the trial n or the influence of how confident the subject was. However, we did not collect subjects' confidence reports and further analysis using sequential performance as a proxy for confidence did not yield any significant results. This effect remains unexplained.

## Discussion

We found a decrease in false alarm rate during these pre-change periods, indicating that subjects implicitly incorporated in their decision strategy the contextual information available at the block level. Task-related pupil response reduced with increasing pre-change period durations, which correlated with subjects' decreased false alarm rate during this time period. We also report an inverted U-shape relationship between EPRs and outcome, where false alarms elicit larger pupil dilation during the trial (McGinley et al. [2015a], Van Den Brink et al. [2016], Lempert et al. [2015]). Both effects are independent, possibly reflecting parallel processes driven by different networks. The relationship between subjects' bias and pupil size modulation for response choice has been associated in de Gee et al. [2014] and Gee et al. [2017] . 'Yes' choices elicited larger pupil size than 'no' choices only if

subjects were conservative. They interpreted this as subjects overcoming their bias. Here, we show that EPRs vary with subject's criterion, independently of pre-choice dilation increase. In addition, we show that pupil size prior to the decision is scaled by the outcome, even within the 'yes' class (hits and false alarms).

Contrary to pupil evoked responses, baseline pupil size does not decrease with fixed pre-change period. Previous studies quantified that baseline pupil size modulation correlates with subject confidence, beliefs and the reliability of prior expectations (Krishnamurthy et al. [2017], Colizoli et al. [2018]). It is entirely possible that pupil size baseline on trial n is influenced by post-choice pupil on trial n-1. We did not collect subjects' confidence ratings and do not have a good measure to explore that possibility.

Most subjects showed onset-related pupil dilation, however, a few subjects showed negative correlation to baseline diameter (3 out of 17). This has been reported before (de Gee et al. [2014], 5 subjects out of 28) and subjects were excluded from the analysis but the effects still hold when included. This slow constriction is puzzling because neuromodulatory systems involved in cognitive control are linked with pupil dilation, not constriction (Joshi et al. [2016], Aston-Jones and Cohen [2005]). We did not exclude the subjects from the analysis, especially because they show the same trend as the other subjects (see Fig. 50A).

In summary, theses results suggest that subjects integrate the context of target event temporal distribution and adapt their strategy accordingly. EPRs reflect subject's shift in criterion and trial outcome independently. The delayed EPR observed in ferret M's pupil size dynamics (see Fig. 44) could then correspond the change time distribution used during electrophysiological recordings. As neuromodulatory network are driving pupil dilation and cortical state, we could use the pupil to precise the animal's state during recordings.

# Chapter 6: Discussion

## Results summary

**Chapter 2** We investigated how listeners detected changes in spectrotemporally broad acoustic textures, as a model for change detection in complex auditory environments. Listeners are presented with a continuous sound, whose statistics change at a random time. Hence, they are faced with the dual-task of estimating the baseline statistics and detecting a potential change in those statistics at any moment, mimicking real-life challenges. We found that detection performance improves with the time available to sample the baseline statistics before the change. Detection performance also depended on the salience of the change. EEG recordings from auditory projection sites did not exhibit a discernible response related specifically to the change in stimulus statistics. By contrast, EEG signals over parietal cortex appeared after the change time, and displayed an accumulation-to-threshold dynamics whose build-up rate that depended on the size of the change (O'Connell et al. [2012], Kelly and O'Connell [2013]). The peak amplitude of this potential decreased with prechange interval. Performance and reaction times are well predicted by a model of statistical estimation based on the difference in the outputs of two leaky integrators operating at fast and slow timescales. In addition a model of cortical processing augmented with an accumulation-to-bound decision stage also accounted for the EEG responses and subjects' behaviors, thus suggesting that decision-making in such statistically complex environments may only require minor post-processing (channel-selection and averaging) beyond the early auditory cortex. These results demonstrated that listeners estimated the statistics of the stimulus to make their decision, as evidenced by the dependence of performance, reaction times, and the parietal response on the stimulus parameters. We developed a drift-diffusion type model for estimating certain stimulus statistics, which accounted well for the response performance and dynamics in human listeners. Finally, we adapted a model of auditory cortical processing to provide a link between statistical estimation and the underlying physiology.

**Chapter 3** To further describe the extraction of relevant sensory sensory information in complex continuous stimuli along the cortical pathway. To address this question we successfully trained ferrets on a similar task. Similarly to (Fritz et al. [2010], Atiani et al. [2014], Brincat et al. [2018], van Vugt et al. [2018], Rossi-Pool et al. [2016]) we collected electrophysiological data in the primary auditory (A1) cortex, secondary auditory cortices (PEG) and the FC (dlFC/Premotor) of the behaving ferret. A1 neurons exhibited reduced change-related discharges, whereas dlFC neurons presented an enhanced response to change-related events during behavior, possibly being the signature of accumulation of sensory evidence. The LFP recorded in those area shows a similar behavior where the change related-modulation is small in A1, already enhanced in PEG and strong in FC. These area-specific responses to sound mirror EEG recordings in humans. All together these results suggest a behavior-dependent mechanism of selective amplification and accumulation of sensory evidence, leading to decision making. A decoding analysis argues for a gradual abstraction of the stimulus representation. Finally, we show that pre-change activity and post-change activity are correlated in FC arguing for time-varying population activity facilitating crossing of a decision threshold in the neural space.

**Chapter 4** Perceptual decision-making requires the conversion of sensory evidence in a decision signal, a process associated with frontal area or parietal areas (Huk [2005], Latimer et al. [2013], Churchland et al. [2008], Britten et al. [1996], Drugowitsch et al. [2012], Hanks et al. [2006], Kiani et al. [2008, 2014], Shadlen and Kiani [2013], Brunton et al. [2013], Erlich et al. [2015], Scott et al. [2017], Fritz et al. [2010]). Because modulations in FC neurons' firing rate can be correlated with a large variety of (sometimes overlapping) task-relevant and irrelevant events, we used a Linear Non-Linear Poisson model to disentangle the contribution of different predictors (sound onset, change in stimulus statistics, decision, motor activity...) to those modulations. Our model allows us to orthogonalize the responses to each predictor and quantify their specific contribution to the firing rate of individual neuron. By focusing our study on the responses of the neurons at the single trial category level (hit vs. miss, small vs. big changes, etc.), we found that neurons encoded both stimulus changes in a stimulus-dependent manner and perceptual decisions in a categorical stimulus-independent fashion. Using, a demixed PCA, we report dual encoding of these two types of events, suggesting that conversion from sensory evidence towards a decision signal may take place in the FC, within the same population.

**Chapter 5** We wanted to test if modulation of pupil diameter can reflect subject's expectation during a perceptual decision-making task. For that purpose we modified the change time distribution in a

block design. We found a decrease in false alarm rate with increased fixed pre-change duration, indicating that subjects implicitly incorporated the contextual information in their decision strategy. Onset-related pupil dilation was reduced with increasing fixed pre-change duration, correlating with subjects' decreased false alarm rate during this time period. EPR also reflected the outcome of the trial in a classical inverted U-shape. Those two effect were shown to be independent. All together, this suggests that the pupil-related modulation can reflect time-dependent adaptation of subject's criterion.

## Discussion

Overall, those results describe a gradual change detection process unfolding along the cortical pathway and are coherent with a number of perceptual studies (Atiani et al. [2014], Rossi-Pool et al. [2016], Brincat et al. [2018], van Vugt et al. [2018]).

**Estimation of baseline statistics** The stimulus is defined by its first order statistics and the change is a deviation from those statistics. Estimating those statistics is necessary to perform the task. If the behavioral effects of Chapter 2 (change time and initial baseline statistics dependency), we were unable to specify neural correlates directly relating to this process. Because our stimulus statistics are different on every trial, we have not been able to match systematic changes in the initial statistics and activity.

**Ecological relevance** The use of a recation-time task and positive reinforcement enabled us to obtain a more precise estimation of the decision window. It mimicks real-world challenges were action follow a dynamic process. In addition, relevant events are not token-based (Thura and Cisek [2014]) but rather embedded in complex scenes. However, in the real world, sources of information are also rarely modality specific and sensory evidence is pooled across modality to build a robust percept (Ernst and Bülthoff [2004]). It is therefore unclear how relevant within modality decisions mechanisms described above and in the introduction are to real world decision-making.

**Refining behavior** Early trials can be informative when using detection-triggered averaged (Okazawa et al. [2018]), because if they are false alarm in the true sense, they will reflect the sensory template used by the subject to detect the target event. In our paradigm, the stimulus is stochastic in nature, and it is not unlikely that a subset of early trials were "perceptual" false alarms happening after a sensory event resembling the change. We however used them to differentiate premotor from sensory or decision activity. Similarly, a subset of hits are "chance hits", we have not been able to identify

those. Therefore, defining the decision as the first postchange lick is not perfect because we rely on that definition to identify activity related to the decision process. This approach it can induce an underestimation of the decision-related activity. A more systematic approach to disentangle the decision process from the motor command would require recording licks in the absence of stimulus.

Because we have a reaction-time design ferrets tend to have high false alarms rates. Only a sub-part of these will be actual false alarms, i.e., perceptual false alarms. Is it possible to classify FAs, based on behavior itself? Moreover, the same way ferrets can make false false alarms, they can make false hits. Intuitively, since the first lick triggers the valve that gives water only on the second lick, we expect that an animal making a real FA or hit, thinking heard the target sound, is going to lick at least twice. By looking at the number of pot-decision lick (see Fig. 53 A), we show a clearer pattern matching the behavioral template (see Fig. 53 B, on the right) in decision triggered averaged computed on FA during biased sessions. This indicates that based on a behavioral measure it is possible to distinguish “perceptual” false alarm from impulsive responses.

Once ’perceptual’ FA are satisfyingly identified, their decision lick should be taken into account in the decision predictor for the GLM in Chapter 4.

**Control of animal state** Similarly to Fritz et al. [2010] and Atiani et al. [2014], we recorded neurons during passive presentation of the stimuli and during behavior. Behavioral gating mechanisms are reported in all three cases, the passive state is poorly defined. Experiments can last up to 8 hours and the passive sate can vary. Since Stringer et al. [2018] show that most of the explained variance of the spontaneous activity is due to arousal, it is crucial for future experiment to maintain the animal in a quiet but awake state or to measure proxies such as the pupil size to characterize further the state of the animal.

## Future directions

Apart from a full replications (FC and A1 data need to be gathered prior to publication), we will present the future directions for the project.

**The top-down influences: investigating effect of task-engagement on cell selectivity in A1 and Belt area** In Chapter 3, the accuracy of the decoding for the change improved when taking into account cell selectivity only in the passive state, suggesting a difference in the representation of the change between the two states. This could be due to changes in the receptive field of the cells. We therefore will compare receptive field estimated with our stimulus using a spike triggered average, or

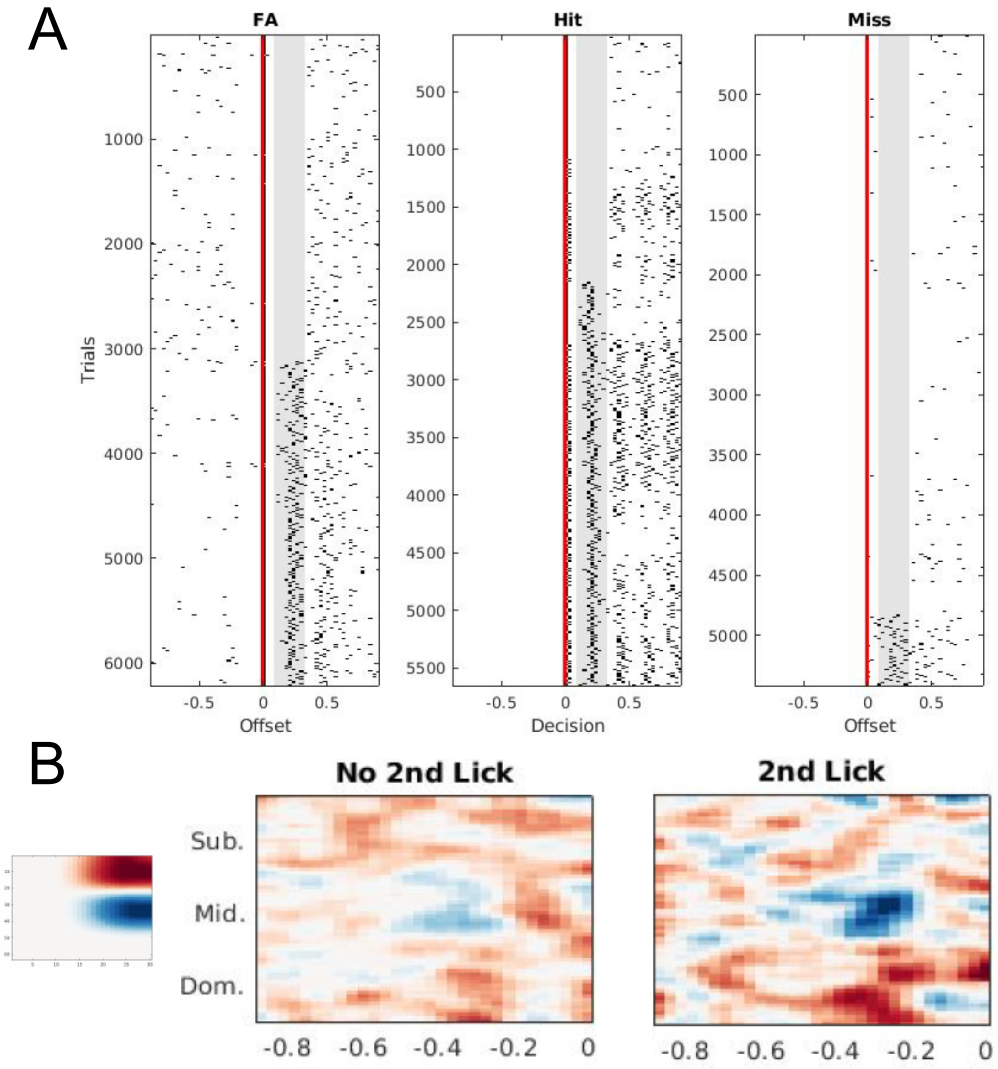


Figure 53: **Post-decision lick pattern informs behavior and decision formation in ferret M** (A) Post-decision lick pattern (post-offset for misses) organised according to the number of lick in the gray window per outcome. For hits after the decision lick a pattern emerges with a rate of roughly 4 Hz. Only a few second licks follow the offset for miss. For half of the false alarms a second lick is present in the grey window, its distribution is more spread than in hits (B) Behavioral pattern (on the left) obtained by averaging decision triggered averages computed on biased sessions (smoothed version of it). Decision triggered average in biased sessions for false alarm trials with or without a second lick. DTA for FA with a second lick matches more closely the behavioral pattern, indicating that some false alarms are more 'perceptual', and that they can be partly identified by the presence of a second lick.

the GLM in between states. In addition ferret T is implanted in both FC and Belt area, we could thus compare the correlation between those areas during behavior (similarly to Fritz et al. [2010]).

**Investigating the correlations between spontaneous cortical activity and pupil size** The precise nature of the relationship between cortical state correlates and performance in behavioral tasks is not yet clear Jacobs et al. [2018]. The pupil size was recorded during a number of physiological recording sessions in ferret M and ferret T in multiple areas. In addition to helping define the state of the animal, the collected data could be use describe the correlation between pupil size, cortical activity (lfp and spontaneous) and performance (McGinley et al. [2015b,a]).

**Template-matching in FC** When using an STA in the biased sessions only on the false alarms, some FC neurons display a template very similar to the behavioral template (increase in one frequency bin and decrease in the adjacent bin, see Fig. 53B, on the right). This intriguing results needs to be further quantified but suggest a match in the FC representation and the behavioral template.

**Inactivating the FC of the behaving ferret** As mentioned in the Introduction, the role of higher cortical areas in the accumulation of evidence and the decision formation are currently being questioned. most of the evidence are neural correlates. If FC is truly responsible for decision formation (like the demixed PCA suggests), then inactivation (bilateral) should impact behavior. We could implant canulas once the electrophysiological recordings are finished to pharmacologically inactivate FC and collect behavior.

# Bibliography

Misha B Ahrens, Jennifer F Linden, and Maneesh Sahani. Nonlinearities and contextual influences in auditory cortical responses modeled with multilinear spectrotemporal methods. *J Neurosci*, 28(8):1929–1942, 2008. doi: 10.1523/JNEUROSCI.3377-07.2008. URL http://dx.doi.org/10.1523/JNEUROSCI.3377-07.2008.

Lefkothea-Vasiliki Andreou, Timothy D Griffiths, and Maria Chait. Sensitivity to the temporal structure of rapid sound sequences - An MEG study. *Neuroimage*, 110C:194–204, 2015. doi: 10.1016/j.neuroimage.2015.01.052. URL http://dx.doi.org/10.1016/j.neuroimage.2015.01.052.

Gary Aston-Jones and Jonathan D Cohen. An integrative theory of locus coeruleus-norepinephrine function: adaptive gain and optimal performance. *Annual review of neuroscience*, 28: 403–50, 2005. ISSN 0147-006X. doi: 10.1146/annurev.neuro.28.061604.135709. URL http://www.ncbi.nlm.nih.gov/pubmed/16022602.

Gary Aston-Jones, Janusz Rajkowski, and Jonathan Cohen. Role of locus coeruleus in attention and behavioral flexibility, 1999. ISSN 00063223.

Serin Atiani, Mounya Elhilali, Stephen V David, Jonathan B Fritz, and Shihab A Shamma. Task Difficulty and Performance Induce Diverse Adaptive Patterns in Gain and Shape of Primary Auditory Cortical Receptive Fields. *Neuron*, 61(3):467–480, 2009. doi: 10.1016/j.neuron.2008.12.027. URL http://dx.doi.org/10.1016/j.neuron.2008.12.027.

Serin Atiani, Stephen V. David, Diego Elgueda, Michael Locastro, Susanne Radtke-Schuller, Shihab A. Shamma, and Jonathan B. Fritz. Emergent selectivity for task-relevant stimuli in higher-order auditory cortex. *Neuron*, 82(2):486–499, 2014. ISSN 10974199. doi: 10.1016/j.neuron.2014.02.029.

Sophie Bagur, Martin Averseng, Diego Elgueda, Stephen David, Jonathan Fritz, Pingbo Yin, Shihab Shamma, Yves Boubenec, and Srdjan Ostojic. Go/No-Go task engagement enhances population representation of target stimuli in primary auditory cortex. *Nature Com-*

*munications*, 9(1):2529, 2018. ISSN 2041-1723. doi: 10.1038/s41467-018-04839-9. URL http://www.nature.com/articles/s41467-018-04839-9.

O Bar-Yosef, Y Rotman, and I Nelken. Responses of Neurons and in Cat and Primary Auditory and Cortex to Bird and Chirps: Effects and of Temporal and Spectral Context. *The Journal of Neuroscience*, 22 (19), 2002.

Nicolas Barascud, Marcus Pearce, Timothy Griffiths, Karl Friston, and Maria Chait. MEG responses in humans reveal ideal-observer-like sensitivity to complex acoustic patterns. *Proc Natl Acad Sci U S A*, pages 1–41, 2016. ISSN 1091-6490. doi: 10.1073/pnas.1508523113.

H. B. BARLOW. Increment thresholds at low intensities considered as signal/noise discriminations. *The Journal of physiology*, 1957. ISSN 00223751. doi: 10.1113/jphysiol.1957.sp005774.

Peter Bartho, Carina Curto, Artur Luczak, Stephan L. Marguet, and Kenneth D. Harris. Population coding of tone stimuli in auditory cortex: Dynamic rate vector analysis. *European Journal of Neuroscience*, 30(9):1767–1778, 2009. ISSN 0953816X. doi: 10.1111/j.1460-9568.2009.06954.x.

Yoav Benjamini and Yosef Hochberg. Controlling the False Discovery Rate: A Practical and Powerful Approach to Multiple Testing. *Journal of the Royal Statistical Society. Series B (Methodological)*, 57(1):289–300, 1995. ISSN 00359246. doi: 10.2307/2346101. URL http://www.jstor.org/stable/2346101.

Andrea Benucci, Aman B Saleem, and Matteo Carandini. Adaptation maintains population homeostasis in primary visual cortex. *Nat Neurosci*, 16(6):724–729, jun 2013. doi: 10.1038/nn.3382. URL http://dx.doi.org/10.1038/nn.3382.

A. Berditchevskaia, R. D. Cazé, and S. R. Schultz. Performance in a GO/NOGO perceptual task reflects a balance between impulsive and instrumental components of behaviour. *Scientific Reports*, 6(August 2015):1–15, 2016. ISSN 20452322. doi: 10.1038/srep27389. URL http://dx.doi.org/10.1038/srep27389.

Celian Bimbard, Charlie Demene, Constantin Girard, Susanne Radtke-Schuller, Shihab Shamma, Mickael Tanter, and Yves Boubenec. Multi-scale mapping along the auditory hierarchy using high-resolution functional UltraSound in the awake ferret. *eLife*, page 249417, 2018. doi: 10.1101/249417. URL https://www.biorxiv.org/content/early/2018/01/17/249417.

Christopher M Bishop. *Pattern Recognition and Machine Learning*. 2006. ISBN 9780387310732. doi: 10.1117/1.2819119.

Jennifer K Bizley, Fernando R Nodal, Israel Nelken, and Andrew J King. Functional organization of ferret auditory cortex. *Cereb Cortex*, 15(10):1637–1653, oct 2005. doi: 10.1093/cercor/bhi042. URL http://dx.doi.org/10.1093/cercor/bhi042.

Jennifer K Bizley, Kerry M M Walker, Fernando R Nodal, Andrew J King, and Jan W H Schnupp. Auditory cortex represents both pitch judgments and the corresponding acoustic cues. *Curr Biol*, 23(7):620–625, apr 2013. doi: 10.1016/j.cub.2013.03.003. URL http://dx.doi.org/10.1016/j.cub.2013.03.003.

Rafal Bogacz, Eric Brown, Jeff Moehlis, Philip Holmes, and Jonathan D Cohen. The physics of optimal decision making: a formal analysis of models of performance in two-alternative forced-choice tasks. *Psychological review*, 113(4):700–765, 2006. ISSN 0033-295X. doi: 10.1037/0033-295X.113.4.700.

Yves Boubenec, Jennifer Lawlor, Urszula Górska, Shihab Shamma, and Bernhard Englitz. Detecting changes in dynamic and complex acoustic environments. *eLife*, 6, 2017. ISSN 2050084X. doi: 10.7554/eLife.24910.

Scott L. Brincat, Markus Siegel, Constantin von Nicolai, and Earl K. Miller. Gradual progression from sensory to task-related processing in cerebral cortex. *Proceedings of the National Academy of Sciences*, 115(30):E7202–E7211, 2018. ISSN 0027-8424. doi: 10.1073/pnas.1717075115. URL http://www.pnas.org/lookup/doi/10.1073/pnas.1717075115.

K.H. Britten, W.T. Newsome, M.N. Shadlen, J.A. Movshon, and S Celebrini. A relationship between behavioral choice and the visual responses of neurons in macaque MT. *Visual Neuroscience*, 13(01):87–100, 1996. ISSN 0952-5238. doi: 10.1017/S095252380000715X. URL http://journals.cambridge.org/abstract_S095252380000715X.

Bingni W Brunton, Matthew M Botvinick, and Carlos D Brody. Rats and humans can optimally accumulate evidence for decision-making. *Science*, 340(6128):95–98, apr 2013. doi: 10.1126/science.1233912. URL http://dx.doi.org/10.1126/science.1233912.

Matteo Carandini and David J. Heeger. Normalization as a canonical neural computation. *Nature Reviews Neuroscience*, 13(1):51–62, 2012. ISSN 1471003X. doi: 10.1038/nrn3136.

Marie Carlen. What constitutes the prefrontal cortex? ( 6 ). *Science*, 482(October):478–482, 2017. ISSN 0036-8075. doi: 10.1126/science.aan8868.

Federico Carnevale, Victor DeLafuente, Ranulfo Romo, Omri Barak, and Néstor Parga. Dynamic Control of Response Criterion in Premotor Cortex during Perceptual Detection under Temporal Uncertainty. *Neuron*, 86(4):1067–1077, 2015. ISSN 10974199. doi: 10.1016/j.neuron.2015.04.014.

Vincent Castranova, Bahman Asgharian, Phil Sayre, West Virginia, and North Carolina. HHS Public Access. 28(3):1922–2013, 2016. ISSN 1527-5418. doi: 10.1080/10937404.2015.1051611.INHALATION.

Nicolas Catz and Arnaud J Noreña. Enhanced representation of spectral contrasts in the primary auditory cortex. *Front Syst Neurosci*, 7:21, 2013. doi: 10.3389/fnsys.2013.00021. URL http://dx.doi.org/10.3389/fnsys.2013.00021.

Francisco Cervantes Constantino, Leyla Pinggera, Supathum Paranamana, Makio Kashino, and Maria Chait. Detection of appearing and disappearing objects in complex acoustic scenes. *PLoS One*, 7(9):e46167, 2012. doi: 10.1371/journal.pone.0046167. URL http://dx.doi.org/10.1371/journal.pone.0046167.

Taishih Chi, Powen Ru, and Shihab A Shamma. Multiresolution spectrotemporal analysis of complex sounds. *J Acoust Soc Am*, 118(2):887–906, 2005.

Anne K Churchland, Roozbeh Kiani, and Michael N Shadlen. Decision-making with multiple alternatives. *Nature Neuroscience*, 11(6):693–702, 2008. ISSN 1097-6256. doi: 10.1038/nn0708-851c.

Paul Cisek, Geneviève Aude Puskas, and Stephany El-Murr. Decisions in changing conditions: the urgency-gating model. *J Neurosci*, 29(37):11560–11571, sep 2009. doi: 10.1523/JNEUROSCI.1844-09.2009. URL http://dx.doi.org/10.1523/JNEUROSCI.1844-09.2009.

Yale E. Cohen, Marc D. Hauser, and Brian E. Russ. Spontaneous processing of abstract categorical information in the ventrolateral prefrontal cortex. *Biology Letters*, 2(2):261–265, 2006. ISSN 1744957X. doi: 10.1098/rsbl.2005.0436.

Olympia Colizoli, Jan Willem de Gee, Anne Urai, and Tobias H. Donner. Task-evoked pupil responses reflect internal belief states. *bioRxiv*, (July):275776, 2018. doi: 10.1101/275776. URL https://www.biorxiv.org/content/early/2018/03/03/275776.

John P Cunningham and Byron M Yu. Dimensionality reduction for large-scale neural recordings. *Nat Neurosci*, 2014. doi: 10.1038/nn.3776. URL http://dx.doi.org/10.1038/nn.3776.

S V David, J B Fritz, and S A Shamma. Task reward structure shapes rapid receptive field plasticity in auditory cortex. *Proc Natl Acad Sci U S A*, 109(6):2144–2149, 2012. doi: 10.1073/pnas.1117717109. URL http://dx.doi.org/10.1073/pnas.1117717109.

Alain de Cheveigné and Lucas C Parra. Joint decorrelation, a versatile tool for multichannel data analysis. *Neuroimage*, 98:487–505, sep 2014. doi: 10.1016/j.neuroimage.2014.05.068. URL http://dx.doi.org/10.1016/j.neuroimage.2014.05.068.

Jan Willem de Gee, Tomas Knapen, and Tobias H Donner. Decision-related pupil dilation reflects upcoming choice and individual bias. *Proceedings of the National Academy of Sciences of the United States of America*, 111(5):E618–25, 2014. ISSN 1091-6490. doi: 10.1073/pnas.1317557111. URL http://www.ncbi.nlm.nih.gov/pubmed/24449874.

V. de Lafuente and R. Romo. Neural correlate of subjective sensory experience gradually builds up across cortical areas. *Proceedings of the National Academy of Sciences*, 103(39):14266–14271, 2006. ISSN 0027-8424. doi: 10.1073/pnas.0605826103. URL http://www.pnas.org/cgi/doi/10.1073/pnas.0605826103.

Arnaud Delorme and Scott Makeig. EEGLAB: An open source toolbox for analysis of single-trial EEG dynamics including independent component analysis. *J. Neurosci. Methods*, 134(1):9–21, 2004. ISSN 01650270. doi: 10.1016/j.jneumeth.2003.10.009.

Arnaud Delorme, Tim Mullen, Christian Kothe, Zeynep Akalin Acar, Nima Bigdely-Shamlo, Andrey Vankov, and Scott Makeig. EEGLAB, SIFT, NFT, BCILAB, and ERICA: New tools for advanced EEG processing. *Computational Intelligence and Neuroscience*, 2011, 2011. ISSN 16875265. doi: 10.1155/2011/130714.

Jochen Ditterich. Stochastic models of decisions about motion direction: Behavior and physiology. *Neural Networks*, 19(8):981–1012, 2006. ISSN 08936080. doi: 10.1016/j.neunet.2006.05.042.

Ja Swets DM Green, D M Green, and J a Swets. Signal detection theory and psychophysics. *Society*, 1966. ISSN 00225002. doi: 10.1901/jeab.1969.12-475.

Jan Drugowitsch, Rubén Moreno-Bote, Anne K Churchland, Michael N Shadlen, and Alexandre Pouget. The cost of accumulating evidence in perceptual decision making. *J Neurosci*, 32(11):3612–3628, mar 2012. doi: 10.1523/JNEUROSCI.4010-11.2012. URL http://dx.doi.org/10.1523/JNEUROSCI.4010-11.2012.

James P. Egan, G Z. Greenberg, and A I. Schulman. Operating Characteristics, Signal Detectability, and the Method of Free Response. *J Acoust Soc Am*, 33(8):993, 1961. ISSN 00014966. doi: 10.1121/1.1908935. URL http://scitation.aip.org/content/asa/journal/jasa/33/8/10.1121/1.1908935.

Jos J Eggermont. Temporal modulation transfer functions in cat primary auditory cortex: separating stimulus effects from neural mechanisms. *J Neurophysiol*, 87(1):305–321, 2002. ISSN 0022-3077.

Einhäuser. Pupil dilation betrays the timing of decisions. *Frontiers in Human Neuroscience*, 2010. ISSN 16625161. doi: 10.3389/fnhum.2010.00018. URL http://journal.frontiersin.org/article/10.3389/fnhum.2010.00018/abstract.

W. Einhauser, J. Stout, C. Koch, and O. Carter. Pupil dilation reflects perceptual selection and predicts subsequent stability in perceptual rivalry. *Proceedings of the National Academy of Sciences*, 105(5):1704–1709, 2008. ISSN 0027-8424. doi: 10.1073/pnas.0707727105. URL http://www.pnas.org/cgi/doi/10.1073/pnas.0707727105.

Mounya Elhilali, Ling Ma, Christophe Micheyl, Andrew J Oxenham, and Shihab A Shamma. Temporal Coherence in the Perceptual Organization and Cortical Representation of Auditory Scenes. *Neuron*, 61(2):317–329, jan 2009. doi: 10.1016/j.neuron.2008.12.005. URL http://dx.doi.org/10.1016/j.neuron.2008.12.005.

B. Englitz, S. V. David, M. D. Sorenson, and S. A. Shamma. MANTA—an open-source, high density electrophysiology recording suite for MATLAB. *Frontiers in Neural Circuits*, 7(May):1–15, 2013. ISSN 1662-5110. doi: 10.3389/fncir.2013.00069. URL http://journal.frontiersin.org/article/10.3389/fncir.2013.00069/abstract.

Jeffrey C. Erlich, Max Bialek, and Carlos D. Brody. A cortical substrate for memory-guided orienting in the rat. *Neuron*, 72(2):330–343, 2011. ISSN 08966273. doi: 10.1016/j.neuron.2011.07.010.

Jeffrey C. Erlich, Bingni W. Brunton, Chunyu A. Duan, Timothy D. Hanks, and Carlos D. Brody. Distinct effects of prefrontal and parietal cortex inactivations on an accumulation of evidence task in the rat. *eLife*, 2015(4), 2015. ISSN 2050084X. doi: 10.7554/eLife.05457.001.

J. B. Fritz. Differential Dynamic Plasticity of A1 Receptive Fields during Multiple Spectral Tasks. *Journal of Neuroscience*, 25(33):7623–7635, 2005. ISSN 0270-6474. doi: 10.1523/JNEUROSCI.1318-05.2005. URL http://www.jneurosci.org/cgi/doi/10.1523/JNEUROSCI.1318-05.2005.

Jonathan Fritz, Shihab Shamma, Mounya Elhilali, and David Klein. Rapid task-related plasticity of

spectrotemporal receptive fields in primary auditory cortex. *Nature Neuroscience*, 6(11):1216–1223, 2003. ISSN 10976256. doi: 10.1038/nn1141.

Jonathan B Fritz, Stephen V David, Susanne Radtke-Schuller, Pingbo Yin, and Shihab A Shamma. Adaptive, behaviorally gated, persistent encoding of task-relevant auditory information in ferret frontal cortex. *Nature neuroscience*, 13(8):1011–9, 2010. ISSN 1546-1726. doi: 10.1038/nn.2598. URL http://www.pubmedcentral.nih.gov/articlerender.fcgi?artid=2921886&tool=pmcentrez&rendertype=abstract.

Jan Willem De Gee, Olympia Colizoli, Niels A Kloosterman, Tomas Knapen, Sander Nieuwenhuis, and Tobias H Donner. Dynamic modulation of decision biases by brainstem arousal systems. (Lc): 1–36, 2017. doi: 10.7554/eLife.23232.

J Gold and M Shadlen. The neural basis of decision making. *Annu. Rev. Neurosci*, 30(1): 535–574, 2007. ISSN 0147-006X. doi: 10.1146/annurev.neuro.29.051605.113038. URL http://www.ncbi.nlm.nih.gov/entrez/query.fcgi?db=pubmed&cmd=Retrieve&dopt=AbstractPlus&list_uids=5656

D M Green and B G Berg. Spectral weights and the profile bowl. *Q J Exp Psychol A*, 43(3):449–458, aug 1991.

D M Green and J a Swets. Signal detection theory and psychophysics. *Society*, 1(3):521, 1966. ISSN 00225002. doi: 10.1901/jeab.1969.12-475. URL http://psycnet.apa.org/psycinfo/1975-00121-000.

D M Green, B G Berg, H Dai, D A Eddins, Z Onsan, and Q Nguyen. Spectral shape discrimination of narrow-band sounds. *J Acoust Soc Am*, 92(5):2586–2597, nov 1992.

DM Green. *Profile Analysis*. Oxford University Press, oxford psy edition, 1988.

Paul S. Hammon, Scott Makeig, Howard Poizner, Emanuel Todorov, and Virginia R. de Sa. Predicting reaching targets from human EEG. *IEEE Signal Processing Magazine*, 25(1):69–77, 2008. ISSN 10535888. doi: 10.1109/MSP.2008.4408443.

Timothy D. Hanks and Christopher Summerfield. Perceptual Decision Making in Rodents, Monkeys, and Humans. *Neuron*, 93(1):15–31, 2017. ISSN 10974199. doi: 10.1016/j.neuron.2016.12.003. URL http://dx.doi.org/10.1016/j.neuron.2016.12.003.

Timothy D Hanks, Jochen Ditterich, and Michael N Shadlen. Microstimulation of macaque area LIP affects decision-making in a motion discrimination task. *Nature neuroscience*, 9(5):682–689, 2006. ISSN 1097-6256. doi: 10.1038/nn1683.

Timothy D. Hanks, Roozbeh Kiani, and Michael N. Shadlen. A neural mechanism of speed-accuracy tradeoff in macaque area LIP. *eLife*, 2014(3):1–17, 2014. ISSN 2050084X. doi: 10.7554/eLife.02260.

Timothy D. Hanks, Charles D. Kopec, Bingni W. Brunton, Chunyu A. Duan, Jeffrey C. Erlich, and Carlos D. Brody. Distinct relationships of parietal and prefrontal cortices to evidence accumulation. *Nature*, 520(7546):220–3, 2015. ISSN 0028-0836. doi: 10.1038/nature14066. URL http://www.ncbi.nlm.nih.gov/pubmed/25600270.

R. Hari, K. Aittoniemi, M. L. Järvinen, T. Katila, and T. Varpula. Auditory evoked transient and sustained magnetic fields of the human brain localization of neural generators. *Experimental Brain Research*, 40(2):237–240, 1980. ISSN 00144819. doi: 10.1007/BF00237543.

Kenneth D Harris and Alexander Thiele. Cortical state and attention. *Nat Rev Neurosci*, 12(9):509–523, sep 2011. doi: 10.1038/nrn3084. URL http://dx.doi.org/10.1038/nrn3084.

W M Hartmann, S McAdams, A Gerzso, and P Boulez. Discrimination of spectral density. *J Acoust Soc Am*, 79(6):1915–1925, jun 1986.

R. J. Herrnstein, Donald H. Loveland, and Cynthia Cable. Natural concepts in pigeons. *Journal of Experimental Psychology: Animal Behavior Processes*, 2(4):285–302, 1976. ISSN 00977403. doi: 10.1037/0097-7403.2.4.285.

A. C. Huk. Neural Activity in Macaque Parietal Cortex Reflects Temporal Integration of Visual Motion Signals during Perceptual Decision Making. *Journal of Neuroscience*, 25(45): 10420–10436, 2005. ISSN 0270-6474. doi: 10.1523/JNEUROSCI.4684-04.2005. URL http://www.jneurosci.org/cgi/doi/10.1523/JNEUROSCI.4684-04.2005.

Elina A K Jacobs, Nicholas A Steinmetz, Matteo Carandini, Kenneth D Harris, and Kenneth Uk. Cortical state fluctuations during sensory decision making. *bioRxiv*, pages 1–22, 2018. doi: 10.1101/348193. URL https://www.biorxiv.org/content/biorxiv/early/2018/06/16/348193.full.pdf.

Peter Janssen and Michael N. Shadlen. A representation of the hazard rate of elapsed time in macaque area LIP. *Nature Neuroscience*, 8(2):234–241, 2005. ISSN 10976256. doi: 10.1038/nn1386.

Bridgette Johnson, Rebeka Verma, Manying Sun, and Timothy D. Hanks. Characterization of decision commitment rule alterations during an auditory change detection task. *Journal of Neu-*

*rophysiology*, 118(5):2526–2536, 2017. ISSN 0022-3077. doi: 10.1152/jn.00071.2017. URL http://www.physiology.org/doi/10.1152/jn.00071.2017.

Siddhartha Joshi, Yin Li, Rishi M. Kalwani, and Joshua I. Gold. Relationships between Pupil Diameter and Neuronal Activity in the Locus Coeruleus, Colliculi, and Cingulate Cortex. *Neuron*, 89(1):221–234, 2016. ISSN 10974199. doi: 10.1016/j.neuron.2015.11.028.

Daniel Kahneman and Jackson Beatty. Pupil diameter and load on memory. *Science*, 1966. ISSN 00368075. doi: 10.1126/science.154.3756.1583.

Leor N. Katz, Jacob L. Yates, Jonathan W. Pillow, and Alexander C. Huk. Dissociated functional significance of decision-related activity in the primate dorsal stream. *Nature*, 535(7611):285–288, 2016. ISSN 14764687. doi: 10.1038/nature18617. URL http://dx.doi.org/10.1038/nature18617.

Emine Merve Kaya and Mounya Elhilali. Investigating bottom-up auditory attention. *Front Hum Neurosci*, 8:327, 2014. doi: 10.3389/fnhum.2014.00327. URL http://dx.doi.org/10.3389/fnhum.2014.00327.

Simon P Kelly and Redmond G O'Connell. Internal and external influences on the rate of sensory evidence accumulation in the human brain. *J Neurosci*, 33(50):19434–19441, 2013. doi: 10.1523/JNEUROSCI.3355-13.2013. URL http://dx.doi.org/10.1523/JNEUROSCI.3355-13.2013.

Simon P. Kelly and Redmond G. O'Connell. The neural processes underlying perceptual decision making in humans: Recent progress and future directions. *Journal of Physiology Paris*, 109(1-3):27–37, 2015. ISSN 17697115. doi: 10.1016/j.jphysparis.2014.08.003. URL http://dx.doi.org/10.1016/j.jphysparis.2014.08.003.

N Y-S Kiang, T Watanabe, E C Thomas, and L F Clark. Discharge patterns of single fibers in the cat's auditory nerve. Technical report, 1965.

R. Kiani, T. D. Hanks, and M. N. Shadlen. Bounded Integration in Parietal Cortex Underlies Decisions Even When Viewing Duration Is Dictated by the Environment. *Journal of Neuroscience*, 28(12):3017–3029, 2008. ISSN 0270-6474. doi: 10.1523/JNEUROSCI.4761-07.2008. URL http://www.jneurosci.org/cgi/doi/10.1523/JNEUROSCI.4761-07.2008.

Roozbeh Kiani, Leah Corthell, and Michael N Shadlen. Choice certainty is informed by both evidence and decision time. *Neuron*, 84(6):1329–1342, 2014. doi: 10.1016/j.neuron.2014.12.015. URL http://dx.doi.org/10.1016/j.neuron.2014.12.015.

J N Kim and M N Shadlen. Neural correlates of a decision in the dorsolateral prefrontal cortex of the macaque. *Nature neuroscience*, 2(2):176–185, 1999. ISSN 1097-6256. doi: 10.1038/5739.

Dmitry Kobak, Wieland Brendel, Christos Constantinidis, Claudia E. Feierstein, Adam Kepecs, Zachary F. Mainen, Xue Lian Qi, Ranulfo Romo, Naoshige Uchida, and Christian K. Machens. Demixed principal component analysis of neural population data. *eLife*, 5(APRIL2016):1–36, 2016. ISSN 2050084X. doi: 10.7554/eLife.10989.

N Kowalski, D A Depireux, and S Shamma. Analysis of Dynamic and Spectra in Ferret and Primary Auditory and Cortex. I. and Characteristics of Single-Unit and Responses to Moving and Ripple Spectra. *J Neurophysiol*, 76 (5), 1996.

Kamesh Krishnamurthy, Matthew R. Nassar, Shilpa Sarode, and Joshua I. Gold. Arousal-related adjustments of perceptual biases optimize perception in dynamic environments. *Nature Human Behaviour*, 1(6):0107, 2017. ISSN 2397-3374. doi: 10.1038/s41562-017-0107. URL http://www.nature.com/articles/s41562-017-0107.

Lakshmi Krishnan, Mounya Elhilali, and Shihab Shamma. Segregating Complex Sound Sources through Temporal Coherence. *PLoS Comput Biol*, 10(12):e1003985, 2014. doi: 10.1371/journal.pcbi.1003985. URL http://dx.doi.org/10.1371/journal.pcbi.1003985.

Christian Lammertmann and Bernd Lütkenhöner. Near-DC magnetic fields following a periodic presentation of long-duration tonebursts. *Clinical Neurophysiology*, 112(3):499–513, 2001. ISSN 13882457. doi: 10.1016/S1388-2457(00)00551-4.

Jack L. Lancaster, Marty G. Woldorff, Lawrence M. Parsons, Mario Liotti, Catarina S. Freitas, Lacy Rainey, Peter V. Kochunov, Dan Nickerson, Shawn A. Mikiten, and Peter T. Fox. Automated Talairach Atlas labels for functional brain mapping. *Human Brain Mapping*, 10(3):120–131, 2000. ISSN 10659471. doi: 10.1002/1097-0193(200007)10:3<120::AID-HBM30>3.0.CO;2-8.

Kenneth W. Latimer, Jacob L. Yates, Miriam L. R. Meister, Alexander C. Huk, and Jonathan W. Pillow. Single-trial spike trains in parietal cortex reveal discrete steps during decision-making. *Science*, 349(6244):184–187, 2013. ISSN 0036-8075. doi: 10.1126/science.aaa4056.

Kenneth W Latimer, Jacob L Yates, Miriam L R Meister, Alexander C Huk, and Jonathan W Pillow. NEURONAL MODELING. Single-trial spike trains in parietal cortex reveal discrete steps during decision-making. *Science*, 349(6244):184–187, 2015. doi: 10.1126/science.aaa4056. URL http://dx.doi.org/10.1126/science.aaa4056.

Vernon Lawhern, Wei Wu, Nicholas Hatsopoulos, and Liam Paninski. Population decoding of motor cortical activity using a generalized linear model with hidden states. *Journal of Neuroscience Methods*, 189(2):267–280, 2010. ISSN 01650270. doi: 10.1016/j.jneumeth.2010.03.024. URL http://dx.doi.org/10.1016/j.jneumeth.2010.03.024.

S. J. Lederman. Auditory texture perception. *Perception*, 8(1):93–103, 1979. ISSN 03010066. doi: 10.1068/p080093.

Karolina M. Lempert, Yu Lin Chen, and Stephen M. Fleming. Relating pupil dilation and metacognitive confidence during auditory decision-making. *PLoS ONE*, 10(5), 2015. ISSN 19326203. doi: 10.1371/journal.pone.0126588.

J J Lentz and V M Richards. Sensitivity to changes in overall level and spectral shape: an evaluation of a channel model. *J Acoust Soc Am*, 101(6):3625–3635, jun 1997.

Daniel T Levin and Daniel J Simons. Failure to detect changes to attended objects in motion pictures. *Psychonomic Bulletin & Review*, 4(4):501–506, 1997. ISSN 1069-9384. doi: 10.3758/BF03214339.

Michael S Lewicki. Efficient coding of natural sounds. *Nature neuroscience*, 5(4):356–363, 2002. ISSN 1097-6256. doi: 10.1038/nn831. URL http://www.ncbi.nlm.nih.gov/pubmed/11896400.

Li Liang, Thomas Lu, and Xiaoqin Wang. Neural representations of sinusoidal amplitude and frequency modulations in the primary auditory cortex of awake primates. *J Neurophysiol*, 87(5):2237–2261, 2002.

A. Luczak, P. Bartho, and K. D. Harris. Gating of Sensory Input by Spontaneous Cortical Activity. *Journal of Neuroscience*, 33(4):1684–1695, 2013. ISSN 0270-6474. doi: 10.1523/JNEUROSCI.2928-12.2013. URL http://www.jneurosci.org/cgi/doi/10.1523/JNEUROSCI.2928-12.2013.

Bernd Lütkenhöner, Annemarie Seither-Preisler, Katrin Krumbholz, and Roy D. Patterson. Auditory cortex tracks the temporal regularity of sustained noisy sounds. *Hearing Research*, 272(1-2):85–94, 2011. ISSN 03785955. doi: 10.1016/j.heares.2010.10.013.

C. K. Machens, R. Romo, and C. D. Brody. Functional, But Not Anatomical, Separation of ”What” and ”When” in Prefrontal Cortex. *Journal of Neuroscience*, 30(1): 350–360, 2010. ISSN 0270-6474. doi: 10.1523/JNEUROSCI.3276-09.2010. URL http://www.jneurosci.org/cgi/doi/10.1523/JNEUROSCI.3276-09.2010.

N A Macmillan and C D Creelman. *Detection Theory: A User's Guide*. 2005. ISBN 0805842306.

Valerio Mante, David Sussillo, Krishna V. Shenoy, and William T. Newsome. Context-dependent computation by recurrent dynamics in prefrontal cortex. *Nature*, 503(7474):78–84, 2013. ISSN 00280836. doi: 10.1038/nature12742.

Stephan L Marguet and Kenneth D Harris. State-dependent representation of amplitude-modulated noise stimuli in rat auditory cortex. *J Neurosci*, 31(17):6414–6420, 2011. doi: 10.1523/JNEUROSCI.5773-10.2011. URL http://dx.doi.org/10.1523/JNEUROSCI.5773-10.2011.

David Marr. *Vision*. 1982. ISBN 9780262514620. URL http://books.google.com/books?id=EehUQwAACAAJ&printsec=frontcover%5Cnpapers2://publication/uuid/FBB059-4C15D54099CE.

Mark E. Mazurek, Jamie D. Roitman, Jochen Ditterich, and Michael N. Shadlen. A Role for Neural Integrators in Perceptual Decision Making. *Cerebral Cortex*, 13(11):1257–1269, 2003. ISSN 10473211. doi: 10.1093/cercor/bhg097.

J H McDermott, D Wrobleski, and A J Oxenham. Recovering sound sources from embedded repetition. *Proceedings of the National Academy of Sciences*, 108(3):1188–1193, jan 2011. doi: 10.1073/pnas.1004765108. URL http://dx.doi.org/10.1073/pnas.1004765108.

Josh H McDermott and Eero P Simoncelli. Sound texture perception via statistics of the auditory periphery: evidence from sound synthesis. *Neuron*, 71(5):926–940, sep 2011. doi: 10.1016/j.neuron.2011.06.032. URL http://dx.doi.org/10.1016/j.neuron.2011.06.032.

Josh H Mcdermott, Michael Schemitsch, and Eero P Simoncelli. No Title. 16(4):493–498, 2013.

Matthew J. McGinley, Stephen V. David, and David A. McCormick. Cortical Membrane Potential Signature of Optimal States for Sensory Signal Detection. *Neuron*, 87 (1):179–192, 2015a. ISSN 10974199. doi: 10.1016/j.neuron.2015.05.038. URL http://dx.doi.org/10.1016/j.neuron.2015.05.038.

Matthew J. McGinley, Martin Vinck, Jacob Reimer, Renata Batista-Brito, Edward Zagha, Cathryn R. Cadwell, Andreas S. Tolias, Jessica A. Cardin, and David A. McCormick. Waking State: Rapid Variations Modulate Neural and Behavioral Responses. *Neuron*, 87 (6):1143–1161, 2015b. ISSN 10974199. doi: 10.1016/j.neuron.2015.09.012. URL http://dx.doi.org/10.1016/j.neuron.2015.09.012.

Richard McWalter and Torsten Dau. Cascaded Amplitude Modulations in Sound Texture Per-

ception. *Frontiers in Neuroscience*, 11(September):1–12, 2017. ISSN 1662-453X. doi: 10.3389/fnins.2017.00485. URL http://journal.frontiersin.org/article/10.3389/fnins.2017.00485/full.

Richard McWalter and Josh H. McDermott. Adaptive and Selective Time Averaging of Auditory Scenes. *Current Biology*, 28(9):1405–1418.e10, 2018. ISSN 09609822. doi: 10.1016/j.cub.2018.03.049. URL https://doi.org/10.1016/j.cub.2018.03.049.

Nima Mesgarani, S.V. David, J.B. Fritz, and S.A. Shamma. Influence of context and behavior on stimulus reconstruction from neural activity in primary auditory cortex. *Journal of neurophysiology*, 102(6):3329, 2009. doi: 10.1152/jn.91128.2008. URL http://jn.physiology.org/cgi/content/abstract/102/6/3329.

Vernon B. Mountcastle. MODALITY AND TOPOGRAPHIC PROPERTIES OF SINGLE NEURONS OF CAT'S SOMATIC SENSORY CORTEX. *Journal of Neurophysiology*, 1957. ISSN 0022-3077. doi: 10.1152/jn.1957.20.4.408.

Peter R. Murphy, Joachim Vandekerckhove, and Sander Nieuwenhuis. Pupil-Linked Arousal Determines Variability in Perceptual Decision Making. *PLoS Computational Biology*, 10(9), 2014. ISSN 15537358. doi: 10.1371/journal.pcbi.1003854.

D L Neff and D M Green. Masking produced by spectral uncertainty with multicomponent maskers. *Percept Psychophys*, 41(5):409–415, may 1987.

Yingjiu Nie, Yang Zhang, and Peggy B Nelson. Auditory stream segregation using bandpass noises: evidence from event-related potentials. *Frontiers in neuroscience*, 8:277, 2014. ISSN 1662-4548. doi: 10.3389/fnins.2014.00277. URL http://www.pubmedcentral.nih.gov/articlerender.fcgi?artid=4162371%7B&%7Dtool=pmcentrez%7B&%7Drend

Shinji Nishimoto, An T. Vu, Thomas Naselaris, Yuval Benjamini, Bin Yu, and Jack L. Gallant. Reconstructing visual experiences from brain activity evoked by natural movies. *Current Biology*, 21(19): 1641–1646, 2011. ISSN 09609822. doi: 10.1016/j.cub.2011.08.031.

Redmond G O'Connell, Paul M Dockree, and Simon P Kelly. A supramodal accumulation-to-bound signal that determines perceptual decisions in humans. *Nat Neurosci*, 15(12):1729–1735, dec 2012. doi: 10.1038/nn.3248. URL http://dx.doi.org/10.1038/nn.3248.

Gouki Okazawa, Long Sha, Braden A. Purcell, and Roozbeh Kiani. Psychophysical reverse correlation reflects both sensory and decision-making processes. *bioRxiv*, (2018):273680, 2018. ISSN 2041-1723. doi: 10.1101/273680. URL https://www.biorxiv.org/content/early/2018/03/13/273680.

Robert Oostenveld, Pascal Fries, Eric Maris, and Jan Mathijs Schoffelen. FieldTrip: Open source software for advanced analysis of MEG, EEG, and invasive electrophysiological data. *Computational Intelligence and Neuroscience*, 2011, 2011. ISSN 16875265. doi: 10.1155/2011/156869.

Ori Ossmy, Rani Moran, Thomas Pfeffer, Konstantinos Tsetsos, Marius Usher, and Tobias H. Donner. The timescale of perceptual evidence integration can be adapted to the environment. *Current Biology*, 23(11):981–986, 2013. ISSN 09609822. doi: 10.1016/j.cub.2013.04.039. URL http://dx.doi.org/10.1016/j.cub.2013.04.039.

A. Oswal, Miriam Ogden, and R.H.S. Carpenter. The Time Course of Stimulus Expectation in a Saccadic Decision Task. *Journal of Neurophysiology*, 97(4):2722–2730, 2007. ISSN 0022-3077. doi: 10.1152/jn.01238.2006. URL http://www.physiology.org/doi/10.1152/jn.01238.2006.

Tobias Overath, Sukhbinder Kumar, Katharina von Kriegstein, and Timothy D Griffiths. Encoding of spectral correlation over time in auditory cortex. *J Neurosci*, 28(49):13268–13273, 2008. ISSN 1529-2401. doi: 10.1523/JNEUROSCI.4596-08.2008.

Tobias Overath, Sukhbinder Kumar, Lauren Stewart, Katharina von Kriegstein, Rhodri Cusack, Adrian Rees, and Timothy D Griffiths. Cortical mechanisms for the segregation and representation of acoustic textures. *J Neurosci*, 30(6):2070–2076, 2010. doi: 10.1523/JNEUROSCI.5378-09.2010. URL http://dx.doi.org/10.1523/JNEUROSCI.5378-09.2010.

Liam Paninski, Matthew R Fellows, Nicholas G Hatsopoulos, P John, Wei Wang, Gustavo P Sudre, Yang Xu, Robert E Kass, Jennifer L Collinger, D Alan, Anto I Bagic, and Douglas J Weber. Spatiotemporal Tuning of Motor Cortical Neurons for Hand Position and Velocity. *Journal of Neurophysiology*, (September 2003):515–532, 2011. ISSN 0022-3077. doi: 10.1152/jn.00587.2002.

Il Memming Park, Miriam L R Meister, Alexander C Huk, and Jonathan W Pillow. Encoding and decoding in parietal cortex during sensorimotor decision-making. *Nat Neurosci*, 17(August):1395–1403, 2014. ISSN 1546-1726. doi: 10.1038/nn.3800. URL http://dx.doi.org/10.1038/nn.3800%5Cnhttp://www.ncbi.nlm.nih.gov/pubmed/25174005.

A. J. Parker and W. T. Newsome. SENSE AND THE SINGLE NEURON: Probing the Physiology of Perception. *Annual Review of Neuroscience*, 21(1):227–277, 1998. ISSN 0147-006X. doi: 10.1146/annurev.neuro.21.1.227. URL http://www.annualreviews.org/doi/abs/10.1146/annurev.neuro.21.1.227.

Kailash Patil, Daniel Pressnitzer, Shihab Shamma, and Mounya Elhilali. Music in our ears: the

biological bases of musical timbre perception. *PLoS Comput Biol*, 8(11):e1002759, 2012. doi: 10.1371/journal.pcbi.1002759. URL http://dx.doi.org/10.1371/journal.pcbi.1002759.

Gordon E. Peterson and Harold L. Barney. Control Methods Used in a Study of the Vowels. *The Journal of the Acoustical Society of America*, 1952. ISSN 0001-4966. doi: 10.1121/1.1906875.

Leopoldo Petreanu, Diego a Gutnisky, Daniel Huber, Ning-long Xu, Dan H O'Connor, Lin Tian, Loren Looger, and Karel Svoboda. Activity in motor-sensory projections reveals distributed coding in somatosensation. *Nature*, 489 (7415):299–303, 2012. ISSN 1476-4687. doi: 10.1038/nature11321. URL http://www.pubmedcentral.nih.gov/articlerender.fcgi?artid=3443316&tool=pmcentrez&rendertype=abstract.

Alex Piet, Ahmed El Hady, and Carlos D Brody. Rats optimally accumulate and discount evidence in a dynamic environment. 2017. doi: 10.1101/204248. URL http://arxiv.org/abs/1710.05945.

D Pins and C Bonnet. On the relation between stimulus intensity and processing time: Piéron's law and choice reaction time. *Perception & psychophysics*, 58(3):390–400, 1996. ISSN 0031-5117. doi: 10.3758/BF03206815.

Bethany Plakke and Lizabeth M. Romanski. Auditory connections and functions of prefrontal cortex. *Frontiers in Neuroscience*, 8(8 JUL):1–13, 2014. ISSN 1662453X. doi: 10.3389/fnins.2014.00199.

Neil C Rabinowitz, Ben D B Willmore, Jan W H Schnupp, and Andrew J King. Contrast gain control in auditory cortex. *Neuron*, 70(6):1178–1191, jun 2011. doi: 10.1016/j.neuron.2011.04.030. URL http://dx.doi.org/10.1016/j.neuron.2011.04.030.

Roger Ratcliff and Gail McKoon. The diffusion decision model: theory and data for two-choice decision tasks. *Neural computation*, 20(4):873–922, 2008. ISSN 0899-7667. doi: 10.1162/neco.2008.12-06-420.

J P Rauschecker, B Tian, T Pons, and M Mishkin. Serial and parallel processing in rhesus monkey auditory cortex. *J Comp Neurol*, 382(1):89–103, 1997.

Ofri Raviv, Merav Ahissar, and Yonatan Loewenstein. How recent history affects perception: the normative approach and its heuristic approximation. *PLoS Comput Biol*, 8(10):e1002731, 2012. doi: 10.1371/journal.pcbi.1002731. URL http://dx.doi.org/10.1371/journal.pcbi.1002731.

Jacob Reimer, Emmanouil Froudarakis, and Cathryn R. Cadwell. Pupil fluctuations track fast switching of cortical states during quiet wakefulness. *Neuron*, 84(2):355–362, 2015. doi: 10.1016/j.neuron.2014.09.033.Pupil.

Alfonso Renart and Christian K. Machens. Variability in neural activity and behavior, 2014. ISSN 18736882.

Ronald A Rensink, J K O'Regan, and J J Clark. On the failure to detect changes in scenes across brief interruptions. *Visual Cognition*, 7(1): 127–145, 2000. ISSN 1350-6285. doi: 10.1080/135062800394720. URL http://www.informaworld.com/10.1080/135062800394720%5Cnpapers3://publication/uuid/F0F795BA-370B-49 8C0BDE0A3022.

Mattia Rigotti, Omri Barak, Melissa R. Warden, Xiao Jing Wang, Nathaniel D. Daw, Earl K. Miller, and Stefano Fusi. The importance of mixed selectivity in complex cognitive tasks. *Nature*, 497(7451): 585–590, 2013. ISSN 00280836. doi: 10.1038/nature12160.

Jamie D Roitman and Michael N Shadlen. Response of Neurons in the Lateral Intraparietal Area during a Combined Visual Discrimination Reaction Time Task. *J Neurosci*, 22(21):9475–9489, 2002. ISSN 1529-2401. URL http://www.jneurosci.org/content/22/21/9475.short.

L M Romanski, B Tian, J Fritz, M Mishkin, P S Goldman-Rakic, and J P Rauschecker. Dual streams of auditory afferents target multiple domains in the primate prefrontal cortex. *Nat Neurosci*, 2(12): 1131–1136, 1999. doi: 10.1038/16056. URL http://dx.doi.org/10.1038/16056.

Lizabeth M Romanski and Patricia S Goldman-Rakic. An auditory domain in primate prefrontal cortex. *Nat Neurosci*, 5(1):15–16, jan 2002. doi: 10.1038/nn781. URL http://dx.doi.org/10.1038/nn781.

R Romo, A Hernandez, and A Zainos. Neuronal correlates of a perceptual decision in ventral premotor cortex. *Neuron*, 2004. ISSN 0896-6273 (Print). doi: S0896627303008171 [pii].

Ranulfo Romo and Victor de Lafuente. Conversion of sensory signals into perceptual decisions, 2013. ISSN 03010082.

Román Rossi-Pool, Emilio Salinas, Antonio Zainos, Manuel Alvarez, José Vergara, Néstor Parga, and Ranulfo Romo. Emergence of an abstract categorical code enabling the discrimination of temporally structured tactile stimuli. *Proceedings of the National Academy of Sciences*, 113(49):E7966–E7975, 2016. ISSN 0027-8424. doi: 10.1073/pnas.1618196113. URL http://www.pnas.org/lookup/doi/10.1073/pnas.1618196113.

J. E. Roy, M. Riesenhuber, T. Poggio, and E. K. Miller. Prefrontal Cortex Activity during Flexible Categorization. *Journal of Neuroscience*, 30(25):8519–

8528, 2010. ISSN 0270-6474. doi: 10.1523/JNEUROSCI.4837-09.2010. URL http://www.jneurosci.org/cgi/doi/10.1523/JNEUROSCI.4837-09.2010.

Matthew T Schmolesky, Youngchang Wang, Doug P Hanes, Kirk G Thompson, Stefan Leutgeb, Jeffrey D Schall, Audie G Leventhal, T Matthew, Youngchang Wang, Doug P Hanes, Kirk G Thompson, Stefan Leutgeb, and Jeffrey D Schall. Signal Timing Across the Macaque Visual System. 1998.

O Schwartz and E P Simoncelli. Natural signal statistics and sensory gain control. *Nat Neurosci*, 4 (8):819–825, 2001. doi: 10.1038/90526. URL http://dx.doi.org/10.1038/90526.

Zachary P. Schwartz and Stephen V. David. Focal suppression of distractor sounds by selective attention in auditory cortex. *Cerebral Cortex*, 2018. ISSN 14602199. doi: 10.1093/cercor/bhx288.

Benjamin B. Scott, Christine M. Constantinople, Athena Akrami, Timothy D. Hanks, Carlos D. Brody, and David W. Tank. Fronto-parietal Cortical Circuits Encode Accumulated Evidence with a Diversity of Timescales. *Neuron*, 95(2):385–398.e5, 2017. ISSN 10974199. doi: 10.1016/j.neuron.2017.06.013. URL http://dx.doi.org/10.1016/j.neuron.2017.06.013.

M N Shadlen and W T Newsome. Neural basis of a perceptual decision in the parietal cortex (area LIP) of the rhesus monkey. *J Neurophysiol*, 86(4):1916–1936, oct 2001.

Michael N. Shadlen and Roozbeh Kiani. Decision making as a window on cognition. *Neuron*, 80(3):791–806, 2013. ISSN 08966273. doi: 10.1016/j.neuron.2013.10.047. URL http://dx.doi.org/10.1016/j.neuron.2013.10.047.

M.N. Shadlen, K.H. Britten, W.T. Newsome, and J.A. Movshon. A computational analysis of the relationship between neuronal and behavioral responses to visual motion. *The Journal of Neuroscience*, 16(4):1486, 1996. ISSN 0270-6474.

Sara J. Shettleworth. Animal cognition and animal behaviour, 2001. ISSN 00033472.

Markus Siegel, Timothy J Buschman, and Earl K Miller. BRAIN PROCESSING. Cortical information flow during flexible sensorimotor decisions. *Science*, 348(6241):1352–1355, 2015. doi: 10.1126/science.aab0551. URL http://dx.doi.org/10.1126/science.aab0551.

Evan C Smith and Michael S Lewicki. Efficient auditory coding. *Nature*, 439(7079):978–982, feb 2006. doi: 10.1038/nature04485. URL http://dx.doi.org/10.1038/nature04485.

Ediz Sohoglu and Maria Chait. Neural dynamics of change detection in crowded acoustic scenes. *NeuroImage*, 126:164–172, 2016. ISSN 10959572. doi: 10.1016/j.neuroimage.2015.11.050.

Saul Sternberg. The discovery of processing stages: Extensions of Donders' method. *Acta Psychologica*, 30:276–315, 1969. ISSN 00016918. doi: 10.1016/0001-6918(69)90055-9. URL http://linkinghub.elsevier.com/retrieve/pii/0001691869900559.

Carsen Stringer, Marius Pachitariu, Nicholas Steinmetz, Charu Bai Reddy, Matteo Carandini, and Kenneth D. Harris. Spontaneous behaviors drive multidimensional, brain-wide population activity. *bioRxiv*, page 306019, 2018. doi: 10.1101/306019. URL https://www.biorxiv.org/content/early/2018/04/22/306019.

Maik C. Stüttgen, Cornelius Schwarz, and Frank Jäkel. Mapping spikes to sensations. *Frontiers in Neuroscience*, 5(NOV):1–17, 2011. ISSN 16624548. doi: 10.3389/fnins.2011.00125.

Wensheng Sun, Ellisha N. Marongelli, Paul V. Watkins, and Dennis L. Barbour. Decoding sound level in the marmoset primary auditory cortex. *Journal of Neurophysiology*, 2017. ISSN 0022-3077. doi: 10.1152/jn.00670.2016.

Sruthi K Swaminathan and David J Freedman. Preferential encoding of visual categories in parietal cortex compared with prefrontal cortex. *Nature Neuroscience*, 15(2):315–320, 2012. ISSN 1097-6256. doi: 10.1038/nn.3016. URL http://dx.doi.org/10.1038/nn.3016.

Tobias Teichert, Vincent P. Ferrera, and Jack Grinband. Humans optimize decision-making by delaying decision onset. *PLoS ONE*, 9(3), 2014. ISSN 19326203. doi: 10.1371/journal.pone.0089638.

Sundeep Teki, Maria Chait, Sukhbinder Kumar, Shihab Shamma, and Timothy D Griffiths. Segregation of complex acoustic scenes based on temporal coherence. *Elife*, 2:e00699, 2013. doi: 10.7554/eLife.00699. URL http://dx.doi.org/10.7554/eLife.00699.

Etienne Thoret, Mitsuko Aramaki, Richard Kronland-Martinet, Jean-Luc Velay, and Sølvi Ystad. From sound to shape: auditory perception of drawing movements. *Journal of experimental psychology. Human perception and performance*, 40(3):983–94, 2014. ISSN 1939-1277. doi: 10.1037/a0035441. URL http://www.ncbi.nlm.nih.gov/pubmed/24446717.

D. Thura, J. Beauregard-Racine, C.-W. Fradet, and P. Cisek. Decision making by urgency gating: theory and experimental support. *Journal of Neurophysiology*, 108 (11):2912–2930, 2012. ISSN 0022-3077. doi: 10.1152/jn.01071.2011. URL http://jn.physiology.org/cgi/doi/10.1152/jn.01071.2011.

David Thura and Paul Cisek. Deliberation and commitment in the premotor and primary motor cor-

tex during dynamic decision making. *Neuron*, 81(6):1401–1416, 2014. ISSN 10974199. doi: 10.1016/j.neuron.2014.01.031. URL http://dx.doi.org/10.1016/j.neuron.2014.01.031.

N. Tinbergen. The Curious Behavior of the Stickleback, 1952. ISSN 0036-8733.

Joji Tsunada, Andrew S K Liu, Joshua I Gold, and Yale E Cohen. Causal contribution of primate auditory cortex to auditory perceptual decision-making. *Nature neuroscience*, 19(1):135–42, 2016. ISSN 1546-1726. doi: 10.1038/nn.4195. URL http://www.nature.com/neuro/journal/v19/n1/full/nn.4195.html?WT.ec_id=NEURO-201601&spMailingID=50354

Yoshiaki Tsunoda and Shinji Kakei. Reaction time changes with the hazard rate for a behaviorally relevant event when monkeys perform a delayed wrist movement task. *Neuroscience Letters*, 433 (2):152–157, 2008. ISSN 03043940. doi: 10.1016/j.neulet.2007.12.063.

Richard Turner and Maneesh Sahani. Modeling natural sounds with modulation cascade processes. *Advances in Neural Information Processing Systems 20*, 20:1–8, 2007. URL http://eprints.pascal-network.org/archive/00003788/.

Deirdre M Twomey, Peter R Murphy, Simon P Kelly, and Redmond G O'Connell. The classic P300 encodes a build-to-threshold decision variable. *Eur J Neurosci*, 2015. doi: 10.1111/ejn.12936. URL http://dx.doi.org/10.1111/ejn.12936.

Anne E Urai and Thomas Pfeffer. An action-independent signature of perceptual choice in the human brain. *The Journal of Neuroscience*, 34(15):5081–5082, 2014. ISSN 0270-6474. doi: 10.1523/JNEUROSCI.0477-14.2014. URL http://search.ebscohost.com/login.aspx?direct=true&db=psyh&AN=2014-17043-001&site=ehost-live%5Cnthms.pfffr@gmail.com%5Cnanne.urai@gmail.com.

Ruud L. Van Den Brink, Peter R. Murphy, and Sander Nieuwenhuis. Pupil diameter tracks lapses of attention. *PLoS ONE*, 11(10):1–16, 2016. ISSN 19326203. doi: 10.1371/journal.pone.0165274.

Bram van Vugt, Bruno Dagnino, Devavrat Vartak, Houman Safaai, Stefano Panzeri, Stanislas Dehaene, and P R Roelfsema. The threshold for conscious report: Signal loss and response bias invisual and frontal cortex. *Science*, 7186(March):537–542, 2018. URL http://science.sciencemag.org/content/early/2018/03/21/science.aar7186/tab-pdf.

Jonathan D. Wallis and Earl K. Miller. Neuronal activity in primate dorsolateral and orbital prefrontal cortex during performance of a reward preference task. *European Journal of Neuroscience*, 18(7): 2069–2081, 2003. ISSN 0953816X. doi: 10.1046/j.1460-9568.2003.02922.x.

Xiaoqin Wang, Thomas Lu, Ross K Snider, and Li Liang. Sustained firing in auditory cortex evoked by preferred stimuli. *Nature*, 435(7040): 341–6, 2005. ISSN 1476-4687. doi: 10.1038/nature03565. URL http://dx.doi.org/10.1038/nature03565%5Cnhttp://www.nature.com.proxy.ubn.ru.nl/nature/journal/v435/n7040/f

Y. Wang, N. Ding, N. Ahmar, J. Xiang, D. Poeppel, and J. Z. Simon. Sensitivity to temporal modulation rate and spectral bandwidth in the human auditory system: MEG evidence. *J Neurophysiol*, 107 (8):2033–2041, 2012. ISSN 0022-3077. doi: 10.1152/jn.00310.2011.

Barry Wark, Brian Nils Lundstrom, and Adrienne Fairhall. Sensory adaptation. *Current Opinion in Neurobiology*, 17(4):423–429, 2007. ISSN 09594388. doi: 10.1016/j.conb.2007.07.001.

Paul V. Watkins and Dennis L. Barbour. Specialized neuronal adaptation for preserving input sensitivity. *Nature Neuroscience*, 11(11):1259–1261, 2008. ISSN 10976256. doi: 10.1038/nn.2201.

D. E. Winkowski, S. Bandyopadhyay, S. A. Shamma, and P. O. Kanold. Frontal Cortex Activation Causes Rapid Plasticity of Auditory Cortical Processing. *Journal of Neuroscience*, 33 (46):18134–18148, 2013. ISSN 0270-6474. doi: 10.1523/JNEUROSCI.0180-13.2013. URL http://www.jneurosci.org/cgi/doi/10.1523/JNEUROSCI.0180-13.2013.

Matthew G. Wisniewski, Eduardo Mercado III, Barbara A. Church, Klaus Gramann, and Scott Makeig. Brain dynamics that correlate with effects of learning on auditory distance perception. *Frontiers in neuroscience*, 8:1, 2014.

Adrien Wohrer, Mark D. Humphries, and Christian K. Machens. Population-wide distributions of neural activity during perceptual decision-making, 2013. ISSN 03010082.

X Yang, K Wang, and S Shamma. Auditory representations of acoustic signals. *IEEE Trans Inf Theory*, 38:824–839, 1992.

Michael M Yartsev, Timothy D Hanks, Alice M Yoon, and Carlos D Brody. Causal contribution and dynamical encoding in the striatum during evidence accumulation. *bioRxiv*, page 245316, 2018. ISSN 2050-084X. doi: 10.1101/245316. URL http://dx.doi.org/10.1101/245316%0Ahttps://www.biorxiv.org/content/early/2018/01/10/245316.

Pingbo Yin, Jonathan B Fritz, and Shihab A Shamma. Do ferrets perceive relative pitch? *J Acoust Soc Am*, 127(3):1673–1680, mar 2010. doi: 10.1121/1.3290988. URL http://dx.doi.org/10.1121/1.3290988.

Mu Zhou, Feixue Liang, Xiaorui R Xiong, Lu Li, Haifu Li, Zhongju Xiao, Huizhong W Tao, and Li I Zhang. Scaling down of balanced excitation and inhibition by active behavioral states in auditory cortex. *Nature neuroscience*, 17(6):841–50, 2014. ISSN 1546-1726. doi: 10.1038/nn.3701. URL http://www.ncbi.nlm.nih.gov/pubmed/24747575.

Zhe Charles Zhou, Chunxiu Yu, Kristin K. Sellers, and Flavio Fröhlich. Dorso-Lateral Frontal Cortex of the Ferret Encodes Perceptual Difficulty during Visual Discrimination. *Scientific Reports*, 6 (December 2015), 2016a. ISSN 20452322. doi: 10.1038/srep23568.

Zhe Charles Zhou, Chunxiu Yu, Kristin K. Sellers, and Flavio Fröhlich. Dorso-Lateral Frontal Cortex of the Ferret Encodes Perceptual Difficulty during Visual Discrimination. *Scientific Reports*, 6(March):23568, 2016b. ISSN 2045-2322. doi: 10.1038/srep23568. URL http://www.nature.com/articles/srep23568.

# Appendix

## Surgery Protocol

### Day before

Check everything (isofluorane level, O2 concentrator, sufficient number of gauze, drugs quantity and expiration date, etc. - add details). Prepare everything (tools, surgery room, etc. - add details). Do not forget to autoclave surgical light handle and pencil. Put into alcool stereotaxic tools, including stuff to grasp the needle. Inject antibiotics (Baytril, SC). Deprive the animal of food (4h before induction - 2h might be sufficient). Rehearse the surgery and make sure that all the plans are set beforehand (type of implant, EEG implantation or not, screw positions, stereotaxic coordinate, etc.).

### Before starting, in the morning

Deprive the animal of water, 1h before induction. Turn on heating pads. Inject Méloxicam SC (Metacam), 30 min before induction. Adjust the surgeons' seats.

### Anesthesia induction & intubation

Inject IM Medetomidine (Domitor) - wait for sedation to kick in. Inject IM Ketamine (Imalgène) - common source of delay, if done SC. Inject SC Baytril and Atropine . Put some eye protection gel (Lubrithal) on the eyes. Shave the animal (then clean the place to remove the cut fur). Inject SC lidocaine along the future cut. Put local anesthesia cream (Tronothane) on the intubation tube. Give the animal a short shot of isoflurane (30s 5%), then rapidly proceed to intubation. Using gauze to maintain the mouth of the animal open, reach for the trachea (you should see the vocal cords). Check that the intubation is correct with a mirror. If so, add some tape around the tube and sew it to the cheek. Bring the animal to the surgery room, and attach the intubation tube to the isoflurane tube. Turn on isoflurane to 1%. Don't forget to robustly attach all different parts of the breathing system with tape and magnets.

**Surgery**

Hook up all the monitoring. Put the animal's teeth in the snout holder - add some gauze on top of its snout to protect it when clamping. Put the ear bars. This step is crucial for the good proceedings of the surgery: make sure the head of the animal is not wobbly by pressing a little on it. While one surgeon gets prepared (scrubbing hands, then putting on sterile clothes - in that order: hygiene cap, mask, coat, gloves), the other one cleans the head of the animal with alcohol 70%, then iodine (Vétédine 10%) not diluted, 3x, from the center outwards: alternate alcohol and iodine, finish by iodine). When the first surgeon is ready, and the animal hooked up, the second surgeon helps the surgery assistant to give the first surgeon the two sterile fields and the tools needed for the beginning (scissors, scalpel, forceps, gauzes, cup, cautery...). The second surgeon gets prepared when the first one put the sterile field over the animal. Cut a hole in the head/neck region. Add the sticky sterile field Ioban (cut beforehand at the right size), starting from the head and unfolding it on both sides. Make sure the field sticks to the skin and the rest of the skin. Avoid tensions on the holding apparatus. Surgery assistant put the iodine 1% and saline into the cup.

**Getting to the skull** Incise the skin of the animal, along the medial crest (you can feel it with your fingers), from the flat frontal part down to the neck (2-3cm after the posterior crest). Use clamps to spread aside the two banks of the skin. The tools used to touch the skin (scalpel, broad forceps) needs to be discarded as they are not sterile anymore. Use a dilution of iodine (1%) to irrigate the opening. Use the iodine dilution everytime a new layer is open. With the spatula, scratch and scrub the muscles away, starting from the medial crest; careful scalpel cuts can be useful. Remove the muscles until you see the beginning of the zygomatic arch and the lateral wing at the lateral end of the nuchal crest. Be careful here because the external acoustic meatus is just in between, and should not be damaged.

Clamp the muscles as lateral as possible. Wait 5-10 minutes. Cut the muscles (the other surgeon must be ready to cauterize). Add gauze gorged with saline on the freshly cut muscles (especially because you're only cutting one side at a time). Scrub the skull to remove every piece of tissue, then clean the skull with oxygen peroxyde. Wash with saline. Wash with iodine.

**Skull alignment and stereotaxic positioning** One surgeon loses perfect sterility and sets up the stereotaxic apparatus. Good time to add some eye protection gel (Lubrithal) on the eyes ! Using the Stereotaxis support sheet, verify that the skull is well aligned along all axis (A-P, M-L and D-V). Position the wells. Position the headpost. Using superbond, fix it on the skull: this implies using the

green liquid first (10 seconds), drying with a q-tip, and then adding the superbond on the skull and on the bottom of the headpost, then pressing the headpost down onto the skull (the last part needs to be fast). Hold it still until cement has got hard (do not hesitate to wait a little more).

**Building the implant** Position the screws wherever needed. Think ahead for the design of your craniotomies. To fix one screw, drill slowly but persistently (in just one shot, otherwise the thread can be too wide) until it gives in, then wash and cool down the hole with saline, and screw (2 ½ turns). If bleeding occurs, make sure it stops before screwing in, otherwise an increasing pressure will provoke epileptic seizures and/or damage the brain. Note that if when piercing through, a black deposit occurs, you are not doing this properly. You can change the drill bit if you have any doubts. Take pictures! Carefully add bone cement around the screws and around the headpost. Use bone wax to design the shape and size of the wells (and make a bone wax snowman). Using custom plastic bands inserted laterally (just above the muscle), progressively add liquid then semi-liquid bone cement to build the implant. The first layer can be a thin layer of liquid cement everywhere on the skull. Make sure no bubble is present between the implant and the bone. Build up the implant using the plastic shapes. Make sure that the implant is smooth and has no shards. Remove the bone wax from the wells, and cast some liquid dental cement in the wells to guarantee impermeability. Holding the skin at the neck level using a clamp so that the two banks meet, draw the cut you'll make in the skin. Cut the skin. Stitch the skin (usually, 1-2 stitches in front, 5-6 on the neck). On the neck, don't forget to include the fascia on every stitch. Clean the implant with saline/iodine. Add Dermaflon all around the wound. Stay in the lab until the animal wakes up and make sure no bleeding occurs. Rehydrate and feed the animal (use Fortol, water with sugar is one solution). Inject Méloxicam (Metacam) Put the animal back in a sick bay cage, with a heating pad (~25°C), moist food, and water.

**Post-op**

Give Baytril SC, 10 days and Metacam orally for 5 days. Make sure everything is fine: balance, eyes, food and water intake, etc.

## Multi-array implantation protocol

Antibiotics are administered the day before (Baytril) and continue to be administered for 5 days, IC. Inject metacam, surgery dose, IC. Place the ferret in tube with the mask. Use oxygen for the first part of the implantation. Enlarge the well as much as possible. You may want to remove part of the lateral

wall. The surface needs to be straight and smooth before starting the craniotomy (play around with an unmounted drive to see how much of the cement should be drilled). Start isoflurane at 1.5, then if possible reduce to 1 after 3 minutes. Drill a square craniotomy (little more than the array size, say 5*5 for the 32 channels) + duratomy (use the tip of a thin needle, scratch very gently the dura until it opens and then use bent and sterilised needle to enlarge duratomy). Have everything prepared before the duratomy because the brain will bulge. Find an adequate position with the help of the surrogate drive (Trying to be as perpendicular as possible to the brain surface); note X/Y/Z position and the angle. This is extremely important for the removal. Take pictures. Hold the actual drive at the same position and slowly go down while monitoring the ferret. If possible record the signal at the same time and wake the ferret up. Stop when the Z coordinate has been reached + add 500µm. Fill the gap with sterile conductor gel (use a syringe). Seal it with UV viscous flow cement. Start from the remaining sides and create a structure encasing the array. Make sure the cement fills the cavity. Leave a small opening to insert a thin cable in the gel that will be use for grounding. Position the Falcon tube or the printed part that will protect the mounted electrode. Make sure the lateral part of the drive is NOT in contact with the protection and seal it to the implant using dental cement. Attach the connector. Wires need to be protected (shrink cable works well) and encased in dental cement. Finish the construction with liquid dental cement if necessary, to ensure maximum protection. Remove the ferret from the tube. Metacam post-op given orally and ferret is returned to the cage.

## Change representation depends on FC recording location

Flexibility in recording location enabled by the use of single tungsten electrodes in semi-chronic recordings allowed us to record at different locations in FC. Similarly to Fritz et al. [2010], Zhou et al. [2016a], task-relevant modulations here displayed as averaged population response to the change (Fig. 54) are present in the most posterior recording locations, thought to correspond to the ferret dorso-lateral/premotor FC. Histology will be necessary to confirm the position of our recordings.

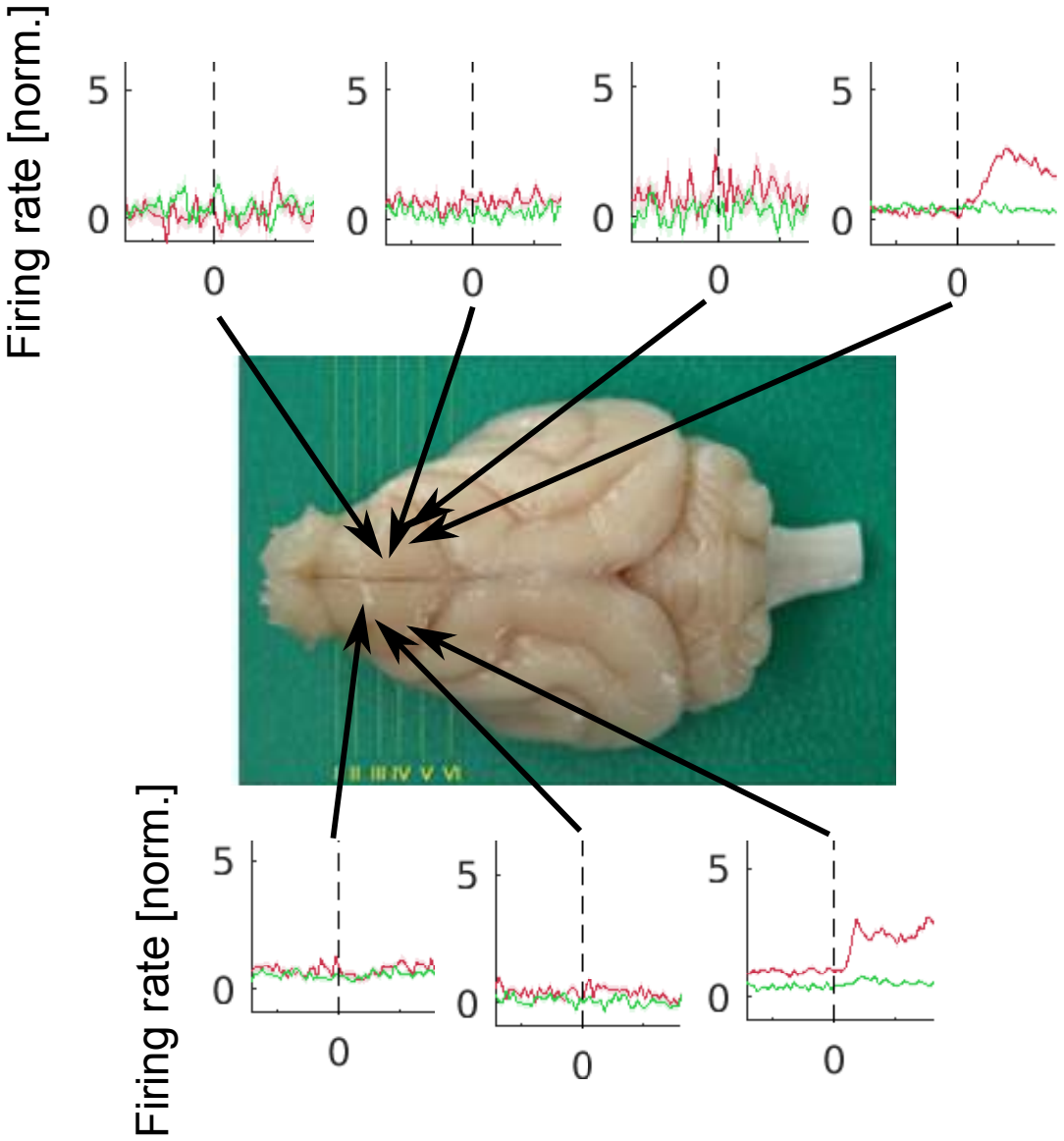


Figure 54: **Behavior-dependent modulations as a function of recording location in ferret FC** Averaged population responses displayed in PSTHs locked to the change as a function of approximate recording sites in Ferret M (ferret brain image is not ferret M) FC shows modulation only for the most posterior recording sites.

## Résumé

Se déplacer dans une rue tout en discutant au téléphone est une action triviale pour une majorité de la population. Cependant, comment le cerveau parvient à extraire les informations pertinentes d'un environnement acoustique aussi complexe afin de produire un comportement adéquat reste encore actuellement peu compris. La thèse présentée explore les bases neurales de l'extraction d'informations pertinentes dans un flux complexe et continu afin de produire un comportement. Les sujets (humains et furets) détectent des changement dans les statistiques de nuages de tons pendant que leur activité électrique cérébrale (sur le scalp pour les humains, cellulaire pour le furet) est enregistrée. Les différentes zones du cortex enregistrées présentent des activités spécifiques: les réponses liées au changement se généralisent le long de la hiérarchie corticale. De plus, l'engagement dans la tâche module spécifiquement les réponses frontales au changement et à la décision.



## Mots Clés

prise de décision, détection de changement, statistiques du stimulus,cortex auditif, cortex frontal, électrophysiologie



## Abstract

Navigating a busy street while talking on the phone is trivial for a majority of the population. However, how the brain extracts the relevant information from the ever-changing and cluttered acoustic environment to produce the appropriate behavior remains poorly understood. The proposed thesis investigates neural basis of the extraction of relevant information in complex continuous streams for goal-directed behavior using a combination techniques linking electrophysiology to psychophysics. Humans and ferrets performed a similar change detection task that consisted of reporting changes in the underlying statistics of a tone cloud. The brain electrical activity was recorded (scalp level for humans and cell level for ferrets) while subjects engaged in the task. Overall, we find area-specific cortical responses: change-related responses are generalized along the cortical pathway. In addition, task engagement strongly modulates the frontal cortex where decision-related responses are found.



## Keywords

perceptual decision-making, change detection, stimulus statistics, auditory cortex, frontal cortex, electrophysiology